UNIVERSITY OF CALIFORNIA SAN DIEGO

Migrating Eastern North Pacific Gray Whale Behavior Compared Over Multiple Timescales

A dissertation submitted in partial satisfaction of the
requirements for the degree
Doctor of Philosophy

in

Oceanography

by

Regina Anne Guazzo

Committee in charge:

John A. Hildebrand, Chair
Jay Barlow
Sarah C. Creel
Gerald L. D'Spain
Mark D. Ohman
David W. Weller

2018

The dissertation of Regina Anne Guazzo is approved, and it is acceptable in quality and form for publication on microfilm and electronically:

_____

_____

_____

_____

_____

_____

Chair

University of California San Diego

2018

EPIGRAPH

"Unless someone like you
cares a whole awful lot,
nothing is ever going to get better.
It's not."

—Dr. Seuss

TABLE OF CONTENTS

LIST OF FIGURES

LIST OF TABLES

ACKNOWLEDGEMENTS

This dissertation would not have been possible without the confidence from my advisor, John Hildebrand. John welcomed me into his lab and helped me start my own research project right away. He seized the opportunity to deploy a hydrophone array offshore of the Granite Canyon visual and IR station and provided me with more long-term datasets than I could have ever worked through in the time of a PhD.

My committee members greatly improved the contents of this dissertation. Gerald D'Spain contribued to each of my chapters and made sure that everything I did was mathematically and physically correct. I am so grateful for our long meetings, detailed email conversations, and your thorough critique of my papers. Dave Weller helped to design the setup for the Granite Canyon study and is a gray whale expert. Without Dave, this project studying the gray whale migration would have never begun. Thank you for your constant encouragement and for helping me understand the whales from a biological point of view. Jay Barlow was a wonderful resource for statistical advice and helped me design the GAM model used in Chapter 4. Thank you for class which first introduced me to Bayesian statistics and your thoughtful feedback about how to apply statistical tests to marine mammal datasets. Mark Ohman helped me to think about my research questions from a biological oceanography mindset. Thank you especially for offering a seminar course last year, which helped me improve my presentation, writing, and peer-review skills, and allowed me to create a solid draft of my abstract and introduction chapter. Thank you, James Nieh, for being a part of my committee for two years and for your advice particularly about publishing my work. And finally, Sarah Creel jumped on my committee in the last five months. Thank you for your interest in my work and for bringing an outside perspective with your suggestions.

The Science, Mathematics, and Research for Transformation (SMART) Scholarship, funded through the Department of Defense, supported me for the last three years of my PhD. I am so grateful that through this scholarship I got the opportunity to collaborate with Tyler Helble

at SPAWAR Systems Center Pacific (SSC-PAC). I would especially like to thank Dave Nieman, John Bily, and Jim Crowder for their coordination of the SMART scholarship at SSC-PAC.

Tyler Helble designed the Generalized Power Law detector that was used in each of these chapters and provided code and assistance for localizing and tracking whales acoustically. During my SMART summer internships, Tyler allowed me to continue working on my dissertation while using SSC-PAC technology and resources. I greatly admire his work and have been honored to contribute to his recent conference presentations. I am excited to begin working with him at SSC-PAC this fall.

I am thankful for Alisa Schulman-Janiger and Michael Smith who generously shared their visual data with me and offered insightful comments regarding Chapter 4 from their years of experience observing these whales.

Several other members of the NOAA Southwest Fisheries Science Center contributed to this dissertation. Thank you to Wayne Perryman who has spent his career studying gray whales and took time to listen to my ideas and teach me what he has learned. Thank you to John Durban who created the model that NOAA uses to estimate gray whale population size and who contributed to Chapter 3. Thank you to Alexa Kownacki who first showed me the IR camera system and to Hollis Europe who manually detected gray whale blows for Chapter 3.

I have worked with an amazing team at the Scripps Whale Acoustics Lab. They designed, deployed, and retrieved all the acoustic recording packages, processed the data, and were always available to answer questions. These tireless workers include: Sean Wiggins, Simone Baumann-Pickering, Marie Roch, Ana Širović, Bruce Thayer, Ryan Griswold, Erin O'Neill, Greg Campbell, Virginia Lehr, Sean Herbert, Frank Chang, Elioth Fraijo, Alex Luu, Rohen Gresalfi, Amanda Debich, Ally Rice, Jenny Trickey, Arial Brewer, Sarah Kerosky, Sienna Thomas, Beverly Kennedy, and Lauren Roche, who taught me how to identify baleen whale calls and shared what she had learned about gray whale vocalizations when I first started in the lab.

The other graduate students and post-docs in the Scripps Whale Acoustics Labs have

been a wonderful source of encouragement, advice, and friendship. They have been office mates, cruise partners, and conference roommates. Thank you to Karlina Merkins, Martin Gassman, Liz Vu, Kait Frasier, Grace Teller, Leah Varga, Leah Lewis, Anne Simonis, Josh Jones, Katherine Cameron Wilson, Rebecca Cohen, Angela Szesciorka, Anna Krumpel, Alba Solsona Berga, Camille Pagniello, Ashlyn Giddings, Eadoh Reshef, Morgan Ziegenhorn, Natalie Posdaljian, Eric Snyder, and post-docs Goldie Phillips and Jack Butler.

A huge thank you to the 2013 Biological Oceanography cohort: Ben Whitmore, Jess Carrière-Garwood, Matt Costa, AJ Schlenger, Lilly McCormick, Bellineth Valencia, Abby Cannon, and Josh Jones. We survived departmentals, qualifying, and are now defending! I always look forward to our brunch/lunch/ice cream dates. You are going to be amazing at whatever you do. A special thank you to the 2012 Biological Oceanography cohort for guiding us through our time at SIO. Thank you also to my friends from other curricular groups, especially Anna Merrifield, Maddie Harvey, Sarah Shackleton, Dara Goldberg, and Katherine Cameron. You have made these past five years so much better and I am so happy to have met you!

Thank you to all the faculty and staff at SIO who make it a warm, supportive environment. Whenever I have had a question, everyone has been so generous with their time. The Scripps Graduate Program office deserves an extra thank you for all their hard work to make the academic programs run seamlessly. I am amazed at how they remember details about every student and ensure that we know we matter.

I am lucky to have friends from outside of SIO who encouraged me through this journey. Thank you to Alex Cameron, Rosa Valdez, and Casey Converse who provided many laughs, honesty, and support in our careers, marriages, and faith. Thank you to Sarah Blatsos who has been a wonderful friend through our husbands' deployments and training trips. Thank you to Samantha Coy and Marissa Vigar who I met at Duke Marine Lab and who share my excitement for marine life and outdoor exploration. Our long-distance friendship has meant so much to me. Thank you to Melissa Meola and Serena Lu who have been my friends through every stage of life

and who have always believed in me.

I am grateful for the Rutgers Marine Science program that helped me get started in oceanography. Scott Glenn, Oscar Schofield, and Josh Kohut believed in undergrads and allowed us to participate in research projects through the RU COOL program. Heidi Fuchs supervised my independent study and made me a co-author on my first scientific publication. Judy Grassle was a wonderful advisor. Peter Smouse inspired me and encouraged me as I left for graduate school.

I had the opportunity to study bottlenose dolphin signature whistles during the summer of 2012 at Duke University Marine Lab through NSF's Research Experiences for Undergraduates program. Thank you to Doug Nowacek for his advice and mentorship during that summer and the following year and for giving me my first opportunity to study marine mammal bioacoustics.

Since I was in elementary school, most of my teachers knew I dreamed of being a marine biologist. I am thankful for all the teachers in the Bridgewater-Raritan Regional School District who saw potential in me and challenged me, but would like to extend a special thanks to my orchestra director, Joseph Lalumia, my physics teacher, Walt Gibbons, and my math teacher, David Weth.

I am incredibly blessed to have parents, Dana and Frank Guazzo, who love me and support me in all of my passions. Thank you to my mom who inspired me by having a PhD, a successful career, and a wonderful marriage. Throughout my grad school journey, my mom has been a constant source of encouragement. Thank you to my dad whose humor has always kept me laughing and who has been a role model for me with his kind, patient nature. Thank you to my sister, Julia Guazzo, who has continued to love me despite our many similarities and (even more) differences. I am so lucky to have had you living close by for the past three years and I really appreciate the time we have gotten to spend together. Thank you to Brian's parents, Heidi and Jeff McShea, who have welcomed me into their family.

Finally, the biggest thank you goes to my husband, Brian McShea. Brian, you mean the world to me. I am so glad we met five years ago. It has been a difficult journey, but your

never-ending pep talks, spontaneous date nights, adventure-filled get-aways, and attempts to solve my many problems have helped me finish. Whether you were right by my side hugging me or whether there was an ocean (and lots of whales) between us, I have always known I had your unwavering love and support. I am so excited to see what is next for us!

This dissertation is a collection of papers that have been accepted, submitted, or are in preparation for publication.

Chapter 2, in full, is a reprint of the material as it appears in *PloS ONE*, 2017: Regina A. Guazzo, Tyler A. Helble, Gerald L. D'Spain, David W. Weller, Sean M. Wiggins, and John A. Hildebrand, "Migratory behavior of eastern North Pacific gray whales tracked using a hydrophone array." The dissertation author was the primary investigator and author of this paper.

Chapter 3, in full, has been submitted for publication in *Scientific Reports*, Regina A. Guazzo, David W. Weller, Hollis M. Europe, John W. Durban, Gerald L. D'Spain, and John A. Hildebrand, "Migrating eastern North Pacific gray whale cue rates estimated from acoustic recordings, infrared camera images, and visual sightings." The dissertation author was the primary investigator and author of this paper.

Chapter 4, in full, is currently being prepared for submission for publication. Regina A. Guazzo, Alisa Schulman-Janiger, Michael H. Smith, Jay Barlow, Gerald L. D'Spain, and John A. Hildebrand, "Gray whale migration patterns through the Southern California Bight from multi-year visual and acoustic monitoring." The dissertation author was the primary investigator and author of this paper.

VITA

2013	B.S., Marine Science Rutgers, the State University of New Jersey
2016	M.S., Marine Biology Scripps Institution of Oceanography, University of California San Diego
2018	Ph.D., Oceanography Scripps Institution of Oceanography, University of California San Diego

PUBLICATIONS

Journal Articles

1. Guazzo, R. A., Helble, T. A., D'Spain, G. L., Weller, D. W., Wiggins, S. M., and Hildebrand, J. A. (2017) Migratory behavior of eastern North Pacific gray whales tracked using a hydrophone array. *PloS ONE*, 12(10):e0185585.
2. Fuchs, H. L., Hunter, E. J., Schmitt, E. L., and Guazzo, R. A. (2013). Active downward propulsion by oyster larvae in turbulence. *Journal of Experimental Biology*, 216(8):1458–1469.

Conference Presentations

1. Guazzo, R. A., Helble, T. A., D'Spain, G. L., Weller, D. W., Durban, J. W., Wiggins, S. M., and Hildebrand, J. A. (2018). Multi-year investigation of migrating gray whale acoustic and swimming behavior at two sites in California. Southern California Marine Mammal Workshop. Newport Beach, CA. Poster.
2. Guazzo, R. A., Helble, T. A., Hildebrand, J. A., Wiggins, S. M., D'Spain, G. L., and Weller, D. W. (2016). Tracking gray whale behavior with a sparse hydrophone array. Joint Meeting of the Acoustical Society of America and the Acoustical Society of Japan. Honolulu, HI. Oral Presentation.
3. Guazzo, R. A., Weller, D. W., Wiggins, S. M., and Hildebrand, J. A. (2015). Combining acoustic array localizations with visual observations to track migrating gray whales. Society of Marine Mammalogy Biennial Conference. San Francisco, CA. Poster.
4. Guazzo, R. A., Wiggins, S. M., and Hildebrand, J. A. (2014). Using acoustics to study extreme migrations: Gray whales in Monterey Bay National Marine Sanctuary. Meeting of the Acoustical Society of America. Indianapolis, IN. Oral Presentation.

5. Guazzo, R. A. and Hildebrand, J. A. (2014). Acoustic detection of migrating gray, humpback, and blue whales in the coastal, northeast Pacific. BioAcoustics Summer School (SeaBASS). Leesburg, VA. Poster.
6. Guazzo, R. A., Nowacek, D. P., and Schofield, O. S. (2013). Evaluating the stability of signature whistles of bottlenose dolphins (*Tursiops truncatus*) off Beaufort, NC. Rutgers University Senior Honors Thesis. New Brunswick, NJ. Oral Presentation.

ABSTRACT OF THE DISSERTATION

Migrating Eastern North Pacific Gray Whale Behavior Compared Over Multiple Timescales

by

Regina Anne Guazzo

Doctor of Philosophy in Oceanography

University of California San Diego, 2018

John A. Hildebrand, Chair

Mysticetes (baleen whales) often make long, annual migrations from high latitude summer feeding areas to low latitude wintering areas. Eastern North Pacific gray whales (*Eschrichtius robustus*) migrate within a few kilometers from shore for most of their route from summer feeding areas in the Bering, Chukchi, and Beaufort Seas to wintering areas in the lagoons along the south-western coast of the Baja California Peninsula in Mexico. This dissertation combines passive acoustic recordings, infrared camera video, and visual sightings to investigate gray whale behavior and how it changes across different timescales. I use a four-element hydrophone array in central California to present the first published full-season acoustic monitoring and

tracking of migrating gray whales. I describe the characteristics of calls produced by migrating gray whales and analyze how these characteristics change due to propagation. I show that gray whale behavior changes on diel and seasonal timescales. Notably, gray whales increase their vocalizations at night but their mean swimming behavior does not change, contrary to previous assumptions used in population size estimates. Over seasonal timescales, vocalizing gray whale swimming behavior aligns with previous observations. I explore how passive acoustic and infrared camera monitoring can help quantify whales by calculating cue rates or call and blow rates for migrating gray whales. Acoustic calling rates indicate that the gray whale population size is greater than estimated using visual sightings alone and that calling rate increases over the southbound migration. Infrared camera blow rates are less affected by whale behavior and are useful for daytime and nighttime monitoring, but are limited by visibility and distance. To understand gray whale behavior over seven migration seasons, I use visual daily counts at two sites and single-hydrophone call detections which indicate that migratory behavior seems to be driven more by intrinsic than the tested environmental factors. I find that the proportion of the population using a coastal route through the Southern California Bight, especially past Los Angeles, increased over these years. Understanding the behavior of migrating gray whales will help improve abundance estimates and determine how these whales may be impacted by nearshore anthropogenic activities and climate change.

Chapter 1

Introduction

1.1 Annual Migrations in Mysticetes

Mysticetes, or baleen whales, often make long, annual migrations from their summer feeding areas in high latitudes to their wintering areas in low latitudes. In the North Pacific, humpback whales (*Megaptera novaeangliae* Borowski) migrate from feeding areas off mainland Russia, the Aleutian Islands, Alaska, Canada, and the United States to breeding areas in the western Pacific Islands, Hawaii, Mexican Islands, Baja California, mainland Mexico, and Central America (Barlow et al., 2011). Blue whales (*Balaenoptera musculus* Linnaeus) in the northeast Pacific feed along the coast of the United States in the summer, concentrated off southern California and migrate in the winter to the southern tip of Baja California, the Gulf of California, and a region west of the Costa Rica Dome (Bailey et al., 2009). Eastern North Pacific gray whales (*Eschrichtius robustus* Lilljeborg) make one of the longest migrations of any mammal, covering 50 degrees of latitude and traveling 15,000 to 20,000 km round-trip between the Bering, Chukchi, and Beaufort Seas where they spend the summer and Baja California, Mexico where they spend the winter (Sumich, 1983) (Figure 1.1). In this dissertation, I will investigate the behavior of gray whales as they migrate through central and southern California and analyze how

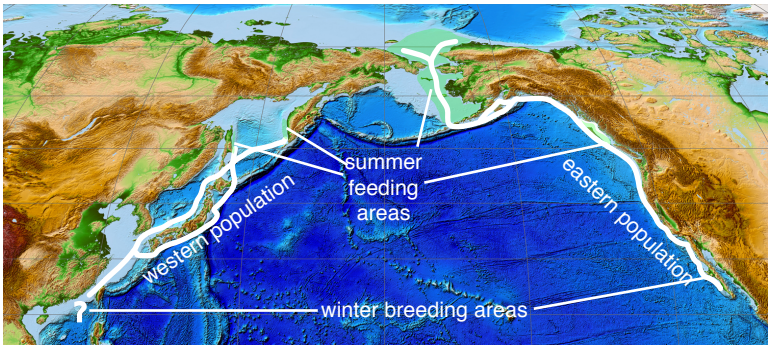

Figure 1.1: Map of the North Pacific Gray Whale Migration. Migration routes (white lines) between summer feeding and winter breeding areas for the western and eastern North Pacific gray whale populations. The majority of the western route is inferred. From Sumich (2014), Figure 2.1, page 23.

this behavior changes over time.

1.2 Whaling History and Current Population Status

At least three populations of gray whales once existed. The North Atlantic gray whales, which may have been divided into separate eastern and western populations, went extinct in the 1700s (Lindquist, 2000). The western North Pacific population of gray whales is critically endangered with an abundance of about 100 individuals and a growth rate of 3% (Bradford et al., 2008).

The eastern North Pacific population of gray whales is a conservation success story. When commercial whaling first began, the eastern North Pacific gray whale population size was around 30,000 (Scammon, 1874). Between 1846 and 1874, whalers killed approximately 10,800 gray whales, with much of the whaling directed toward females and calves, causing the population to shift its migration corridor farther offshore and nearly desert the Mexican lagoons (Scammon, 1874). In the 20th century, the gray whale hunt decreased and only 2,724 whales were taken from the eastern population between 1910 and 1946 (Sumich, 2014). In 1946, the International Whaling Commission was established and gray whales were protected

from commercial whaling (Sumich, 2014). In the 1950s and 1960s, aerial censuses by Hubbs and Hubbs (1967) and shore-based censuses by Gilmore (1960) estimated that the population contained between 2,894 and 4,454 individuals and seemed to be increasing at a rate of up to 10% each year (Gilmore, 1960). Today, eastern North Pacific gray whales are presumed to be at their carrying capacity (Moore et al., 2001) and are listed as a species of least concern (Reilly et al., 2008). The population size was estimated to be 26,960 individuals during the 2015–2016 season (Durban et al., 2017). The dramatic recovery in population size over fifty years and the reoccupation of the lagoons in the winter and the coastal corridor migration route gives hope that species can survive exploitation with proper management and sufficient time.

1.3 The Gray Whale Migration

The eastern North Pacific gray whale migration follows a predictable pattern with different demographic components of the whale population traveling at different times (Rice and Wolman, 1971) (Figure 1.2). The southbound migration starts with late pregnant females, followed by recently ovulated females, adult males, immature females, and lastly immature males (Rice and Wolman, 1971). Gray whales migrate along the continental shelf for most of the route. In the Southern California Bight, however, gray whales split into three corridors with one inshore, one around Santa Catalina Island, and one around San Clemente Island (Sumich and Show, 2011). The whales that swim around the islands mostly pass to the west of the islands and then meet up with the nearshore migrators between La Jolla, California and the United States/Mexico border (Sumich and Show, 2011). Carretta et al. (2000) estimated that most of the population takes the offshore route through the Channel Islands. Since 1980, the timing of the southbound migration has shifted about 7 days later (Rugh et al., 2001). This shift, concurrent with the change to a positive Pacific Decadal Oscillation (PDO) regime, could indicate that gray whales are affected by climate cycles, perhaps because regime shifts may cause changes in prey locations,

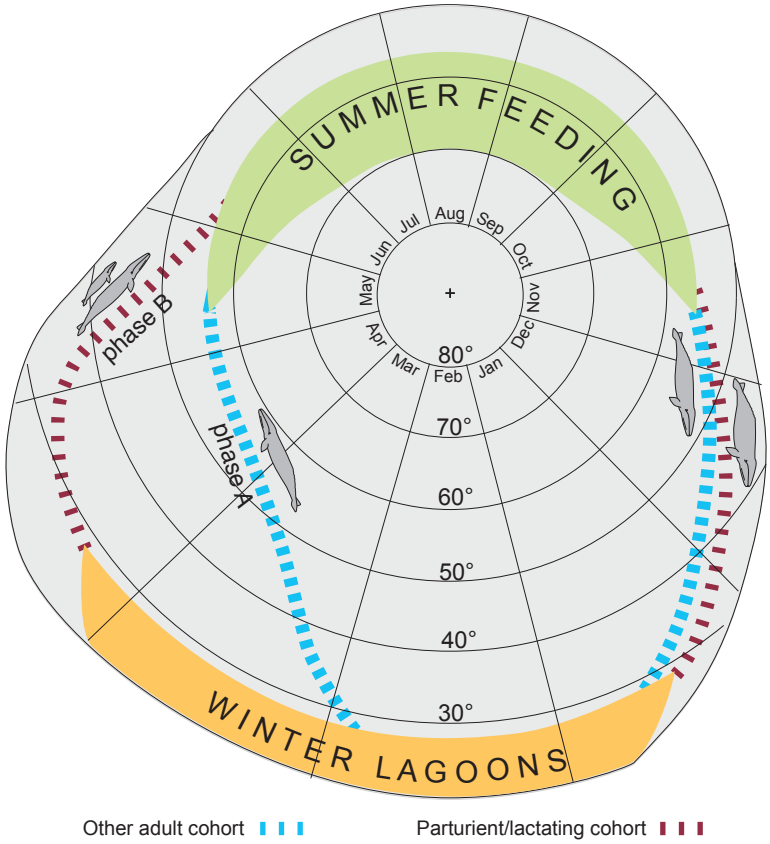

Figure 1.2: Timing of the Eastern North Pacific Gray Whale Migration. This diagram shows month and latitude for pregnant/lactating females (red) and other adult whales (blue). From Sumich (2014), Figure 4.8, page 98.

causing the gray whales to migrate farther (Rugh et al., 2001).

The northward migration from the lagoons of coastal Baja California is slightly more offshore and direct for most whales, except for females with calves which keep, in some areas, within 200–400 m from shore (Poole, 1984; Perryman et al., 2002). Early pregnant females leave the breeding areas first, followed by adult males, adult females that are not pregnant, immature females, immature males, and finally postpartum females with calves (Rice and Wolman, 1971). This migration pattern, hugging the North American coast, makes the eastern North Pacific gray whale migration the most observed whale migration, but also makes these whales more likely to be impacted by nearshore human activities such as shipping, fishing, and increased background noise.

Many studies have quantitatively described the gray whale migration by visually observing whales or tagging a small number of animals with satellite tags. Most pregnant females travel south alone, but groups of two or three are most common for other southward migrating gray whales (Gilmore, 1960; Rice and Wolman, 1971). The mean distance between conspecifics is 4.8 km (Sumich, 1983). Gray whales swim at speeds between 1.1 and 2.8 m/s while migrating (Cummings et al., 1968; Rice and Wolman, 1971; Sumich, 1983; Rugh et al., 1990; Perryman et al., 1999; Mate and Urbán-Ramírez, 2003; Mate et al., 2010) and tend not to deviate from their migration behavior except for occasional courting or mating behavior during the late southbound migration (Gilmore, 1960).

Controversy exists regarding gray whale behavior at night. Hubbs and Hubbs (1967) reported that gray whales continue migrating in bright moonlight, but stop on dark nights. Perryman et al. (1999) used infrared cameras during portions of three southbound migration seasons and observed that gray whales shifted 0.4 km closer to shore at night. After 15 January, gray whales increased their nighttime southbound migration rate and daytime pod size (Perryman et al., 1999). Perryman et al. (1999) hypothesized that gray whales were socializing more during the day and slowing their migration rate. This change in migration behavior is accounted for in population size estimates (Laake et al., 2009). In contrast, a diel change in migration behavior has not been observed during the northbound migration (Mate and Urbán-Ramírez, 2003; Perryman et al., 2002). These results warrant further investigation. Passive acoustic monitoring is another way to increase our understanding of whale behavior during both night and day.

1.4 Gray Whale Vocalizations

Many oceanic animals use sound as their primary method of communication and sensing their environment. Species of fish in several different taxa are known to use acoustic

communication and often these sounds are associated with mating (e.g. Bass and McKibben, 2003). Some crustaceans produce sound. A well-known example is the snapping shrimp which creates sound to stun prey through cavitating bubbles (Versluis, 2000). Pinnipeds also vocalize, often in the form of male displays (e.g. Hanggi and Schusterman, 1994). Species of odontocetes, or toothed whales, use whistles and clicks to communicate (e.g. Janik and Slater, 1998) and echolocation clicks to sense their environment and detect prey (e.g. Au et al., 1974). Mysticetes make low- and mid-frequency vocalizations. One of the best studied and most complex is male humpback whale song (e.g. Payne and McVay, 1971), but all species of mysticetes are thought to vocalize. Passive acoustic monitoring is often used to determine presence of a vocalizing species. The context of these vocalizations can provide clues to their significance.

Previous research has described vocalizations produced by gray whales, but little is known about how gray whales use calls while migrating. Dalheim (1987) named and described six gray whale call types when she studied gray whales in the lagoons of coastal Baja California. She recorded 0.33 calls/whale/hour in February and 0.25 calls/whale/hour in March and found no diel variation in call production (Dalheim, 1987).

Gray whales are reported to produce fewer calls while migrating than while in their breeding areas, but the most common call while migrating, making up 47 to 87% of the repertoire, is the low-frequency M3 call (Cummings et al., 1968; Crane and Lashkari, 1996). Gray whales vocalize less frequently than many other mysticetes in the northeast Pacific. Crane and Lashkari (1996) measured 0.050 calls/whale/hour in water less than 100 meters deep and Cummings et al. (1968) recorded 0.74 calls/hour (not normalized for whale) with a maximum of 53 M3 calls/whale/hour and noted that approximately one-third of lone migrators made detectable sounds. The M3 call is an amplitude- and frequency-modulated call often containing harmonics (Crane and Lashkari, 1996). It has a center frequency below 100 Hz (Crane and Lashkari, 1996), a range from 20–200 Hz, and an average duration of 1.54 s (Cummings et al., 1968). M3 calls have a published source level of 151 dB re : 1μPa at 1 meter (Cummings et al., 1968), but Petrochenko

et al. (1991) measured source levels of 167 to 188 dB re : 1μPa at 1 meter for gray whale calls in general.

Another call type recorded from migrating gray whales is the M1 call. This call has been described as sounding like knocking, metallic pulsing, or bongo drums (Cummings et al., 1968; Fish et al., 1974; Crane and Lashkari, 1996). Crane and Lashkari (1996) reported that M1 calls make up 37.4% of the gray whale repertoire when migrating. M1 pulses are broadband calls containing an average of five pulses per call with the lowest frequency below 100 Hz and the highest frequency over 10 kHz (Fish et al., 1974; Crane and Lashkari, 1996). Cummings et al. (1968) reported that gray whale M1 calls have a source level of 141 dB re : 1μPa at 1 meter. M1 calls have been associated with disruptive circumstances in a captive gray whale (Wisdom, 2000) and with social and sexual behavior in gray whales off Vancouver (Youngson and Darling, 2016).

1.5 Datasets

Previously published work on migrating gray whale swimming and acoustic behavior has been based upon small sample sizes of whales and observation days. In contrast, in this dissertation I use acoustic recordings, infrared cameras, and visual counts to monitor the complete gray whale migration at various locations along the migration route and across several years (Figure 1.3). By recording and localizing gray whale calls, we can reconstruct their underwater behavior based on much larger samples than was previously practical and investigate whether this behavior changes over the migration cycle. Multi-year single hydrophone recordings paired with visual sightings enable us to test whether the gray whale migration changes across years.

1.5.1 NOAA Visual Sightings

The abundance of the eastern North Pacific gray whale population has been estimated by the National Oceanic and Atmospheric Administration (NOAA) National Marine Fisheries

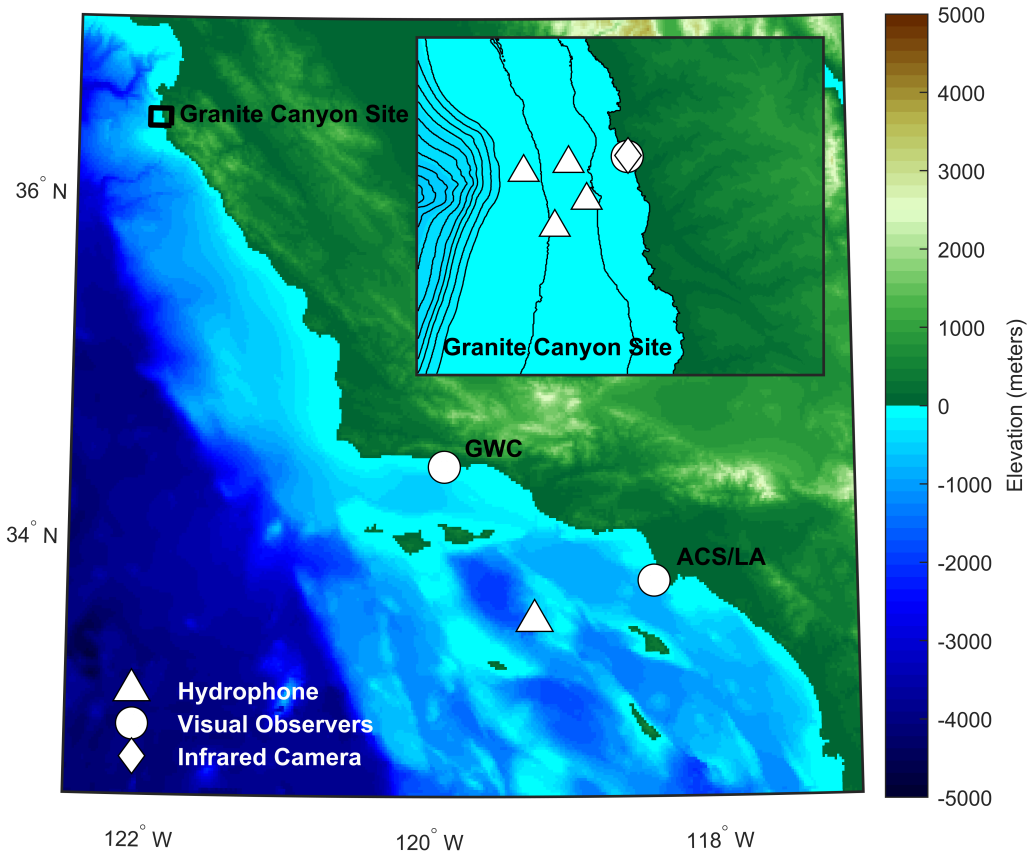

Figure 1.3: Gray Whale Acoustic, Infrared, and Visual Monitoring Locations. At the Granite Canyon site, we were able to monitor the same gray whales using acoustic, infrared cameras, and visual sightings during the 2014–2015 migration season. Four acoustic recording packages were arranged in an array 2–3 km from shore (white triangles, inset map) while the infrared camera (white diamond, inset map) and visual sightings (white circle, inset map) were shore-based. Black contour lines show seafloor depth in 50 m increments. In the Southern California Bight, two shore-based visual censuses (Gray Whales Count and The American Cetacean Society - Los Angeles, white circles) counted gray whales that migrated along the coastal migration corridor, while the High-Frequency Acoustic Recording Package (HARP, white triangle) recorded sound from the 2008–2009 to the 2014–2015 migration seasons. Colors indicate land elevation and seafloor depth with respect to sea level. Relief data from the NOAA National Centers for Environmental Information's Southern California Coastal Relief Model with 1 arc-second resolution (inset map) and ETOPO1 bedrock model with 1 arc-minute resolution (main map).

Service (NMFS) with shore-based surveys during the southbound migration from December through February since the 1967–1968 migration season (Laake et al., 2009). The visual observers for these surveys count groups of gray whales and estimate the number of individuals in each from a vantage point 22.3 m above sea level at Granite Canyon, south of Monterey, California (Rugh et al., 2008; Laake et al., 2009, Figure 1.3). Granite Canyon is an ideal location to enumerate southbound gray whales because of a narrow continental shelf causing gray whales to funnel through this region. The visual census assumes that each whale produces visible cues within the search area, there are no false positives, whales travel in set groups that do not change while passing the visual observers, and whales are traveling south exhibiting their characteristic migratory behavior (Rugh et al., 2008). The data are later corrected to account for probability of detection which is primarily influenced by visibility and number of whales passing per unit time (Durban et al., 2015). Abundance estimates also include corrections for whales that passed when no observers were on watch, which includes the nighttime increase in migration rate observed by Perryman et al. (1999) (Durban et al., 2015). Most discrepancies between independent visual observers are attributable to different estimates of number of whales in each group (Rugh et al., 1990, 1993). In an aerial survey at Granite Canyon, only 1.28% of whales migrating southbound were farther than 3 nautical miles (5.5 km) from shore (Shelden and Laake, 2002). This observation validates the assumption that most whales pass Granite Canyon within visible range of observers and that ignoring whales too far to be sighted does not make a significant difference in abundance calculations (Shelden and Laake, 2002). A hierarchical Bayesian "N-mixture" model corrects counts from a pair of observers to estimate the abundance for that year (Durban et al., 2015). During the 2014–2015 migration season, concurrent with the Scripps Whale Acoustic Lab acoustic monitoring discussed in Section 1.5.3, NOAA observers counted southbound gray whales from 30 December 2014 until 13 February 2015 and estimated the population size to be 28,790 (Durban et al., 2017). In Chapters 2 and 3, I use this abundance estimate to calculate cue rates of gray whales.

1.5.2 NOAA Infrared Camera Videos

NOAA added three infrared cameras to monitor for gray whales at the same location as the visual survey during the 2014–2015 migration (Figure 1.3). These infrared cameras recorded video from December 2014 until June 2015 and pointed different directions offshore. Because marine mammals are warm-blooded and their blow or exhalation is slightly warmer than the surrounding water (Cuyler et al., 1992), whale blows produce infrared signals that appear bright against the dark water. Infrared camera images are a method of monitoring whales visually at night and day and have great potential since whales must surface to breathe. However, these cameras, like visual observations, are limited by sea state, visibility, and, unlike visual observations, humidity since infrared wavelengths are absorbed by water molecules (Baldacci et al., 2005). In chapter 3, I combine manually detected gray whale blows from the middle infrared camera on 5–8 January 2015 with visual sightings. I chose four days with good visibility conditions to test the feasibility of gray whale monitoring with infrared cameras and measure the limitations of the camera under ideal circumstances.

1.5.3 Passive Acoustic Monitoring

To record the underwater vocalizations of gray whales, we use seafloor-mounted hydrophone-recorder packages that are deployed for months at a time. The Scripps Whale Acoustics Laboratory developed the High-Frequency Acoustic Recording Package (HARP) (Wiggins and Hildebrand, 2007). HARPs have been deployed hundreds of times in disparate ocean environments such as the west coast of North America, the Arctic and Antarctic, the Gulfs of Mexico and California, and the waters around Hawaii and other Pacific Islands. Most use a sample rate of 200 kHz to record low-frequency baleen whales as well as high-frequency toothed whales. After recovery, the raw acoustic files are processed and analyzed using MATLAB-(Mathwords, Natick, MA) based custom software (Wiggins and Hildebrand,

2007).

It is important to understand the amplitude transfer function inherent in this data collection process. When a whale produces a sound, the sound is attenuated as it travels though the ocean. This attenuation is estimated using acoustic propagation models. The hydrophone measures the pressure change caused by the received sound. The hydrophone converts pressure into voltage, the preamplifier provides gain to the signal, the low-pass filter corners at the sampling frequency divided by two to avoid aliasing, and the analog-to-digital converter converts volts into counts. The system transfer function is described as sensitivity in units of dB re : counts/μPa and is a function of frequency. The system is designed to have a relatively flat response as a function of frequency across the frequency band of interest. We use the transfer function to convert back to units of pressure so results can be compared across passive acoustic monitoring systems.

Granite Canyon Hydrophone Array

In Chapters 2 and 3 of this dissertation, I use acoustic data from four acoustic recording packages located offshore of the NOAA visual and infrared gray whale surveys at Granite Canyon in Monterey Bay National Marine Sanctuary (Figure 1.3). This is a unique dataset due to concurrent shore-based visual and infrared data collected by NOAA to estimate eastern North Pacific gray whale population size. Each acoustic recording package consists of a hydrophone, a datalogger, subsurface floats, an acoustic release, and weights for anchor (Figure 1.4). These were bottom-moored systems based off the HARP that recorded at low-frequencies from November 2014 until June 2015. The depths and locations of each acoustic recording package are listed in Table 1.1 and each hydrophone is denoted by its relative geographic position as NE, NW, SE, or SW. The locations were chosen to surround the main gray whale migration corridor 2 to 3 km from shore.

To detect gray whale vocalizations, I used the Generalized Power Law (GPL) Detector described by Helble et al. (2012) with parameters specific to gray whale M3 calls. I then localized

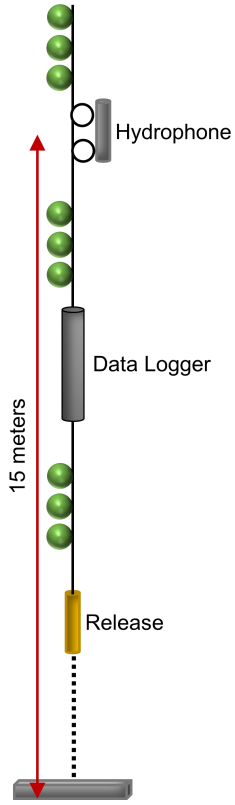

Figure 1.4: Acoustic Recording Package Mooring Diagram. This diagram shows the design of the bottom-moored acoustic recording package. The hydrophones are located 15 m above the seafloor. The green circles indicate the locations of the floats. The data logger contains the batteries, computer, and hard drives. The release is an acoustic release system that is used to retrieve the package along with the data at the end of the deployment. This diagram is not to scale.

whales using localization software developed for use on humpback whales in Hawaii (Helble et al., 2015) and grouped successive localizations into tracks based on estimated swimming behavior of gray whales.

Southern California Bight HARPs

To study migrating gray whales on their offshore route through the Southern California Bight, I apply what I learn about gray whale behavior from the hydrophone array to single HARPs in Chapter 4. Most past recordings are from single hydrophone systems, so to analyze time-series

Table 1.1: Deployment Locations of Acoustic Recording Packages. Hydrophones are named according to their relative positions. Depth is water depth in m. Range is horizontal distance to the NE hydrophone in m. The hydrophone in each recording package was moored 15 m off the bottom in all 4 cases.

Hydrophone	Latitude	Longitude	Depth	Range to NE
NE	36.43778°N	121.94417°W	67	—
NW	36.43512°N	121.96082°W	110	1,530
SE	36.42679°N	121.93743°W	58	1,380
SW	36.41872°N	121.94925°W	94	2,170

of data and monitor change over time, we often have to use single hydrophones. I use recordings from HARPs located in the middle of the Channel Islands, west of Los Angeles, northwest of San Clemente and Santa Catalina Islands, and south of Santa Cruz Island (Figure 1.3). HARPs recorded at this site between 2009 and 2015. The recording dates and locations are listed in Table 1.2.

Table 1.2: Deployment Locations of High-Frequency Acoustic Recording Packages at a Site in the Southern California Bight. Although each deployment was intended to be in the same location, there was some variability. Seafloor depths are in meters.

Migration Season	Dates	Latitude	Longitude	Depth
2008–2009	Jan 2009–Mar 2009	33°30.582′ N	119°15.282′ W	895
2008–2009	Mar 2009–May 2009	33°30.579′ N	119°15.280′ W	1,123
2009–2010	Dec 2009–Jan 2010	33°30.937′ N	119°14.798′ W	912
2009–2010	Jan 2010–Mar 2010	33°30.915′ N	119°14.690′ W	891
2010–2011	Dec 2010–Apr 2011	33°30.897′ N	119°14.888′ W	919
2011–2012	Nov 2011–Mar 2012	33°30.886′ N	119°14.869′ W	927
2012–2013	Dec 2012–Apr 2013	33°30.599′ N	119°15.305′ W	907
2013–2014	Sep 2013–Jan 2014	33°30.584′ N	119°15.252′ W	917
2013–2014	Jan 2014–Apr 2014	33°30.577′ N	119°15.251′ W	877
2014–2015	Nov 2014–Feb 2015	33°30.837′ N	119°14.943′ W	900

1.5.4 Southern California Visual Sightings

Two nonprofit organizations run annual, shore-based gray whale censuses in southern California (Figure 1.3). The American Cetacean Society - Los Angeles Chapter census, led by Alisa Schulman-Janiger, has counted both southbound and northbound gray whales annually since the 1983–1984 migration season from the Palos Verdes Penninsula. The Gray Whales Count census, led by Michael H. Smith, has counted northbound gray whales annually since 2004 from the Coal Oil Point Reserve in Santa Barbara. These volunteers attend mandatory training and many of them have counted whales for multiple migration seasons. An experienced observer is always on duty and ensures that specific protocols are followed. Whales are sighted using binoculars, weather data is recorded regularly, and other opportunistic sightings are noted. Daily counts from these two census efforts are combined with the Southern California Bight HARP recordings to quantify change over time in Chapter 4.

1.6 Dissertation Objectives

The goal of this dissertation is to investigate migrating gray whale behavior. Specifically I ask how behavior changes between night and day, over weeks and months, between the southbound and northbound migration, and over several years. I also explore how cue counting using passive acoustic recordings and infrared camera video can help quantify the abundance of whales with less effort and increased precision than visual surveys. Finally, I investigate whether changes in the gray whale migration between years can be explained by changes in the environment.

In Chapter 2, I use acoustic data from the Granite Canyon hydrophone array to test how gray whale swimming and acoustic behavior changes on daily and seasonal time scales. Using tracks derived from passive acoustic monitoring, I present speed, direction, and water depth of 280 gray whale tracks. I also calculate total number of calls and the percentage of calls part of a track to understand how vocalization behavior changes. In addition, I use the estimated

population size to calculate average calling rate over the entire migration season. Finally, I estimate the source level of M3 calls and call characteristics of both M3 and M1 calls. I analyze the variance in these call characteristics to determine how much of the variance is due to the propagation characteristics and how much is due to the individual animals. This chapter is the first published full-season acoustic monitoring and tracking of migrating gray whales and includes the largest sample size of gray whale calls detected over a single migration season that has been published to date.

In Chapter 3, I use gray whale sightings and abundance estimates from the NOAA southbound visual survey in conjunction with acoustic array call localizations and infrared camera blow detections to calculate gray whale cue rate on a finer time resolution and test how gray whale behavior changes over time. Cues are signs of an animal's presence that can be counted to estimate the total number of animals if the rate at which an animal produces cues is known. Often cues are counted instead of animals when visual sightings of animals are difficult. For whales, cues are often calls or blows. I show how call rate can be used to estimate the number of gray whales that migrated past when visual observers were not present and I calculate that the population size is greater than the population size reported using visual sightings only. I also estimate blow rate over four days and discuss the potentials and limitations of using infrared cameras to monitor for baleen whales. These results suggest that multi-method surveys have great potential for increasing the precision of gray and other whale abundance estimates.

In Chapter 4, I use gray whale acoustic call detections and visual sightings over seven migration seasons to quantify the multi-year variability in the gray whale migration. I estimate the growth rate of number of sightings at two census locations in the Southern California Bight and compare these rates with the population size change over the same time. I find that the proportion of the population using a nearshore route, especially a route past Los Angeles, increased during this time. I also use the calling rate calculated at Granite Canyon to estimate the number of whales that migrated through the acoustic search area each year. Finally, I test if the gray whale

migration quantified by presence of calls or number of sightings in the Southern California Bight can be explained using sea ice data from the gray whale feeding areas or local ocean temperatures.

In Chapter 5, I conclude by synthesizing the results of my three previous chapters. I summarize the novel accomplishments of this dissertation and I suggest future directions for understanding the gray whale migration.

1.7 Significance

Under the Marine Mammal Protection Act (and for certain species, the Endangered Species Act), population assessments of marine mammals must be completed every 1–3 years. Passive acoustic and infrared camera monitoring are tools that have the potential to be used to quantify marine mammals. Visual observation has been the primary method to quantify populations, including the eastern North Pacific gray whale population. This method is very time consuming and is subject to highly variable human error. Instead, passive acoustic and infrared camera video monitoring can record continuously and automatic detection systems with objectively quantified performance can be paired with these methods. One of the variables with the most uncertainty in passive acoustic density and abundance estimation is the calling rate (Marques et al., 2009). In this dissertation, I estimate daily acoustic cue rates for a large sample size of migrating gray whales over a month and a half and seasonal cue rates over the entire migration without disturbing whale behavior. I also estimate blow rates over four days of the southbound migration.

Human noise production poses an increased risk to gray whales compared to species of whales in the open ocean due to the gray whale nearshore migration. Gray whales have been observed to change their behavior to avoid anthropogenic sounds (e.g. Malme et al., 1984; Weller et al., 2002). Understanding the baseline behavior of gray whales in a relatively quiet marine sanctuary is the first step for determining how these whales may be impacted by nearshore

anthropogenic activities.

The impacts of climate change on marine mammals are largely unknown. Passive acoustic monitoring makes it possible to monitor whales continuously over many years and in locations that are difficult to observe visually. Visual shore-based observations have provided regular monitoring over longer periods at locations that are conducive to whale sightings. In this dissertation, I analyze seven gray whale migration seasons with both acoustic and visual data and assess the relationship between the gray whale migration and sea ice and temperature using statistical modeling. Quantifying if and how gray whales respond to short timescale environmental variability can help us better predict how they may be affected by long timescale change. These methods can be applied to other species and the results will allow us to take steps to protect the most sensitive populations and their habitats.

Chapter 2

Migratory Behavior of Eastern North Pacific Gray Whales Tracked Using a Hydrophone Array

2.1 Abstract

Eastern North Pacific gray whales make one of the longest annual migrations of any mammal, traveling from their summer feeding areas in the Bering and Chukchi Seas to their wintering areas in the lagoons of Baja California, Mexico. Although a significant body of knowledge on gray whale biology and behavior exists, little is known about their vocal behavior while migrating. In this study, we used a sparse hydrophone array deployed offshore of central California to investigate how gray whales behave and use sound while migrating. We detected, localized, and tracked whales for one full migration season, a first for gray whales. We verified and localized 10,644 gray whale M3 calls and grouped them into 280 tracks. Results confirm that gray whales are acoustically active while migrating and their swimming and acoustic behavior changes on daily and seasonal time scales. The seasonal timing of the calls verifies the gray whale

migration timing determined using other methods such as counts conducted by visual observers. The total number of calls and the percentage of calls that were part of a track changed significantly over both seasonal and daily time scales. An average calling rate of 5.7 calls/whale/day was observed, which is significantly greater than previously reported migration calling rates. We measured a mean speed of 1.6 m/s and quantified heading, direction, and water depth where tracks were located. Mean speed and water depth remained constant between night and day, but these quantities had greater variation at night. Gray whales produce M3 calls with a root mean square source level of 156.9 dB re : 1μPa at 1 m. Quantities describing call characteristics were variable and dependent on site-specific propagation characteristics.

2.2 Introduction

Eastern North Pacific gray whales (*Eschrichtius robustus* Lilljeborg) undertake one of the longest migrations of any mammal, covering 50 degrees or more of latitude and traveling some 15,000 to 20,000 kilometers roundtrip between Baja California, Mexico and the Bering and Chukchi Seas (Sumich, 1983). By late November, most gray whales in the eastern North Pacific population are moving south from their summer feeding areas in the Bering, Beaufort and Chukchi Seas to wintering areas off Baja California, Mexico (Rugh, 1984). The gray whale migration is segregated by age, sex, and reproductive condition (Rice and Wolman, 1971). The first pulse of migrants is led by (a) near-term pregnant females, followed by (b) estrous females and mature males, and then (c) immature animals of both sexes (Rice and Wolman, 1971). The northward migration is segmented into two phases. The first phase includes (a) newly pregnant females, followed later by (b) adult males and anestrous females, and then (c) immature whales of both sexes (Poole, 1984). The second phase consists mostly of mothers with calves that are observed on the migration route between March and May (Poole, 1984; Perryman et al., 2002, 2010) and generally arrive to the summer feeding areas between May and June (Rice and Wolman,

1971; Sumich, 2014). Animals migrating southward tend to travel within five kilometers from shore (Gilmore, 1960; Shelden and Laake, 2002) while the northward migration is slightly more offshore and direct for most whales, except for cows with calves who keep within 200–400 m from shore in some areas (Poole, 1984; Perryman et al., 2002). This migration pattern, hugging the North American coast, makes the eastern North Pacific gray whale migration the most observed whale migration, and also makes these whales more likely to be impacted by nearshore human activities.

The eastern North Pacific population of gray whales is often cited as a conservation success story. When commercial whaling first began, the eastern North Pacific gray whale population size was around 30,000 (Scammon, 1874). Between 1846 and 1874, whalers killed approximately 10,800 gray whales, causing the population to shift its migration corridor farther offshore and nearly desert the Mexican breeding lagoons (Scammon, 1874). In the 20th century, whaling on gray whales decreased with 2,724 whales taken from the eastern population between 1910 and 1946 (Sumich, 2014). In the 1950s and 1960s, aerial and land-based censuses estimated the population size to be 2,894–4,454 individuals (Gilmore, 1960; Hubbs and Hubbs, 1967). Today, eastern North Pacific gray whales are presumed to be at their carrying capacity (Moore et al., 2001) and are listed as a species of least concern (Reilly et al., 2008). The population size was estimated to be 28,790 individuals for the 2014–2015 season (Durban et al., 2017). The dramatic recovery in population size over fifty years and the reoccupation of the lagoons in the winter and the coastal corridor during the migration gives hope that endangered marine mammals can survive with proper management and time.

The abundance of gray whales has been estimated by the National Oceanic and Atmospheric Administration (NOAA) Southwest Fisheries Science Center (SWFSC) with shore-based visual surveys during the southbound migration from December through February since the 1967–1968 migration season (Laake et al., 2009). The visual observers for these surveys count pods and estimate the number of whales in each from a vantage point at or near

Granite Canyon, south of Monterey, California, approximately 20 m above sea level (Rugh et al., 2008; Laake et al., 2009). Observations are limited to daylight periods, suitable environmental conditions, and, in part, the ability to track and record multiple whales simultaneously migrating past the observation station. NOAA SWFSC added an infrared camera system in 2014–2015 that can detect whales based on the heat difference between their warm blows and the backdrop of the cool ocean during both the day and night.

Many studies have quantitatively described the gray whale migration by visually observing whales or satellite tagging a small sample. These studies show that most pregnant females travel south alone, but small, unstable groups of two or three are most common for the rest of the southbound migration (Gilmore, 1960; Rice and Wolman, 1971). Migrating gray whales move steadily in one direction, breathing and diving in predictable patterns and generally swim at speeds between 1.1 and 2.8 m/s (Cummings et al., 1968; Rice and Wolman, 1971; Sumich, 1983; Rugh et al., 1990; Perryman et al., 1999; Mate and Urbán-Ramírez, 2003; Mate et al., 2010). In order to minimize their cost of transport, gray whales should spend most of their time at depths below 2.5 times their maximum body width, or 6–7 m deep for an adult gray whale (Sumich, 2014). Most do not engage in other activities besides traveling although some later southbound gray whales display courting and mating behavior (Gilmore, 1960). Acoustic monitoring using hydrophone arrays, as reported herein, offers an additional method to investigate migratory timing and behavior and provides data day and night and in all types of weather conditions.

Controversy exists regarding gray whale behavior at night because it is difficult to observe. Hubbs and Hubbs (1967) reported that gray whales continue migrating in bright moonlight, but stop on dark nights. Perryman et al. (1999) used infrared cameras for portions of three southbound migration seasons and observed that gray whales shifted 0.4 km closer to shore at night. In addition, after 15 January, gray whales increased their southbound migration rate at night and increased their pod size during the day (Perryman et al., 1999). Perryman et al. (1999) hypothesized that gray whales were socializing more during the day and slowing their

migration rate. A diel change in migratory behavior has not been observed during the northbound migration (Mate and Urbán-Ramírez, 2003; Perryman et al., 2002). These results warrant further investigation and since gray whales are known to make underwater sounds, acoustic monitoring provides another way to increase understanding of whale behavior during both night and day.

The acoustic behavior and role that vocalizing may serve during the gray whale migration is poorly understood. Dalheim (1987) named and described six gray whale call types from sounds recorded in the Baja California lagoons. She recorded 0.33 calls/hour/whale in February and 0.25 calls/hour/whale in March and found no diel variation in call production (Dalheim, 1987). Gray whales are reported to produce fewer calls while migrating than while in their breeding areas. Crane and Lashkari (1996) measured 0.050 calls/hour/whale in water less than 100 meters deep and Cummings et al. (1968) recorded 0.74 calls/hour with a maximum of 53 calls/hour/whale and noted that approximately one-third of solitary gray whales made detectable sounds during migration.

The M3 call is the most common call while migrating and makes up 47 to 87% of the total calls (Cummings et al., 1968; Crane and Lashkari, 1996). The M3 call is an amplitude- and frequency-modulated call often containing harmonics (Crane and Lashkari, 1996). It has been previously reported to have a peak frequency (which corresponds to Crane and Lashkari's "center frequency") below 100 Hz (Crane and Lashkari, 1996), a bandwidth from 20–200 Hz, and an average duration of 1.54 s (Cummings et al., 1968). The gray whale M3 calls have a reported source level of 151 dB re : 1μPa at 1 m off San Diego (Cummings et al., 1968), but source levels of 167 to 188 dB re : 1μPa at 1 m have been reported for all gray whale call types in the Chukchi Sea (Petrochenko et al., 1991). The metric of the received call used to estimate source level (e.g. root mean square, 0-to-peak, peak-to-peak) was not reported in these published studies.

Another call type produced by migrating gray whales is the M1 call and makes up about 37% of the total calls (Crane and Lashkari, 1996). This call is described to sound like knocking, metallic pulsing, or bongo drums (Cummings et al., 1968; Fish et al., 1974; Crane and

Lashkari, 1996). M1 pulses are broadband calls containing an average of five pulses per call with the lowest frequency below 100 Hz and the highest frequency over 10 kHz (Fish et al., 1974; Crane and Lashkari, 1996). The M1 calls have a reported source level of 141 dB re : 1μPa at 1 m (Cummings et al., 1968).

Earlier studies on the acoustic behavior of gray whales during migration have relied on relatively small sample sizes recorded over short time periods (Cummings et al., 1968; Crane and Lashkari, 1996). The aim in this study was to use passive acoustic recorders offshore of the Granite Canyon visual survey site to monitor the gray whale migration and localize gray whale calls over a full migration season. In this way, we developed an understanding of their underwater movement and vocalizations with a large sample size and investigated whether this behavior changed over the migration cycle. We show that gray whales are acoustically active when migrating and their behavior changes over seasonal and daily time scales.

2.3 Materials and Methods

We deployed four acoustic recording packages offshore of the NOAA SWFSC survey site at Granite Canyon (Figure 2.1) under the Monterey Bay National Marine Sanctuary Research permit MBNMS-2014-039. Each acoustic recording package mooring consisted of a hydrophone, a datalogger, subsurface floats, an acoustic release, and weights for anchor (Supporting Information). They are based on Scripps Institution of Oceanography's High-frequency Recording Package (HARP) (Wiggins and Hildebrand, 2007). These recording systems were bottom-moored systems that sampled at 2,000 Hz for an effective bandwidth from 10 to 1,000 Hz and recorded continuously from November 2014 until June 2015. The depths and locations of each acoustic recording package are listed in Table 2.1 and each hydrophone is denoted by its relative position as NE, NW, SE, or SW. The locations were chosen to surround the visually-determined main gray whale migration corridor 2 to 3 km from shore and to record the same whales detected during

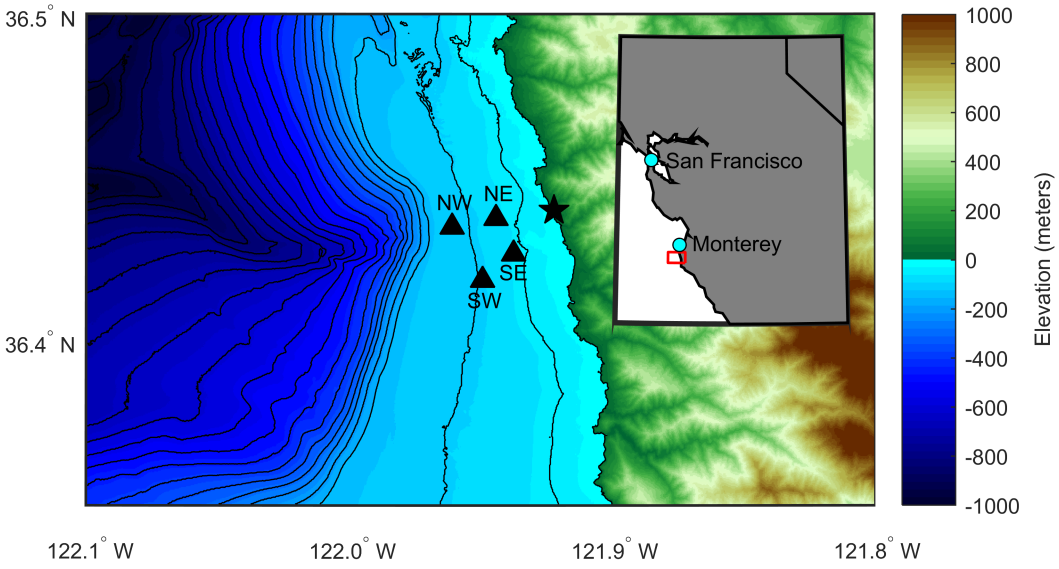

Figure 2.1: Deployment Locations of Acoustic Recording Packages. The study area is off central California as denoted by the red box in the inset map. Acoustic recording packages are indicated with black triangles and labeled according to their relative positions. The location of the NOAA Southwest Fisheries Science Center surveys are indicated with a black star. Colors indicate land elevation and seafloor depth with respect to sea level. Black contour lines show seafloor depth in 50 m increments. Bathymetry data from the NOAA National Centers for Environmental Information's Southern California Coastal Relief Model with 1 arc-second resolution.

the NOAA surveys.

Table 2.1: Deployment Locations of Acoustic Recording Packages. Hydrophones are named according to their relative positions. Depth is water depth in m. Range is horizontal distance to the NE hydrophone in m. The hydrophone in each recording package was moored 15 m off the bottom in all 4 cases.

Hydrophone	Latitude	Longitude	Depth	Range to NE
NE	36.43778°N	121.94417°W	67	—
NW	36.43512°N	121.96082°W	110	1,530
SE	36.42679°N	121.93743°W	58	1,380
SW	36.41872°N	121.94925°W	94	2,170

After recovery, all audio files were time-aligned by assuming linear clock drift across the deployment period. The clock drifts over the 7-month period were 0.1527, 2.0287, 0.5790, and

14.3578 s for the NE, NW, SE, and SW hydrophones, respectively. The least squared differences of measured time delays from theoretical time delays for localized calls were plotted and the values had a mean close to zero over the entire deployment indicating that linear clock drift was a valid approximation.

To detect gray whale vocalizations, we used the Generalized Power Law (GPL) Detector described by Helble et al. (2012) and modified the parameter file for gray whale detections using a frequency band of 20–100 Hz, call length of 1.2–5 s, and fast Fourier transform (FFT) length of 1024 samples with 95% overlap. The GPL detector was run on the data output from all four hydrophones separately. All gray whale M3 call detections from the NE hydrophone recordings were verified manually.

To localize a gray whale call, a detection must be made on all four hydrophones (only three hydrophones are needed to localize, but we require four to increase precision). Helble et al. (2015) described these localization methods in full detail with humpback whale vocalizations on the U.S. Navy's Pacific Missile Range Facility. Since gray whales call less frequently than humpback whales, single calls were cross-correlated instead of a series of calls. Call spectrograms were normalized in each frequency bin based on the average noise level and the background noise was then set to zero to create a template (as in Section IIA of Helble et al. (2015) and Equations 10,11 in Helble et al. (2012)). Background noise was defined as less than 0.5 times the average noise across all frequency bins and time (as opposed to 5 times the noise in Helble et al. (2015)). Each template was cross-correlated with the template of the same call received on the NE hydrophone to calculate the time delay or time difference of arrival (TDOA) (similar to Section IIB in Helble et al. (2015), except with cross-correlating single calls). Three TDOA measurements were obtained for each localized detection. The peak of each cross-correlation was made more precise using polynomial interpolation between the maximum cross-correlation values.

To obtain theoretical TDOA values, whales were assumed to be calling at 10 m depth,

but since the water depth is an order of magnitude shallower than the spacing of the recording array, the assumed calling depth of the whale is insignificant. We verified whether changing the assumed depth of the whale would change the locations and we did not observe significant changes over the tested depths. On average, changing the assumed calling depth by 40 m (to 50 m deep) changes the estimated horizontal location of the animal by only 15 m, which is a small difference compared to range over which we are localizing.

No data on the sound speed profile in Granite Canyon were collected during the recording period and online oceanographic data bases contain few measurements near the recording site for the time period of data recording. Therefore, a constant sound speed of 1500 m/s was used in this analysis. For calls with primarily low frequency content recorded in this shallow water environment, the results should be insensitive to the sound speed profile details. An alternate sound speed profile of 1,490 m/s was tested, but no significant difference in call localizations were observed. Since the southbound migration peaks in January and the northbound migration peaks in March, we assume the sound speed profile will be about the same across the gray whale migration period. Any differences between the actual sound speed profile and these values will cause a bias in the localizations of calls.

A grid search method with 0.001° resolution over a search area of 36.40°–36.45°N and 121.92°–121.98°W determined the location of a calling whale based on the least-squared difference between the theoretical and measured TDOAs summed over the three TDOA measurements (according to Equation 1 in Helble et al. (2015)). The whale location was refined by cubic interpolation of the sum of the least-squared difference around the location of the minimum.

Localized calls were then grouped into tracks. We developed a graphical user interface that allowed the user to slowly advance in time through the localized detections plotted on a map of the search area and select times with one or more tracks. To be considered valid, a track must consist of at least five calls. Each track was then automatically segmented based on maximum allowable time intervals, distance, and speed between sequential localizations. Since gray whales

often travel in groups, this method allowed us to more easily remove calls that did not fit with the rest of the track and therefore may have been produced by another whale. Occasionally some calls in a track may be produced by another animal in a tight-knit group, but we are assuming that the majority of calls are produced by the focal animal and all track metrics are valid for that animal.

After tracks were defined, we plotted spectrograms of all calls in each track and verified call types and species. In addition to gray whales, tracks of humpback, fin, and blue whales were recorded by the hydrophone array.

Swimming behavior of calling gray whales was quantified by calculating speed and direction of tracks and noting seafloor depth at the track location. A smoothing spline was fit between the localizations in each track. Using a smooth curve as a track better models actual swimming behavior instead of connecting each localization with a straight line. Average speed, heading, and direction index for each track was then calculated. Southbound whales are defined as any track with a heading between +135° and +225° and northbound whales are defined as any track with a heading between -45° and +45°. Direction index is a metric developed to measure how straight or curved a track is and is calculated by dividing the net distance traveled by the total distance traveled. A direction index of one indicates a straight track while an index of zero indicates no net movement in location. The seafloor depth along each track was also recorded. Bathymetry data were retrieved from the NOAA National Centers for Environmental Information using the Southern California Coastal Relief Model with 1 arc-second resolution (https://maps.ngdc.noaa.gov/viewers/wcs-client/). These metrics were compared over seasonal and daily time scales.

Not all calls that were localized contributed to a track. A whale had to call at least five times as it swam through the search area and those calls must have been detected on all four hydrophones to be categorized as a track. M1 calls were not manually verified for localization since few are detected on all four hydrophones. Since the majority of gray whale calls detected

were M3, using the percentage of M3 calls that were part of a track is a valid metric to analyze how calling behavior changes over different time scales. Although M1 calls were not enumerated for total call counts, some tracks with M3 calls also had M1 calls.

Since whales swimming past the study location have a well-defined spatial distribution and abundance from visual observations, we are able to calculate an average population calling rate over the entire deployment. When a whale vocalized an M3 call within the area of the hydrophone array, it had a very high probability of detection and localization. Only calls within the area bounded by the array were used in this calling rate analysis. From aerial surveys at Granite Canyon, it is known that approximately 95% of gray whales migrate south within 4.17 km of shore (Shelden and Laake, 2002). The eastern-most hydrophone in this study was approximately 1.7 km from shore and the western-most hydrophone was approximately 3.4 km from shore. Since we are not counting the small fraction of whales that travel inshore and offshore of the hydrophone array, we assumed that 90% travel through the array. We used the 2014–2015 abundance estimate of 28,790 whales (Durban et al., 2017). Travel time was estimated as the total distance traveled to pass through the array divided by the speed of the whale. Calling rate was calculated by dividing the total calls by the product of the total whales and the travel time. Population calling rate has units of calls/whale/day.

To expand on the description of received call types presented in past gray whale acoustic studies, we measured several aspects of the received calls. For all M3 calls produced within the area of the hydrophone array, we measured the received call duration, peak frequency, 3 dB bandwidth, mean frequency, and $\pm\sigma$ bandwidth. A full description of peak frequency (referred to in Crane and Lashkari as center frequency) and 3 dB bandwidth is given in Crane and Lashkari (1996). Peak frequency is the frequency with the greatest amplitude in the call spectrum and the 3 dB bandwidth is a measure of the bandwidth of that peak frequency (bandwidth of a single harmonic). The 3 dB bandwidth metric was estimated using linear extrapolation from the peak frequency. Mean frequency is a weighted mean where the weighting is determined by the fraction

of total energy at each frequency over the bandwidth of the call. That is, if $A^2(f_i)$ is the magnitude squared in the i-th frequency bin centered at frequency f_i, then

$$\mu(f) = \sum_{i=f_1}^{f_2} w_i f_i \tag{2.1}$$

where the weighting is

$$w_i = \frac{A^2(f_i)}{\sum_{i=f_1}^{f_2} A^2(f_i)} \tag{2.2}$$

and f_1 is 20 Hz and f_2 is 200 Hz for M3 calls and 1,000 Hz for M1 calls. The $\pm\sigma$ bandwidth can be defined as ±1 standard deviation about the mean frequency. The variance is

$$\sigma^2(f) = \sum_{i=f_1}^{f_2} w_i (f_i - \mu(f))^2 \tag{2.3}$$

and so the $\pm\sigma$ bandwidth is $2\sqrt{\sigma^2}$. The hydrophones had a roll-off in sensitivity and recorded high noise below 20 Hz so only frequencies greater than 20 Hz were used in spectral analysis. The upper frequency limit was chosen based on the call characteristics as visualized with spectrograms.

To separate the component of variance of a given call characteristic associated with variation in the environmental properties across the four elements of the array from the total variance, we calculated the variance of the call characteristics three different ways. First we define $a_{i,j}$ as some characteristic of the i^{th} call recorded by the j^{th} hydrophone. The component of the variance that is comprised primarily of the variance due to variations from one call to the next is calculated by taking the mean of the measurements across all four hydrophones and then

calculating the variance of that mean (referred to as SD^2)

$$SD^2 = \frac{1}{N}\sum_{i=1}^{N}(\bar{a}_i - < \bar{a} >)^2 \tag{2.4}$$

where $\bar{a}_i$ is the mean of the characteristics of a single call over all four hydrophones or

$$\bar{a}_i = \frac{1}{4}\sum_{j=1}^{4} a_{i,j} \tag{2.5}$$

and the mean over all calls and hydrophone recordings is

$$< \bar{a} >= \frac{1}{N}\sum_{i=1}^{N}\bar{a}_i = \frac{1}{4N}\sum_{i=1}^{N}\sum_{j=1}^{4} a_{i,j} \tag{2.6}$$

The component primarily associated with the environment is calculated by taking the variance of the measurements for each call across the four hydrophones and then taking the mean of these variances for all the calls (referred to as $SD^2_{per\ call}$)

$$SD^2_{per\ call} = \frac{1}{N}\sum_{i=1}^{N}\left(\frac{1}{4}\sum_{j=1}^{4}(a_{i,j} - \bar{a}_i)^2\right) \tag{2.7}$$

The sum of these variances, i.e., the squares of the corresponding standard deviations, equal the total population variance (SD^2_{all})

$$SD^2 + SD^2_{per\ call} = SD^2_{all} \tag{2.8}$$

where

$$SD^2_{all} = \frac{1}{4N}\sum_{i=1}^{N}\sum_{j=1}^{4}(a_{i,j} - < \bar{a} >)^2 \tag{2.9}$$

In summary, the individual quantities can be interpreted as:

1. SD^2 : The variance of the means of the calls, where the means are calculated across all four hydrophones. This variance is the variance in received characteristics over all calls.

2. $SD^2_{per\ call}$: The mean of the variance of a given call across all four hydrophones, where the mean is calculated over all recorded calls. This variance is the variance due to site-specific effects such as those caused by variations in propagation or variations in the properties of the individual data acquisition systems. For those call characteristics used in time-of-arrival difference estimation, it provides a quantitative measure of the effects of site-specific variations in localization.

3. SD^2_{all} : The total population variance. This variance is the variance over all call recordings by all hydrophones.

M1 calls were rarely detected on all four hydrophones. Since the sample size was only 23 for M1 calls detected within the array with good signal-to-noise ratios on all four hydrophones, analyst-detected M1 calls from a single hydrophone (NE) were used instead. We quantified inter-pulse interval (IPI), peak frequency, 3 dB bandwidth, mean frequency, and $\pm\sigma$ bandwidth for these M1 calls. The variance of IPI was compared both within a single call ($SD^2_{w/in\ call}$) and between all calls (SD^2).

Sound pressure spectral level calculations are used for estimating both received level and noise level. Spectral level integrated across a frequency bandwidth of interest is calculated by

$$RL = \frac{f_s}{nFFT} * \sum_{i=f_1}^{f_n} Sp(f_i) \tag{2.10}$$

where RL is the mean square received level, nFFT is the number of samples used in each FFT

window, and the spectral density $Sp(f_i)$ is

$$Sp(f_i) = 2 * \frac{1}{nT} \sum_{j=1}^{nT} \frac{\left|X_j(f_i)\right|^2}{f_s * nFFT * (\frac{1}{nFFT} * \sum_{i=1}^{nFFT} w_i^2)} \tag{2.11}$$

where the subscript j indicates the j-th time segment and nT is the number of time segments incoherently averaged to obtain the spectral density estimate. The factor of 2 leading the right-hand side of the equation above accounts for the energy at negative frequencies. For gray whale M3 calls, $Sp(f_i)$ is summed from f_1= 20 Hz to f_n =100 Hz. The quantity $X_j(f_i)$ is the fast Fourier transformed complex value in the frequency bin corressponding to f_i. The sum of w_i^2 is the sum of the square of all the points in the window applied to each of the j time series segments before Fourier transforming. We used a Hamming window for this analysis. Dividing by the ratio of the sampling frequency and the FFT length normalizes by the bin width in order to estimate spectral density. This step is necessary for estimating continuous spectra. Ocean noise typically has a continuous spectrum and since the M3 call has energy that spans several frequency bins, we treated it as a continuous spectrum and calculated spectral density. To convert into decibel units, we took $10 * \log_{10}(RL) \equiv RL_{dB}$. This method calculates the root mean square (RMS) received level, equivalent in the decibel domain to mean square amplitude.

Knowing the source level of a call is important for understanding how far away a call can be detected and how this detection range would change with changing background noise and acoustic propagation conditions. To estimate source level, we first measured received level of all calls localized within the area bounded by the hydrophones of the array. Since localization precision decreases with distance from the array, we only used calls within the array for this analysis. We subtracted the background noise from the spectrum to obtain the signal level without the noise and used the formulas above. At ranges from the source to the hydrophone greater than

the seafloor depth at the source location, source level was estimated from received level by

$$SL_{dB} = RL_{dB} + 20 * \log_{10}(r_T/1\text{m}) + 10 * \log_{10}(r/r_T) + \alpha * (r - r_T) \tag{2.12}$$

where SL_{dB} is source level in decibel units, RL_{dB} is received level in decibel units, r_T is the transition range at which geometrical spreading transitions from spherical to cylindrical, α is the empirically determined attenuation/absorption coefficient due to bottom interaction, and r is the horizontal distance from the whale to the hydrophone (Urick, 1967). At ranges less than the seafloor depth, source level was calculated using spherical spreading only over the slant range

$$SL_{dB} = RL_{dB} + 20 * \log_{10}(r/1\text{m}) \tag{2.13}$$

These equations are approximately derived by incoherently averaging TL over range and frequency. They assume homogenity and isotropy in the acoustic propagation conditions.

For the same call (i.e. the same SL) recorded at two different receivers at ranges r_1 and r_2 where $r_1 \geq r_T$ and $r_2 \geq r_T$ and assuming the source radiation pattern is omnidirectional

$$RL_2 - RL_1 = 10 * \log_{10}(r_1/r_2) + \alpha * (r_1 - r_2) \tag{2.14}$$

If $r_1 \geq r_T$ but $r_2 \leq r_T$

$$RL_2 - RL_1 = 10 * \log_{10}(r_T * r_1/r_2^2) + \alpha * (r_1 - r_T) \tag{2.15}$$

This equation can be solved for r_T using the empirically-derived value for α obtained from Equation (2.14).

Unfortunately, only three calls occurred where the range to one of the hydrophones was less than the water depth. Therefore, data from only nine pairs of hydrophones were available

to empirically estimate r_T, too small a sample size for a reliable estimate. Instead, we assumed spherical spreading from the location of the source to the seafloor. Since the assumed depth of the source is at 10 m and is therefore close to the surface, an estimated transition range (r_T)(defined in Urick (1967)) of the seafloor depth at the source location (D_{src}) was used. It is unknown at what depth or depths the whales are calling, although it is estimated that the whales spend most of their time around 6–7 m deep (Sumich, 2014). This assumption of a transition range of D_{src} affects the overall source level estimates somewhat. For example, using values of r_T of D_{src} and $D_{src}/2$ results in differences in transmission loss of $10 * \log_{10}(2) - \alpha * D_{src}/2$, or about 3 dB. Therefore, the use of D_{src} as the transition range may over-estimate the transmission loss and the resulting source level estimate by up to 3 dB.

For each call, there were 6 pairs of hydrophones from which to estimate the attenuation/absorption coefficient α. To protect against outliers, we took the median of the pairwise α calculations for each call. We then used the mean of α for all calls to estimate the RMS source level.

Source sound exposure level (SEL) was calculated from the RMS source level

$$SEL = SL_{RMS} + 10 * \log_{10}(t_{call}) \tag{2.16}$$

where t_{call} is the call duration in seconds. Finally peak-to-peak source level was calculated in the same way as RMS source level. Peak-to-peak level is the difference between the time series maximum and minimum no matter where in the call the maximum and minimum occur.

We estimated the sound pressure spectral level of the background noise to ensure that changes in numbers of calls were due to changes in animal behavior and not due to changes in probability of detection (Helble et al., 2013). Background noise was estimated on each hydrophone recording for each minute of recording and calculated using root median square over the same 20–100 Hz band. Root median square is the same as root mean square except calculated

by taking the median spectral level across time instead of the mean. Root median square was used so as to not overly emphasize time periods with isolated high-level short-duration pulses from the instrument's self-noise. We did not remove other marine mammal vocalizations from the background noise calculations because the presence of other calls can also influence the probability of detection.

We calculated probability of localization during each minute bin for a grid of locations within the area of the array. The passive sonar equation

$$SNR_{dB} = SL_{dB} - TL_{dB} - NL_{dB} \tag{2.17}$$

was used with SL randomly chosen from the distribution of real RMS source levels, the transmission loss (TL) from a source at each location in the grid to each hydrophone, and the noise level at each hydrophone in that minute. We repeated the random selection of SL values 100 times for each grid location. A minimum signal-to-noise ratio (SNR) of 0.5 dB was required for detection, determined by adding an M3 call to various levels of Gaussian noise. The probability of detection at a hydrophone was equal to the percent of time that a random source level call had a received SNR greater than or equal to 0.5 dB. We repeated these calculations for each hydrophone and then used the minimum probability of detection across the four hydrophones at each location. Much of the high noise was due to instrument cable strumming because of the shallow-water environment, so it was important to calculate the probability of detection on each of the hydrophones to determine which hydrophone was limiting the localization. To calculate the probability of localization at each time, we took the mean of the probability of localization across the area within the array. This method assumes even spatial distribution of whales across the area within the array. To correct for noise, the number of calls localized during each minute was divided by the probability of localization in that minute. However, if the probability of localization in a minute was less than 50%, we did not count any calls detected in that minute and

categorized that as a time with no effort. We then divided the corrected call count for each day by the proportion of minutes with a probability of localization at least 50% to get a normalized daily call count within the area of the array. All detections localized within the area of the array were manually verified on all four hydrophones.

2.4 Results

In total, we detected, verified, and localized 10,644 gray whale M3 calls from 1 December 2014 to 3 May 2015. The majority of calls were M3. Figure 2.2 shows example time series and corresponding spectrograms of high signal-to-noise ratio M3 and M1 call types recorded on the NE hydrophone. Audio files of the pictured calls are provided in the Supporting Information available online.

Gray whale calls were grouped into 280 tracks consisting of at least five calls with a total of 154 southbound gray whale tracks and 112 northbound gray whale tracks. The remaining 14 tracks did not have a clear northbound or southbound direction. Examples of four tracks are shown in Figure 2.3. Every detection that was part of a track was manually verified as being a gray whale call. The mean number of calls in the tracks (biased high because of the requirement that at least 5 calls define a track) was 8.4 and the maximum was 32. The mean of the mean inter-call interval in each track was 3.89 minutes with a standard deviation of 2.31 minutes. No trend was present in inter-call interval over time.

2.4.1 Vocalization Characteristics

The variance is separated by the amount attributable to variability from call to call (SD^2) and the amount attributable to change on a single call during propagation ($SD^2_{per\ call}$). These values are also shown as percentages of the total variance for each measurement. It was not possible to discern between these two types of variance for M1 calls because the sample size of

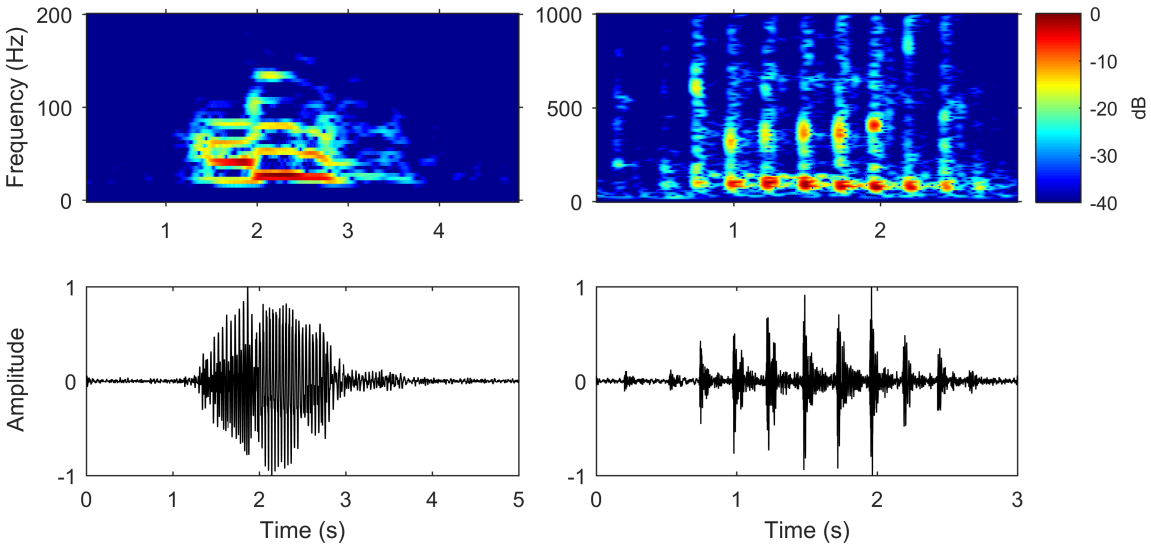

Figure 2.2: Gray Whale M3 and M1 Recorded Vocalizations. An example (A) M3 call and (B) M1 call recorded on the NE hydrophone. Spectrograms are on top with frequency on the y-axis, time on the x-axis, and color indicating pressure magnitude squared (or equivalently pressure magnitude) in dB. A 40 dB dynamic range was used and all magnitudes were normalized to the greatest dB magnitude of the spectrogram. Note the different axes limits for the two call types. Time series plots are on the bottom with normalized amplitude on the y-axis and time on the x-axis. The M3 spectrogram has an FFT length of 512 with 99% overlap and a Hamming window and is bandpass filtered from 20 to 200 Hz. The M1 spectrogram has an FFT length of 256 with 99% overlap and a Hamming window and is bandpass filtered from 20 to 1,000 Hz.

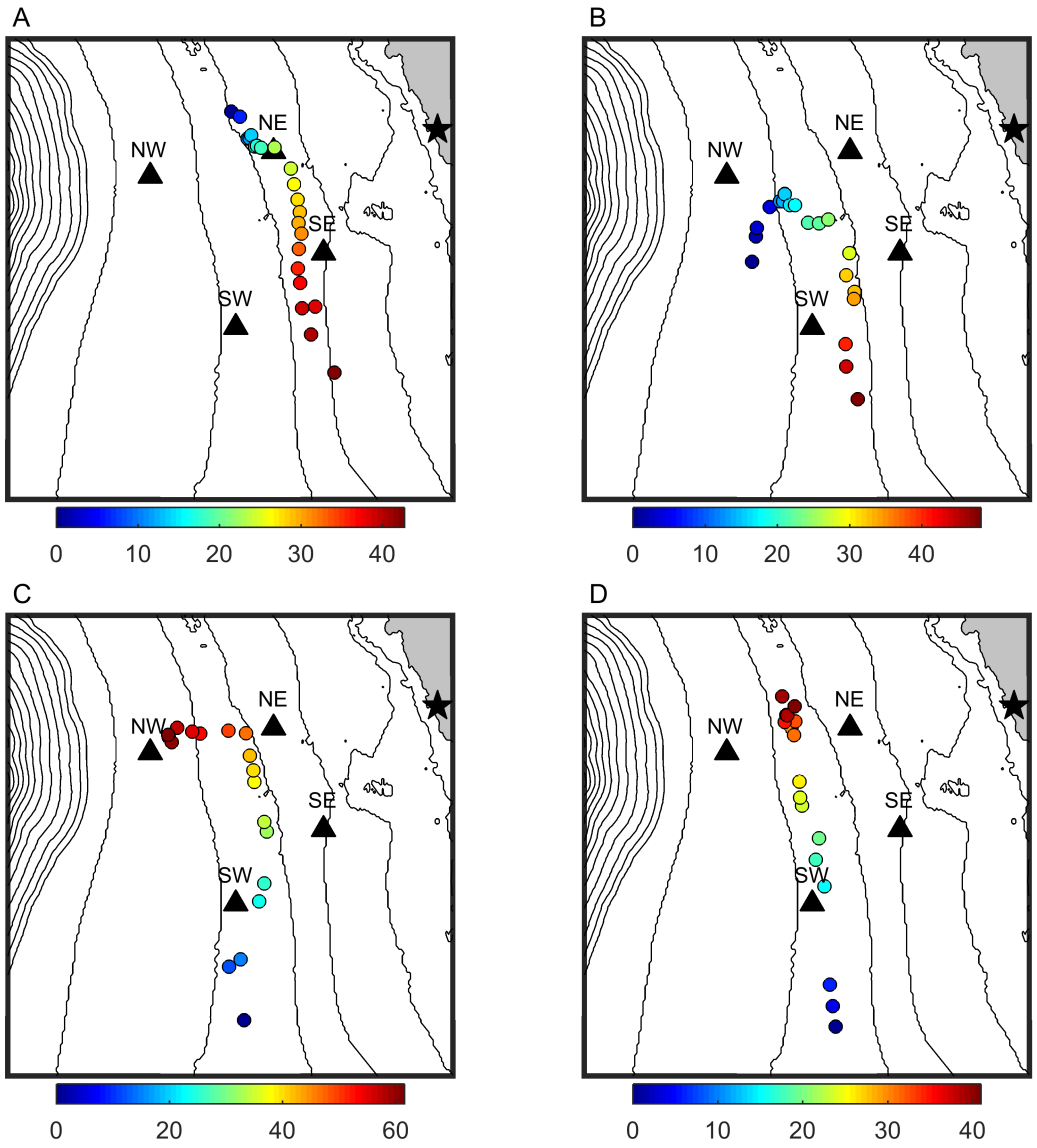

Figure 2.3: Examples of Gray Whale Tracks from Acoustic Localization. Gray whale positions determined by localizing their vocalizations on the hydrophone array. Plots (A) and (B) show southbound whales (21 January 2015 and 10 February 2015, respectively) and plots (C) and (D) show northbound whales (13 March 2015 and 9 April 2015, respectively). Dots indicate position of the calling animal and their color matches the minutes since the start of the track with earlier in time in blue and later in red. The four black triangles mark the positions of the four bottom-mounted hydrophones and the black star marks the position of the NOAA visual and infrared camera research site. Contour lines show water depth in 20 m increments. The axes limits are 36.4° to 36.45° for latitude and -121.98° to -121.92° for longitude.

calls clearly detected on all four hydrophones was not adequate. The received M1 call inter-pulse interval, peak frequency, 3 dB bandwidth, mean frequency, and $\pm\sigma$ bandwidth for 190 calls consisting of at least four pulses detected on the NE hydrophone are presented in Table 2.3. The percentage of variance from changes in inter-pulse interval within a call is compared with the percentage of variance from changes in inter-pulse interval between calls. The frequencies chosen over which to integrate for mean frequency and $\pm\sigma$ bandwidth can dramatically influence the results so it is important that these are stated.

Table 2.2: Characteristics of Received Gray Whale M3 Calls. All calls were received and measured on all four hydrophones. These quantities are highly dependent on the site-specific propagation properties. SD^2 is the variance of the mean values for each call and $SD^2_{per\ call}$ is the mean of the variances for each call across the four hydrophones. The relative contribution of each type of variance is shown as a percentage of the total variance.

M3 n=2,368	**Signal Duration** (s)	**Peak Frequency** (Hz)	**3 dB Bandwidth** (Hz)	**Mean Frequency** (Hz)	**$\pm\sigma$ Bandwidth** (Hz)
Mean	1.79	38.1	4.17	48.1	44.9
$\boldsymbol{SD^2}$	0.0460	228	9.36	88.6	95.3
$\boldsymbol{SD^2_{per\ call}}$	0.0425	130	26.9	27.7	51.8
% $\boldsymbol{SD^2}$	52.0%	63.7%	25.8%	76.2%	64.8%
% $\boldsymbol{SD^2_{per\ call}}$	48.0%	36.3%	74.2%	23.8%	35.2%

Gray whale M3 calls have a mean RMS source level of 156.9 dB re : 1μPa at 1 m measured with bandwidth 20–100 Hz (n=2,368 calls). The variance of the source level is 11.4 dB (calculated in the decibel domain). The attenuation/absorption coefficient α was estimated to be 4.26×10^{-4} which indicates that attenuation/absorption has little effect on the call and most transmission loss is due to spherical and cylindrical spreading. Estimated received level can vary by about 2 dB depending on the signal-to-noise ratio due to errors from subtracting the

Table 2.3: Characteristics of Received Gray Whale M1 Calls. Calls were only measured on one (NE) hydrophone. SD^2 is the variance of the mean values for each call and $SD^2_{w/in\ call}$ is the mean of the variances within each call. The relative contribution of each type of variance for inter-pulse interval is shown as a percentage of the total variance.

M1 n=190	**Inter-Pulse Interval** (s)	**Peak Frequency** (Hz)	**3 dB Bandwidth** (Hz)	**Mean Frequency** (Hz)	**$\pm\sigma$ Bandwidth** (Hz)
Mean	0.208	149	8.07	377	556
$\boldsymbol{SD^2}$	4.78×10^{-3}	1.19×10^4	35.7	8.14×10^3	6.06×10^3
$\boldsymbol{SD^2_{w/in\ call}}$	4.62×10^{-3}				
% $\boldsymbol{SD^2}$	50.8%				
% $\boldsymbol{SD^2_{w/in\ call}}$	49.2%				

background noise from the signal level. This value was determined by inserting an M3 call in various levels of Gaussian noise. As a result, signals in high noise are reported as having a greater received level than signals in low noise. Means and variances of the calculated RMS, SEL, and peak-to-peak source levels are summarized in Table 2.4 and are plotted in Figure 2.4. Similar to Au et al. (2006) with respect to humpback whale calls, we found that on average, gray whale M3 call peak-to-peak source level was 18.1 dB greater than RMS source level. SEL was 2.5 dB greater than RMS source level, which is what is expected from a mean call duration of 1.79 s.

2.4.2 Seasonal Cycle

Background Noise and Probability of Localization

Noise level was calculated for each minute of the deployment on the NE hydrophone. The 25th, 50th, and 75th percentiles of root median square noise were 92.3, 93.5, and 94.9 dB re : 1μPa, respectively.

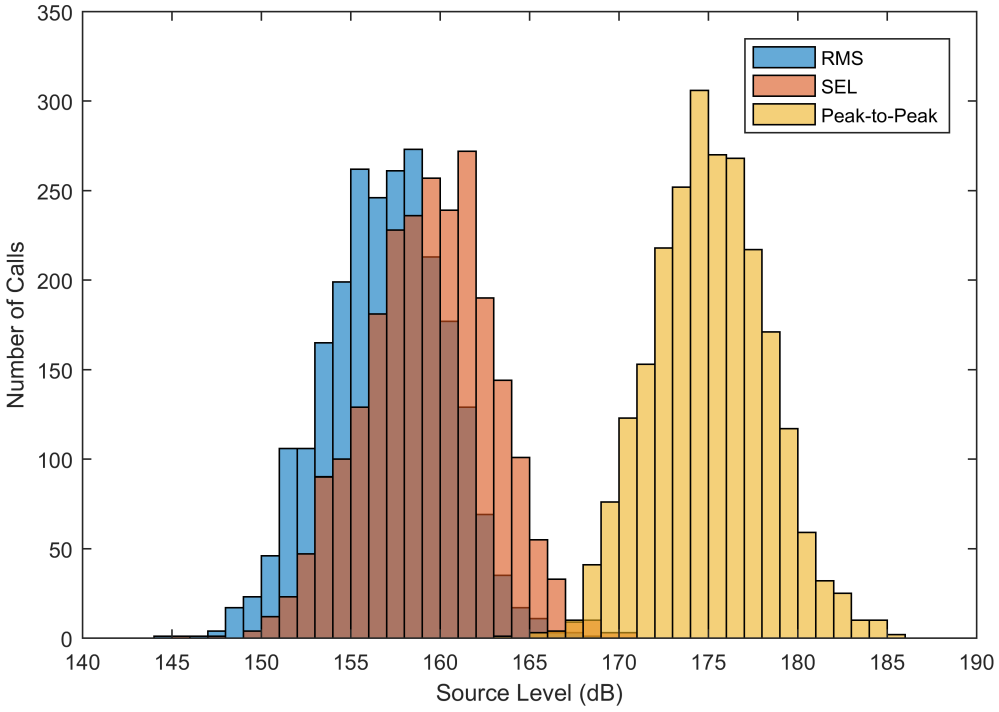

Figure 2.4: Estimated Source Level of Gray Whale M3 Calls. These histograms show the source level of gray whale M3 calls. RMS is shown in blue (dB re : 1μPa at 1 m), SEL is shown in orange (dB re : 1μPa^2 s at 1 m), and peak-to-peak is shown in yellow (dB re : 1μPa at 1 m).

Table 2.4: Source Level of Gray Whale M3 Calls. The source level of gray whale M3 calls calculated three different ways. SD^2 is the variance of the mean values for each call and $SD^2_{per\ call}$ is the mean of the variances for each call across the four hydrophones as in Table 2.2. Mean α is the environment-dependent attenuation/absorption coefficient and has units of dB/m. The mean and variance of α were calculated from the median for each call measured across all pairs of hydrophones. α is the same for RMS and SEL because the SEL was calculated from RMS. All means and variances were calculated in the dB domain.

	RMS (dB re : 1μPa)	**SEL** (dB re : 1μPa^2 s)	**Peak-to-Peak** (dB re : 1μPa)
Mean	156.9	159.4	175.0
$\boldsymbol{SD^2}$	11.4	12.4	10.4
$\boldsymbol{SD^2_{per\ call}}$	6.82	6.94	6.56
% $\boldsymbol{SD^2}$	62.5%	64.1%	61.2%
% $\boldsymbol{SD^2_{per\ call}}$	37.5%	35.9%	38.8%
Mean α	4.26×10^{-4}	4.26×10^{-4}	6.60×10^{-5}
Variance α	3.37×10^{-5}	3.37×10^{-5}	2.67×10^{-5}

At the median noise level of 93.5 dB re : 1μPa, the probability of localization within the array was approximately 100% (Figure 2.5). A total of 4,247 M3 calls were localized within the area of the array, but after correcting for the probability of localization, we estimate that 4,854 calls were produced within the area of the array. This call count is likely an underestimate because infrequent calling results in many minutes having zero calls and these values stay zero even after the noise correction. Only 10.1% of minutes over the entire deployment had a probability of localization below the 50% threshold. In a single day, the greatest percentage of the day considered to have no effort due to low probability of localization was 49%. High noise was most common during the first month of the deployment due to strumming of the acoustic recording package cables.

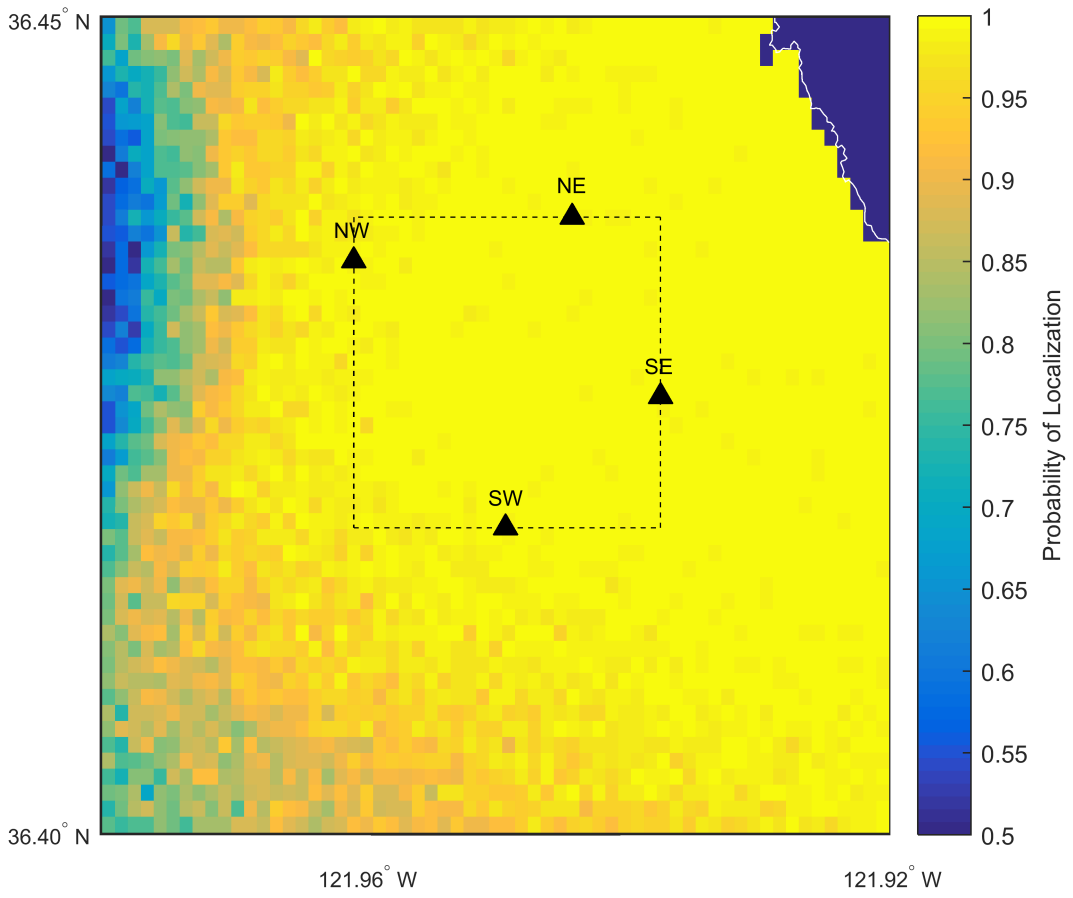

Figure 2.5: Probability of Localization in 93.5 dB re : 1μPa Root Median Square Noise This map shows the probability of localization of a call produced at locations close to the hydrophone array in 93.5 dB re : 1μPa root median square background noise. In the 50th percentile noise conditions, the probability of localization within the area of the array was approximately 100%. Probability of localization increases as noise levels decrease. The four black triangles mark the positions of the four bottom-mounted hydrophones. The dashed box indicates the area inside the hydrophone array. The axes limits are 36.4° to 36.45° for latitude and -121.98° to -121.92° for longitude.

Total Number of Calls and Percentage Part of a Track

The total number of localized calls within the array per day increased from December 2014 until the middle of February with a maximum value of 139 localized calls (152 normalized calls) within the area bounded by the array on 25 February 2015 and then the total number of localized calls decreased until the middle of April (Figure 2.6). These calls were recorded on all four hydrophones and verified as M3 calls, but were not necessarily part of a track. The percentage of M3 calls within the array that were also part of a track had high variability, but in general a higher percentage of calls were part of a track at the beginning and end of the migration (Figure 2.6). This trend was confirmed by using a generalized additive model (GAM) that modeled whether a call was part of a track with a logistic link function and the date and time of the call with both LOESS (LOcally Estimated Scatterplot Smoothing) and smoothing spline functions.

Localization precision can be estimated several different ways. In the time domain, the theoretical timing error is given by

$$\Delta t = \frac{1}{(f_2 - f_1)\sqrt{RL/NL}} \tag{2.18}$$

(from Woodward (1964)) where $f_2 - f_1$ is the bandwidth of the signal and RL/NL is the signal to noise ratio. We use 20–100 Hz for M3 cross-correlation or a bandwidth of 80 Hz. M3 calls within the hydrophone array have a median signal to noise ratio of about 10 dB (3.19). The timing error is therefore 7 ms. Using the assumed sound speed of 1500 m/s, the localization error is 10.5 m. However, we are cross-correlating calls in the spectrogram domain. The spectrogram resolution is 26 ms, which corresponds to a localization error of 38 m. Helble et al. (2015) (Section IID) use Monte Carlo simulations to calculate the estimated timing error in humpback whale calls. For a single grunt humpback call in medium noise, the expected timing delay error is approximately 10 ms, which would correspond with a location error of 15 m. Propagation

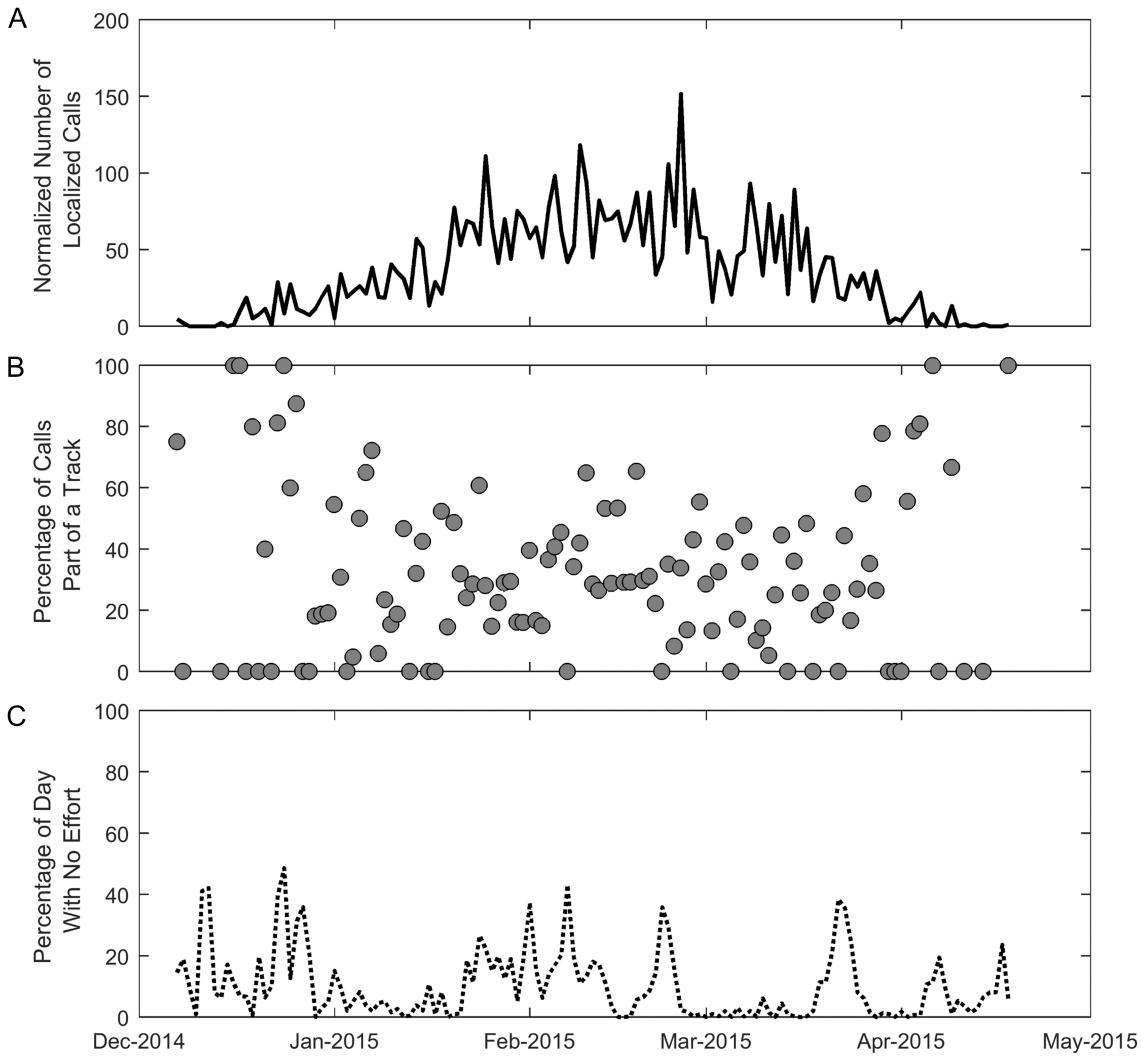

Figure 2.6: Seasonal Cycle: Normalized Calls and Percentage of Calls That Were Part of a Track. The normalized number of localized calls per day is shown in (A), the percentage of those calls that were part of a track is shown in (B), and the percentage of the day with no effort due to probability of localization less than 50% is shown in (C). The first localized gray whale call within the area bounded by the array was detected on 7 December 2014 and the last was detected on 18 April 2015. All of the calls counted were manually verified on all four hydrophones to be gray whale M3 calls.

effects are not modeled in this method and could further increase the timing delay errors. Another way to estimate localization precision is to compare the call localizations with the “corrected" localizations based on the smoothing spline used to make tracks. We assume that the smoothing spline better models animal movement than straight lines connecting each successive localization. The mean of the median difference between the original localization and the smoothing spline “corrected" localization is 39 m with a standard deviation of 26 m. We therefore estimate that our call localizations have a precision of approximately 40 m.

Swimming Behavior

Vocalizing whales swam with a mean speed of 1.6 m/s (standard deviation 0.59 m/s) (Figure 2.7A). No change in speed occurred over the migration season. Southbound whales dominated until the middle of February and then northbound whales became most prevalent (Figure 2.7B). The direction index shows that vocalizing gray whales are usually traveling along relatively direct paths, but may meander more in the first half of January and the second half of February into March (Figure 2.7C).

Seafloor Depth

The depth of water in which the tracks were located increased over the migration season (Figure 2.8). We used track heading to separate southbound and northbound migrators and found that northbound tracks were in significantly deeper water than southbound tracks (2-sample t-test, $p=7.0 \times 10^{-9}$). The mean seafloor depth for southbound tracks was 79 m and the mean seafloor depth for northbound tracks was 89 m.

Average Calling Rate

A total of 4,247 gray whale M3 calls were localized within the bounds of the hydrophone array. From the probability of localization corrections described in detail above, we estimate

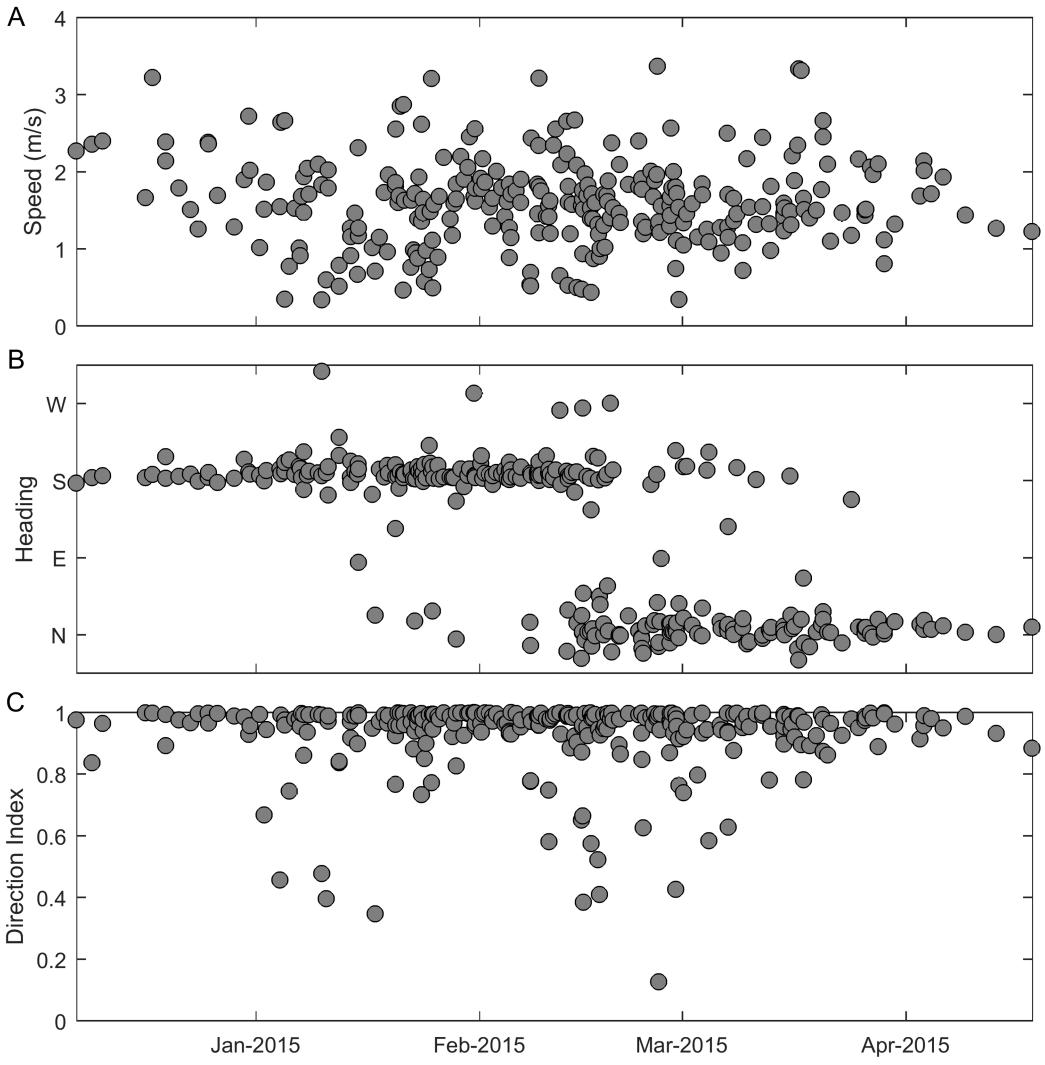

Figure 2.7: Seasonal Cycle: Swimming Behavior. Three track metrics used to assess swimming behavior of vocalizing gray whales. (A) displays average speed, (B) displays average heading, and (C) displays direction index.

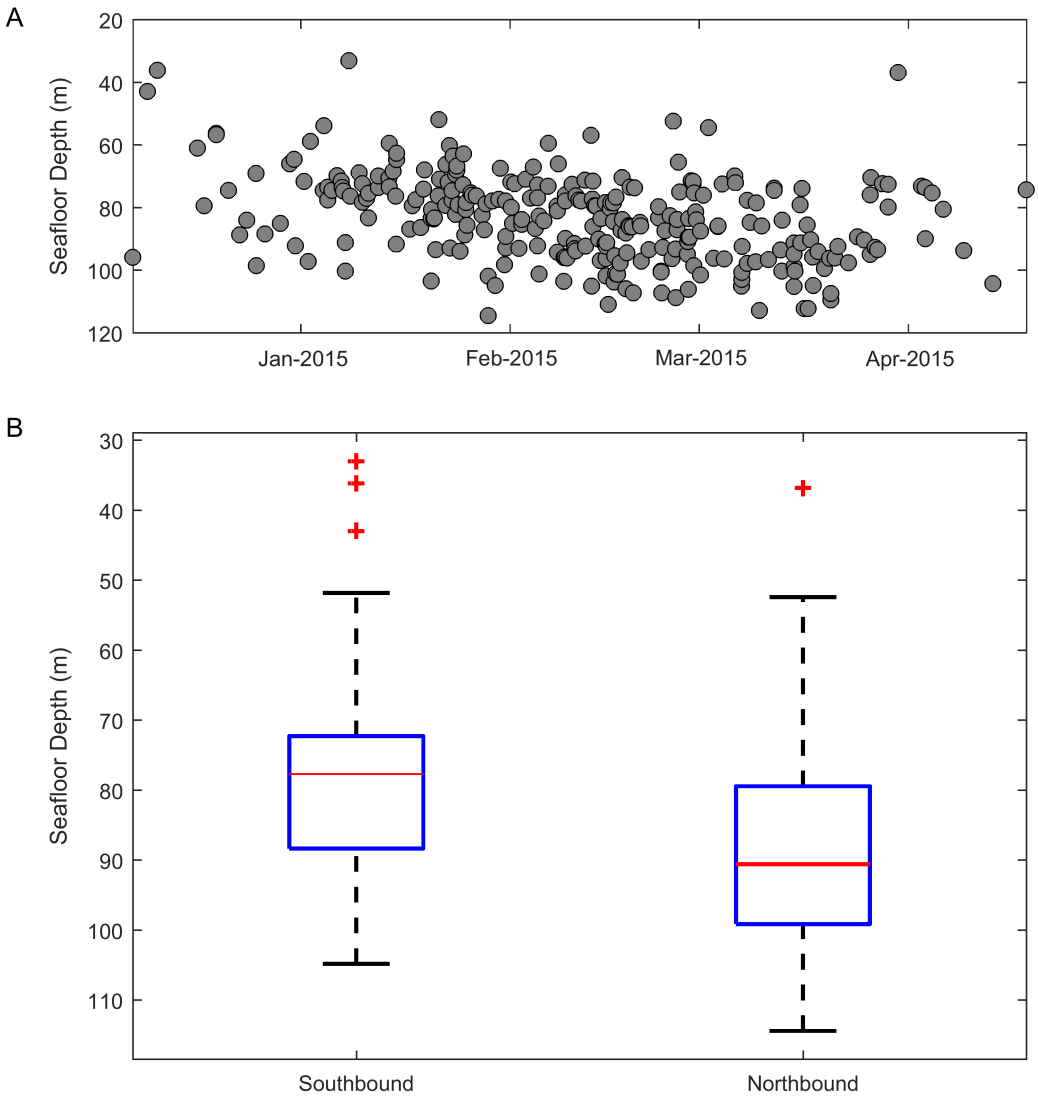

Figure 2.8: Seasonal Cycle: Seafloor Depth. The mean seafloor depth at the position of tracks over the migration season. (A) shows depth as a function of time and (B) categorizes tracks as southbound or northbound based on their heading and shows the same data in boxplot format.

that 4,854 calls were actually produced within the array. Using a distance of 2.28 km, a straight line distance approximating the 80 m bathymetric contour, and an average speed of 1.6 m/s, we estimated that it took 1.6×10^{-2} days (23.75 minutes) for a whale to swim through the array. Assuming that 90% of the 28,790 (Durban et al., 2017) whales migrated through the array and each whale traveled through during both the southbound and northbound migration, we estimated the calling rate as 5.7 calls/whale/day (0.24 calls/whale/hour).

2.4.3 Diel Cycle

Background Noise and Probability of Localization

The mean background noise levels during the day (94.25 dB re : 1μPa root median square in the 20–100 Hz band) were not meaningfully different from the mean background noise levels during the night (94.09 dB re : 1μPa root median square in the 20–100 Hz band). In both cases, the probability of localization in the search area was close to 1. Therefore, diel calling differences cannot be explained by a change in noise level.

Total Number of Calls and Percentage Part of a Track

Over twice as many localized gray whale calls occurred during the night than during the day and the percentage of calls that were part of a track also increased (Figure 2.9A) (Fisher's exact test, p=3.4×10^{-4}). In order to test if a statistically significant difference in diel calling between southbound and northbound migrants existed, we categorized all calls before 15 February as southbound and all calls on or after 15 February as northbound. Again, about twice as many calls occurred during the night than during the day for both halves of the migration. The percentage of calls that were part of a track was similar between day and night for the first half (Fisher's exact test, p=0.43) (Figure 2.9B), but the percentage of calls that were part of a track was greater at night during the second half (Fisher's exact test, p=3.6×10^{-5}) (Figure 2.9C).

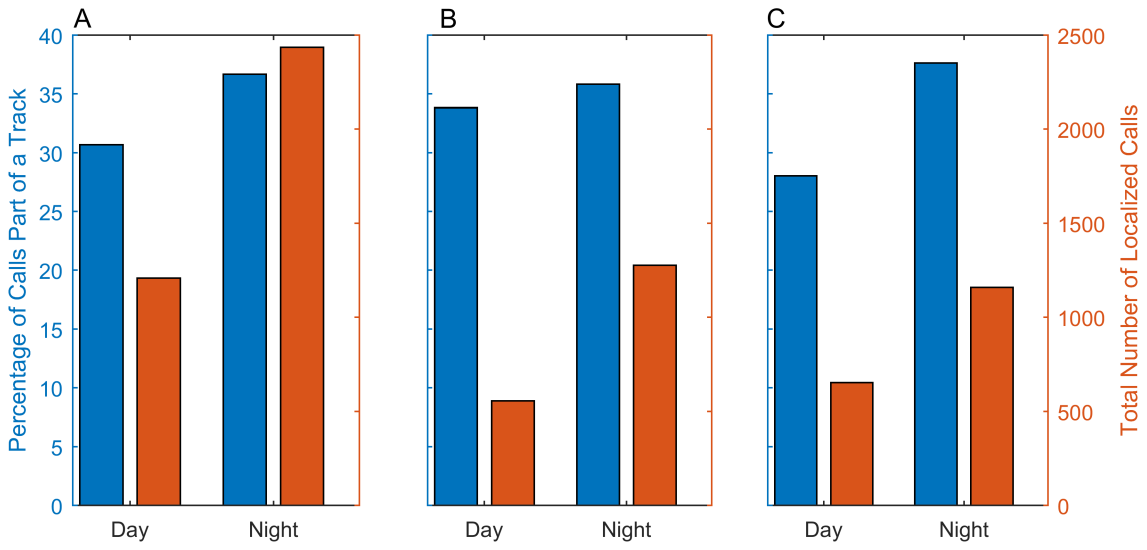

Figure 2.9: Diel Cycle: Total Calls and Percentage of Calls That Were Part of a Track. The total number of localized calls (orange) compared with the percentage of those calls that were part of a track (blue). The calls are binned in daytime or nighttime according to the time they occurred with respect to the local sunrise and sunset. (A) shows the data for the full migration, (B) shows the data for calls before 15 February, and (C) shows the data for calls on or after 15 February. All of the calls included were manually verified to be gray whale M3 calls.

The change in calling over the diel cycle was further examined by looking at the number of tracks throughout the day. Since the time of sunrise and sunset varied throughout the migration, we used a scaled start time for each track and represented sunrise as 0, sunset as 1 and the following sunrise as 2. We compared the timing distribution of tracks to the distribution that would be expected if the timing of tracks within each day was random. Using a one-sided two-sample Kolmogorov-Smirnov test, we concluded that the distribution of calls was significantly different than a randomized distribution and that more tracks existed at night ($p=2.7 \times 10^{-7}$ for the entire migration, $p=8.1 \times 10^{-4}$ for southbound whales, and $p=1.3 \times 10^{-6}$ for northbound whales) (Figure 2.10). Of the 280 gray whale tracks, 73 occurred entirely during the day, while 197 occurred entirely during the night (108/154 during the night versus 42/154 during the day for southbound whales, 78/112 during the night versus 28/112 during the day for nourthbound whales). In this case and for the rest of the results, since only calls that were part of a track are

included, heading is a valid metric to determine the migration direction of the whale.

Swimming Behavior

The mean speed did not change in a statistically significant way over the diel cycle. This observation holds true when grouping all the tracks together from the entire migration (Figure 2.11) and when separating the tracks by southbound and northbound heading (Figure 2.12). However, the variance in speed was greater at night and this difference was significant for the entire migration and for whales swimming southbound (Levene's test, p=0.010 for the entire migration, p=0.0044 for southbound whales). The direction of the tracks did not change between night and day.

Seafloor Depth

Tracks were in the same mean water depth during both night and day, however the variance at night was greater than the variance during the day (Levene's test, p=0.041) (Figure 2.13).

2.5 Discussion

These results show that gray whales are acoustically active while migrating and have an average population calling rate that is about five times that previously reported on the migration route (Crane and Lashkari, 1996) and is approximately equal to the reported lagoon calling rate in March (Dalheim, 1987). The calling rate is highly variable and those animals whose calls form tracks are calling much more frequently than the average calling rate. Other species of baleen whales have also been shown to have highly variable calling rates and tend to either be in a behavioral state in which they are vocalizing often or a behavioral state in which they are not vocalizing. For example, in a tagging study focused on North Atlantic right whales, over half of the individuals were silent for the duration of the tag recording and call rates ranged from 0 to

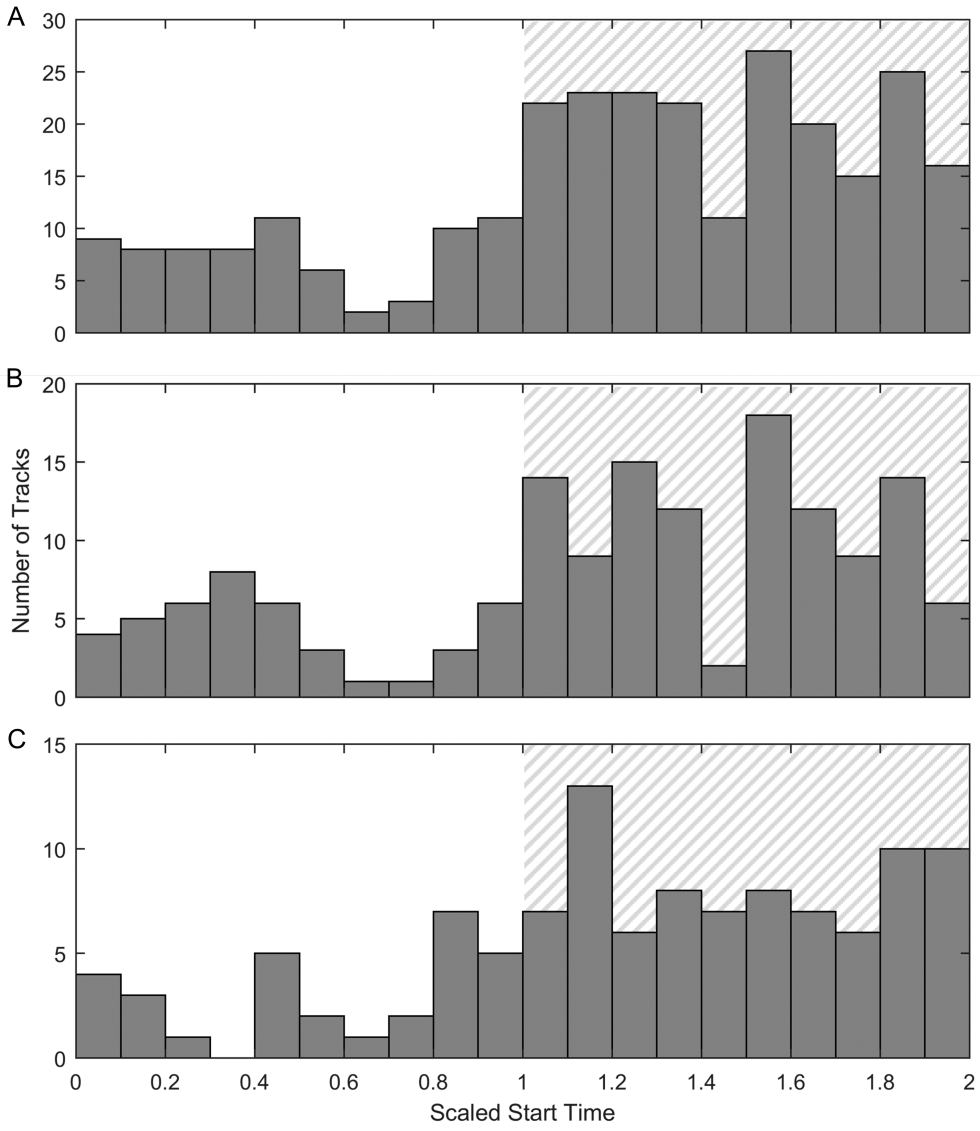

Figure 2.10: Diel Cycle: Number of Tracks. The total number of gray whale tracks binned into different start times. Since the time of sunrise and sunset changes substantially throughout the migration, these plots use scaled start time of each track where 0 indicates sunrise, 1 indicates sunset, and 2 indicates the following sunrise with gray hatching indicating night. (A) shows the entire migration, (B) shows all tracks with a southbound heading, and (C) shows all tracks with a northbound heading.

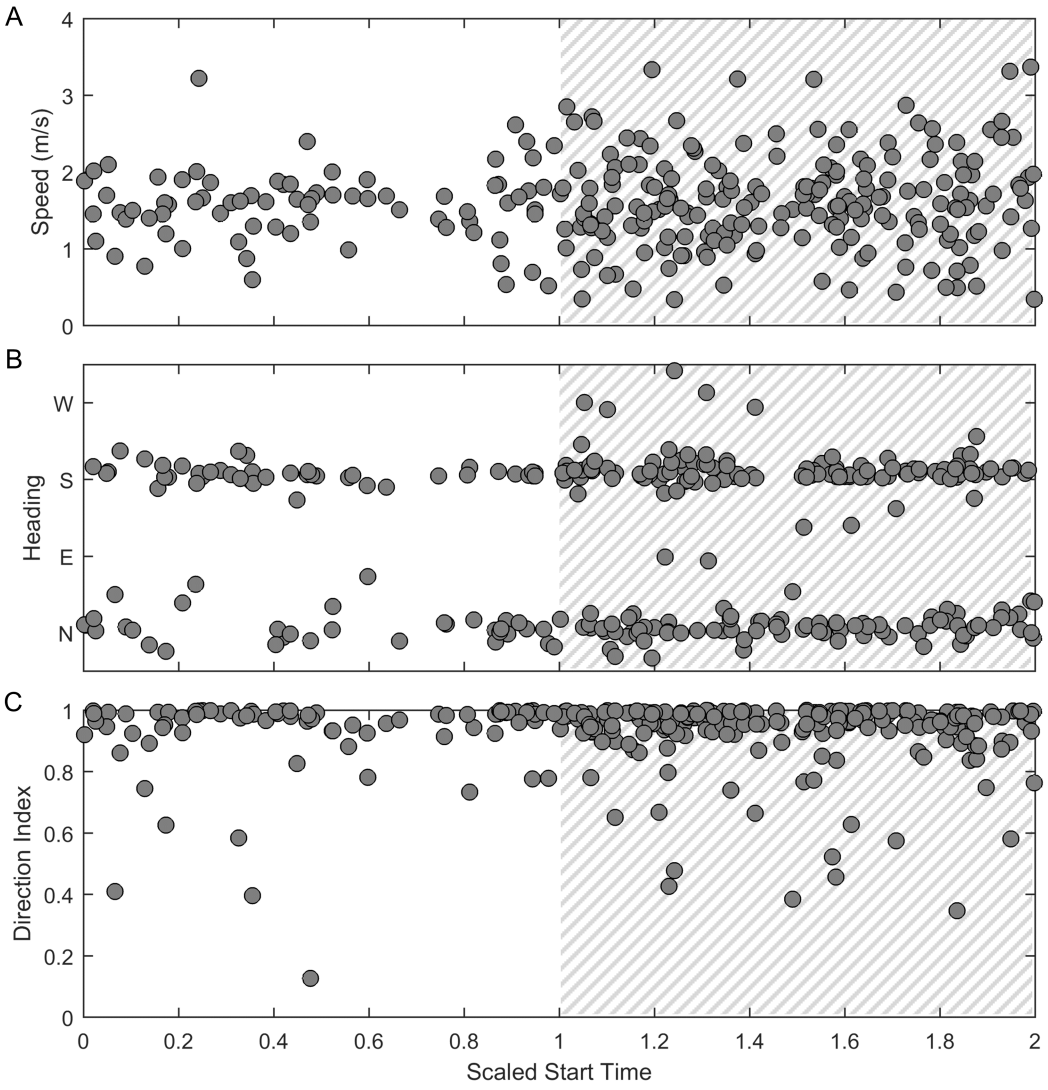

Figure 2.11: Diel Cycle: Swimming Behavior, Entire Migration. Three track metrics used to assess swimming behavior of vocalizing gray whales. (A) displays speed, (B) displays heading, and (C) displays direction index. All track metrics are shown as a function of scaled start time of the tracks where 0 indicates sunrise, 1 indicates sunset, and 2 indicates the following sunrise with gray hatching indicating night.

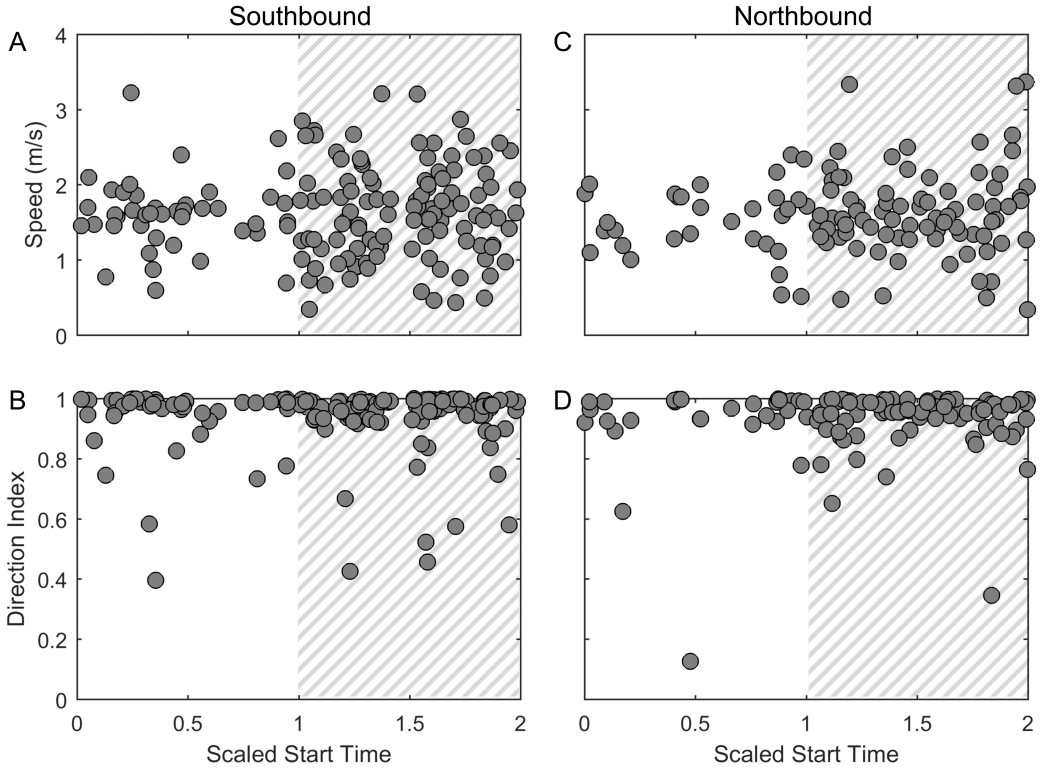

Figure 2.12: Diel Cycle: Swimming Behavior, Split by Heading. The speed (A and C) and direction index (B and D) split based on track heading. All track metrics are shown as a function of scaled start time of the tracks where 0 indicates sunrise, 1 indicates sunset, and 2 indicates the following sunrise with gray hatching indicating night.

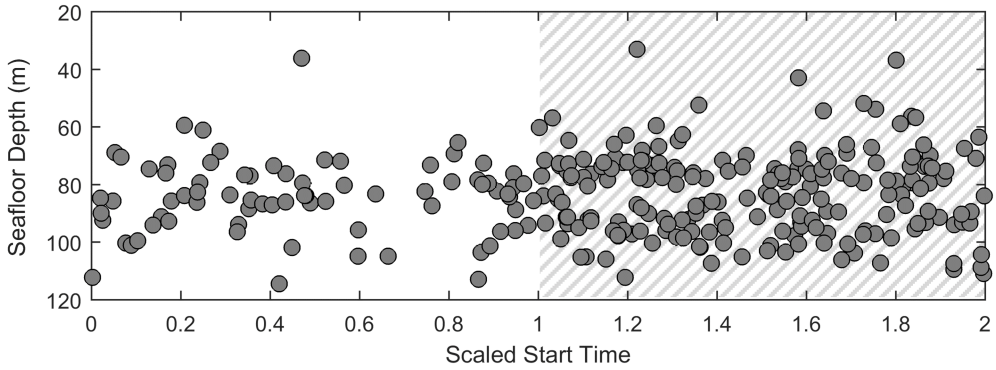

Figure 2.13: Diel Cycle: Seafloor Depth. The mean seafloor depth of tracks as a function of scaled start time where 0 indicates sunrise, 1 indicates sunset, and 2 indicates the following sunrise with gray hatching indicating night.

200 calls/hour (Parks et al., 2011). The seasonal timing of the gray whale calls confirms the gray whale migration timing reported by visual observers. These findings suggest that gray whales change their swimming and acoustic behavior over seasonal and daily time scales.

This study describes the longest duration acoustic dataset focused on migrating gray whales with the greatest number of detected calls that has been published to date. This study is also the first to show full-season acoustic tracking of migrating gray whales. Using multiple hydrophones to localize calls is an effective method for reducing the false alarm rate of an automated detector because even though an automated detector may produce false detections in individual hydrophone sound files, the likelihood of noise detections at approximately the same time on all hydrophones is extremely low. Using multiple hydrophones allows for creating a known study area that can be monitored with a high probability of detection in nearly all noise conditions, unlike a single sensor where source locations are unknown and probability of detection changes with noise (Helble et al., 2013). Acoustic localization and tracking is an important tool that can be applied to many regularly vocalizing species.

2.5.1 Vocalization Characteristics

Characteristics of the M1 and M3 calls were quantified and described as has been done in past studies. These results illustrate the importance of stating and understanding the methods to calculate each quantity. As is apparent in the mean values for each of the characteristics for the M3 and M1 call types, similar sounding metrics could be measuring very different aspects of the call. For M3 calls for example, the “peak frequency" is the frequency of the harmonic with the highest amplitude and is usually either the first or second harmonic, while the “mean frequency" is approximately the frequency of the second harmonic. The “3 dB bandwidth" is the bandwidth of the strongest harmonic, while the “$\pm\sigma$ bandwidth" is the bandwidth of the entire received call. Confusion about call characteristics can lead to mis-categorization of call types. These mean values are helpful for identification of gray whale calls in other datasets, but it is imperative to

note that these values are of the received call and not of the call produced by the whale and can be highly dependent on the environment. Constructive and destructive interference of multipaths will change the received waveform. High frequencies attenuate faster than low frequencies and in shallow water, sound cannot propagate at frequencies below the cutoff frequency of the first mode.

In this study, the variance in call characteristics due to the environment was separated from the total variance. The actual statistical separation of the variance due to the environment and the variance due to the calling animals themselves is limited by the sampling size of the recording sites. Increasing the number of recording sites to greater than four in order to provide greater variability in recording location would provide greater statistical separation. At the least, however, the variance of the characteristics of a given call across recording sites provides quantitative information on the impact of site-specific effects on localization. We would expect gray whales to use call properties that are robust to propagation to convey information. Again, propagation effects are apparent in the variance of a characteristic of a single call across the four sensors ($SD^2_{per\ call}$). The property most robust to environmental propagation (lowest percentage of total variance from variance per call) is mean frequency (23.8% of total variance is from variance per call). The other quantities are sensitive functions of the propagation characteristics and are good indicators of propagation variability but not good metrics for the call characteristics themselves. The same call could not be compared between hydrophones for M1 calls since few were detected with high SNR on all four hydrophones. Instead variation of inter-pulse interval was compared within a single call and between calls. Much of the variation in inter-pulse interval is due to differences between individual calls, but over one-third of the variation is from variability within a single call. Both the received M1 and M3 call types are highly variable. The best way to identify calls is to compare the general frequencies, duration, spacing between calls or pulses, and spectrogram contour shape with known gray whale calls. In addition, these quantities are affected by hydrophone sensitivities, so the frequency band monitored must be stated.

Using the hydrophone array setup, gray whale M3 call source levels were estimated. These source levels were in the range of those reported by Cummings et al. (1968) from migrating whales and by Petrochenko et al. (1991) from whales in the northern feeding areas. However, neither of these previously published results stated how source level was calculated (RMS, SEL, or peak-to-peak) or the bandwidth and only one publication stated the transmission loss assumptions. A 18.1 dB difference exists between the RMS estimate and peak-to-peak estimate, which is equal to a $10^{1.81} = 64.6$ difference in pressure amplitudes squared, equivalent to the ratio of potential energy densities. Transmission loss assumptions affect the estimated source level. We assumed that the whale was calling near the surface and that neither source level nor attenuation and absorption were dependent on the location of the whale. If attenuation/absorption is dependent on specific call properties such as frequency content or location, then a call-specific α value should be used. Using a call-specific α value, the mean source levels are equivalent to those calculated using a mean α value within experimental accuracy (source level values are 0.1 dB greater with a call-specific α), however the source level values have higher variance (RMS SD^2 is 53.5 dB when a call-specific α is used compared to 11.4 dB when a mean α is used). If the whales do not call near the surface, the estimated source level will change more significantly. For example, changing whether the whale vocalizes at the surface or at a depth of half the water depth would result in a change in transmission loss and therefore estimated source level of approximately 3 dB. For this analysis, the variation in the estimated source level due to variations in transmission loss can be estimated by the variance for the same call across all four hydrophones. The standard deviation of the means for M3 call source levels was just over 3 dB. The transmission loss could be expected to vary on this order if the animals call over a wide interval of depths rather than close to a single depth. In addition, since the environmental properties are not homogenous across the survey area due to the sloping bottom and possibly other characteristics, the attenuation and absorption will be different even for a single call as it travels to each of the four hydrophones. This simple spherical and cylindrical spreading model

does not take these propagation differences into account, but the variation in source level due to differences propagating to each of the hydrophones for a single call is quantified in the mean of the variances for a single call. Further, the reported source levels may be slightly in error due to full wavefield propagation effects such as the Lloyd's mirror effect and the different excitation of modes at the depths of the whale compared to the depths of the hydrophones. We have reduced some of these impacts by averaging the results from four hydrophones at different depths and locations.

2.5.2 Seasonal Cycle

The fidelity of the direction of migration and its dependence on season was quantitatively evaluated, as well as other metrics of the migration paths. Most of the acoustically tracked southbound whales passed Granite Canyon between the beginning of December and mid-February with the steadiest stream of tracks during January and the first half of February. This result matches the migratory timing reported by visual surveys.

Although there exists high variability in the percentage of calls that were part of a track over the entire migration season, the increase in percentage of calls that were part of a track at the beginning and end of the migration (Figure 2.5) could indicate a change in how vocalizations are used by different demographics of whales. Pregnant females are the first to migrate south and postpartum females with calves are the last to migrate north (Rice and Wolman, 1971). The beginning and end of the migration season is marked by the least total number of gray whale calls, but the highest percentage of calls that were part of a track. We hypothesize that the pregnant females and those same females with their calves may call more often than other whales as they migrate, which makes their calls more likely to form a track, but the number of whales is more sparse, resulting in a lower total call count. This difference in behavior may be because these females are usually traveling alone, or at least without another mature whale, and are calling to keep in contact with more distant whales.

The gray whale swimming behavior results obtained from acoustic tracking confirm many of the results reported by previous studies. Using acoustic tracking allowed us to monitor for an entire migration cycle and obtain a sample size of 280 tracks which is larger than those of previous behavior studies that used tagging and visual methods. The mean speed of the acoustic gray whale tracks was 1.6 m/s, which is near the middle of the range reported by previous publications (Cummings et al., 1968; Rice and Wolman, 1971; Sumich, 1983; Rugh et al., 1990; Perryman et al., 1999; Mate and Urbán-Ramírez, 2003; Mate et al., 2010). Most of the tracks were very direct supporting the idea that the whales are primarily migrating to their destination and do not deviate to engage in other behaviors. The meandering tracks in the middle of the migration season may be examples of the social and sexual behavior that visual observers have noted at similar times in other years (Gilmore, 1960; Perryman et al., 1999). The tracks were slightly farther offshore in deeper water during the northbound migration than the southbound migration. This shift was not an extreme difference, which could be in part because of the narrow shelf in the study area, but the shift to deeper water agrees with previous observations that most whales travel north farther offshore, perhaps to get to their feeding areas more quickly (Poole, 1984). Females with calves migrate north very nearshore, but calves make up a very small percentage of the entire population(Perryman et al., 2002, 2010). In addition, the very nearshore sounds of breaking waves create an acoustic environment with an unknown probability of detection, so we did not attempt to track gray whales in or near the surf zone. Acoustic masking in kelp beds has been suggested by others as a way for gray whales to avoid predation from killer whales (*Orcinus orca*) (Poole, 1984).

2.5.3 Diel Cycle

Gray whale behavior within the study area changed between night and day. Most significantly, an increase in calls detected occurred at night even though the probability of detection did not change. An increase in nighttime calling has also been reported in several other

mysticete species such as humpback whales, blue whales, and North Pacific right whales (Au et al., 2000; Wiggins et al., 2005; Munger et al., 2008). In addition, an increase occurred in the percentage of calls that were part of a track at night. We hypothesize that gray whales may call more often when they can no longer see their nearest neighbor.

One assumption of population size estimates is that gray whales are increasing their southbound migration rate at night (Laake et al., 2009). In contrast to Perryman et al. (1999), we did not observe a change in mean speed over daily or seasonal time scales. Speed variance did increase at night however. If gray whales are not changing their mean migration speed between night and day, this result would warrant a change in how daytime visual counts are extrapolated to the night which would result in a population size that is lower than reported.

Similar to speed, mean water depth over which the tracks were located was the same at night and day but depth variance increased at night. If gray whales are using visual cues of land or the seafloor to aid their navigation, we would expect less direct tracks at night indicated by a decrease in direction index. In contrast, the direction index of tracks remained the same at night and day. We speculate that since more calling occurs at night, more individuals are producing sounds and these individuals have a wider variance in swimming behavior than the individuals that are calling during both the day and night. However, even though these individuals show a wider range of migration speeds and distance offshore, they still have the same migration goal and therefore their direction index is about the same.

This research was limited in that we were sampling at one location, during one migration cycle, and we are only able to track vocalizing animals. Future studies should investigate whether gray whale behavior changes at different locations along the migration, from year to year, or between vocalizing and non-vocalizing animals.

2.6 Conclusion

The recordings of a set of marine mammal calls by three or more receivers allows both for 1) localization and potential tracking of a calling animal, and 2) separation of the total variance of the calls into a component associated with environmental variability and a component associated with the calling animals themselves. In order to quantify the effects of environment-specific propagation characteristics, no additional numerical modeling or signal processing is required.

Acoustic localization and tracking of animals deepens our understanding of behavior that is difficult or impossible to observe visually. For example, we determined that gray whales increase calling at night and call more regularly toward the beginning and end of the migration season. These results provide clues as to the utility of calls for the gray whale migration. In addition, we observed that vocalizing gray whales swim at the same average speed at night and day. This finding challenges an assumption that is used in population size calculations based on visual surveys.

In the past, researchers have relied on categorization of calls using measured characteristics. In this study, multiple recordings of the same call on separate hydrophones demonstrate that received call characteristics can be highly variable and are dependent on both the animal producing the sound and the local propagation effects. These values can be helpful for initial identification of potential calls, but the variability due to environmental effects must be appreciated. Moreover, different methods of calculating source levels and other call characteristics significantly change the resulting quantities, so detailed methods and assumptions should always be stated so that results can be compared to the analyses of other datasets.

Using multiple hydrophones in close proximity to study marine mammals can greatly increase our knowledge about both acoustic and swimming behavior. This methodology has the potential to allow us to quantify aspects of behavior that are actually due to modification of produced signals within the environment and determine the true behaviors of the animals.

2.7 Supporting Information

Supporting Information is available in the published version of this chapter: https://doi.org/10.1371/journal.pone.0185585

2.8 Acknowledgments

We are grateful to Ryan Griswold and the other engineers at the Scripps Whale Acoustics Lab for designing, building, deploying, and recovering the hydrophone-recorder packages. We would like to thank Jay Barlow for suggesting statistical tests. Glenn Ierley co-wrote most of the GPL detection and localization code with Tyler A. Helble and answered questions about the algorithms within GPL. Graduate students at Scripps Institution of Oceanography and members of the Scripps Whale Acoustics Lab provided useful feedback throughout the research and writing process.

Chapter 2, in full, is a reprint of the material as it appears in *PloS ONE*, 2017: Regina A. Guazzo, Tyler A. Helble, Gerald L. D'Spain, David W. Weller, Sean M. Wiggins, and John A. Hildebrand, "Migratory behavior of eastern North Pacific gray whales tracked using a hydrophone array." The dissertation author was the primary investigator and author of this paper.

Chapter 3

Migrating Eastern North Pacific Gray Whale Cue Rates Estimated from Acoustic Recordings, Infrared Camera Images, and Visual Sightings

3.1 Abstract

During the eastern North Pacific gray whale 2014–2015 southbound migration, acoustic call recordings, infrared blow detections, and visual sightings were combined to estimate cue rates, needed to convert detections into abundance. The gray whale M3 acoustic call rate was 2.3–24 calls/whale/day with an average of 7.5 calls/whale/day over the entire migration (southbound and northbound) and showed a positive trend from 30 December–13 February. The infrared camera blow rate averaged 49 blows/whale/hour over 5–8 January. With a call rate model, we estimated that 4,340 gray whales migrated south before visual observations began on 30 December, which is 2,829 more gray whales than used in the visual abundance estimate. This

finding highlights the usefulness of cue rates to increase precision in abundance estimates. We suggest that visual observers increase their survey effort to all of December to verify gray whale abundance corrections. Probability of detection of a whale blow by the infrared camera was the same at night as during the day. However, probability of detection decreased beyond 2.1 km offshore, whereas visual sightings revealed consistent whale densities up to 3 km offshore. We suggest that future infrared camera surveys use multiple cameras optimized for different ranges offshore.

3.2 Introduction

Estimating population sizes of marine mammals is a challenging problem. Eastern North Pacific gray whales (*Eschrichtius robustus* Lilljeborg) annually migrate between summer feeding areas in the Bering and Chukchi Seas and wintering areas in the lagoons of Baja California, Mexico. While migrating, gray whales tend to swim over the continental shelf, and in many places along the west coast of North America, can easily be seen from land. The abundance of the eastern North Pacific population of gray whales has been estimated using shore-based visual surveys during the southbound migration since the 1967–1968 migration (Laake et al., 2012). Marine mammal observers from the National Oceanic and Atmospheric Administration (NOAA) count whales as they pass through a pre-defined study area, where the continental shelf is narrow, from a vantage point approximately 22 m above sea level at Granite Canyon in central California. Even though gray whales travel along a very nearshore route in this area, the ability to estimate their abundance using visual techniques is limited to daytime periods with adequate visibility and environmental conditions on days when trained visual observers are available. The NOAA visual survey estimated the eastern North Pacific gray whale population to be 28,790 individuals during the 2014–2015 season (Durban et al., 2017).

Underwater passive acoustic sensors are able to continuously record sound produced by

marine mammals. Marques et al. (2009) showed how the number of animals could be estimated from the number of acoustic cues or calls. A required variable in this calculation is the calling rate of the species, which may change over time, location, and/or with behavioral state. Noad et al. (2017) compared visual sightings with acoustic tracks of singing humpback whales off the east coast of Australia over an 18 year period, and found that as the population size increased, the singing rate decreased. This study exemplifies the importance of estimating calling rate for the time and location of interest. Guazzo et al. (2017) estimated that 4,854 gray whale M3 calls were produced within the area bounded by the 4-element hydrophone array offshore of the NOAA visual observation site during the 2014–2015 migration. This number corresponds to an average calling rate of 5.7 calls/whale/day if 90% of the whales are assumed to travel through the array.

Since whales must surface to breathe and their blows are slightly warmer than the surrounding water (Cuyler et al., 1992), infrared cameras are another method for monitoring whales. These cameras are capable of detecting whale exhalations (hereafter called blows) both at night and during the day. Even though the core body temperature of baleen whales is around 36° (Brodie and Paasche, 1985), the blow of a gray whale is composed mostly of seawater that is entrained in the air due to a subsurface exhalation (Kooyman et al., 1975), resulting in a small temperature difference between the blow and the seawater. In Arctic waters, the mean temperature of whale blows was estimated to be 0.2–3.0°C above the water temperature (Cuyler et al., 1992). Sumich (1983) visually observed 74 migrating gray whale groups for at least 15 minutes each and reported an average blow rate of 0.72 blows/whale/min (43.2 blows/whale/hour) with a series of short dives marked by 2–4 blows 20–30 seconds apart followed by a longer dive lasting 3–4 minutes. The range in blow rates was 0.45–1.12 blows/whale/min (27–67.2 blows/whale/hour). Perryman et al. (1999) used infrared cameras to study gray whale migration behavior during the day and night for three different migration seasons. They found no difference in surfacing interval between day and night and reported an average surfacing interval for single animals tracked using infrared cameras of 27 s (133 blows/whale/hour; Perryman et al., 1999),

which is much shorter than those reported by Sumich (1983). However, in order for Perryman et al. (1999) to measure the time intervals between surfacings, a single animal had to blow more than once in the narrow camera field of view. Therefore, their results pertain only to the sequence of short-duration dives and their value of 27 s is consistent with the 20–30 s interval reported by Sumich (1983). A benefit of thermal sensing over acoustic sensing is that whales are required to breathe while vocalization patterns are more strongly affected by behavioral state. That said, infrared cameras are sensitive to environmental parameters and factors such as humidity, sea state, and glare from the sun can reduce the probability of detection of whale blows (Baldacci et al., 2005).

The objective of the present study was to estimate acoustic and infrared cue rates of migrating gray whales for use in estimating whale abundance in future population censuses. We combine the number of calls and blows detected with the number of gray whales estimated from a visual sighting census. We use the gray whale calling rate to estimate the number that migrated through the study area prior to the date when visual observations began and find that the population may be underestimated by almost 10%.

3.3 Results

Southbound migrating eastern North Pacific gray whales were successfully detected and localized using visual sightings, acoustic recordings, and infrared camera video during the 2014–2015 migration season (Figure 3.1). Visual observers counted 2,951 southbound migrating gray whales during daylight hours with good visibility on 34 days and estimated the population size to be 28,790 (95% Highest Posterior Density Interval: 23,620–39,210) (Durban et al., 2017). Guazzo et al. (2017) verified and localized 4,247 gray whale M3 calls within the bounds of the hydrophone array over the entire 2014–2015 migration season. During the four days that blows were manually detected on the infrared camera recordings, 1,882 gray whale blows were

identified. Figure 3.2 shows two example times during this four-day period of overlap in data processing of sensing system recordings when we were able to detect the same whales using multiple methods.

3.3.1 Acoustic Recordings and Visual Sightings

By using visual sightings, we were able to estimate with more accuracy the proportion of gray whales that migrated through the area bounded by the hydrophone array than by using the more general results from aerial surveys presented by Shelden and Laake (2002). Guazzo et al. (2017) estimated that only 5% of gray whales swam inshore of the array, but using visual sightings we found that this proportion was greater than assumed, which decreases the proportion that migrated through the hydrophone array. We update our 90% estimate (Guazzo et al., 2017) and estimate that about 68% of whales migrate within the area bounded by the hydrophone array. This decrease in number of animals within the array increases the average calling rate over the entire migration season from 5.7 calls/whale/day (Guazzo et al., 2017) to 7.5 calls/whale/day (0.31 calls/whale/hour) (using abundance 95% probability interval: 5.5–9.1 calls/whale/day).

The calling rate measured with the four hydrophones increased over the southbound migration from 30 December 2014 until 13 February 2015 (Figure 3.3). Calling rate ranged from 2.3 calls/whale/day on 5 January to 24.0 calls/whale/day on 9 February. Using the acoustic call counts from 6 December, when calls began, until 29 December and the two-term power model for calling rate, we estimate that 4,340 whales passed through the study area prior to the onset of visual observations on 30 December 2014 (minimum of 2,248 whales using positive 67% confidence bound for calling rate).

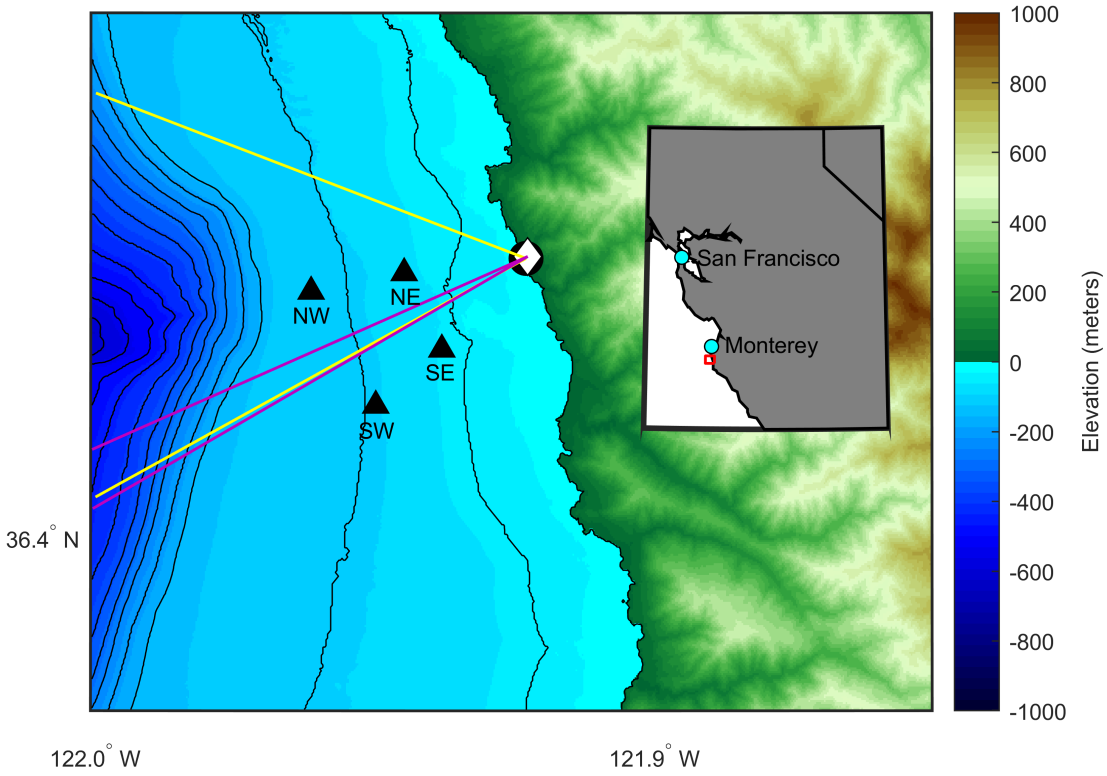

Figure 3.1: Map of the Study Area for the Combined Visual, Infrared, and Acoustic Survey of Migrating Gray Whales. The black circle indicates the location of the visual observers and the white diamond indicates the location of the infrared camera. The four black triangles indicate the locations of the four hydrophones and are labeled according to their positions. The visual field of view is shown with yellow lines and the infrared field of view is shown with pink lines. Colors indicate the land elevation and seafloor depth with respect to sea level and the black contour lines show the seafloor depth in 50 m increments. Bathymetry data are from the NOAA National Centers for Environmental Information's Southern California Coastal Relief Model with 1 arc-second resolution. The latitude bounds are 36.375°–36.475°N and the longitude bounds are 122.000°–121.850°W. For reference, the SE hydrophone is about 1.5 km from shore and the NW hydrophone is about 3.6 km from shore.

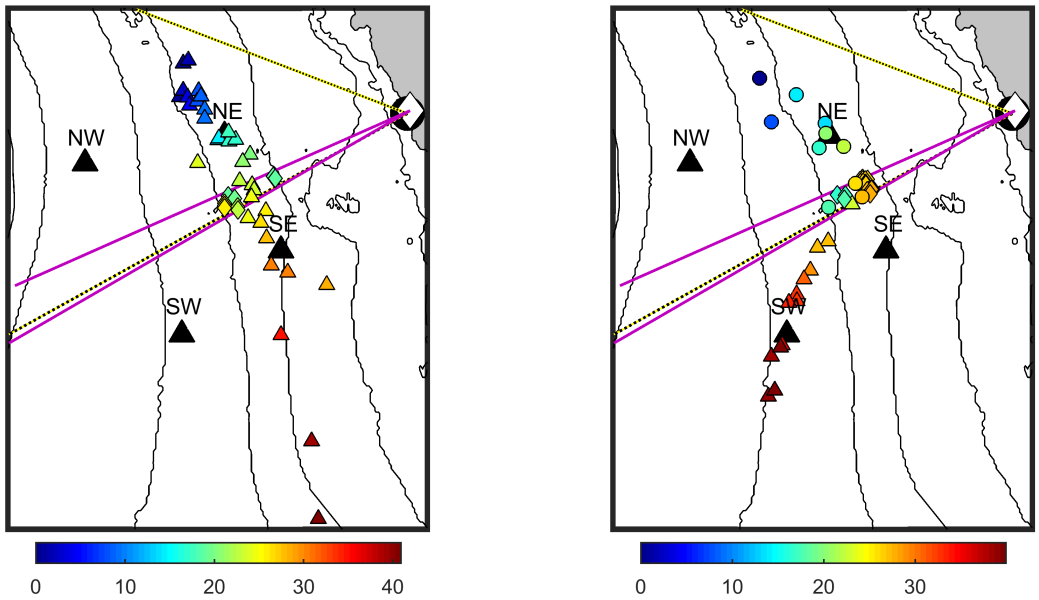

Figure 3.2: Example Gray Whale Tracks from Visual, Acoustic, and Infrared Localizations. Visual sightings are shown with colored circles, acoustic calls are shown with colored triangles, and infrared blows are shown with colored diamonds. Color indicates the amount of time in minutes since the start of the detections. The left plot spans 06 January 2015 02:14:15–02:55:10 local time (at night so no circles for visual sighting locations are plotted) and the right plot spans 07 January 2015 08:31:01–09:10:58 local time. Four black triangles indicate the positions of hydrophones, the black circle indicates the location of the visual observers, and the white diamond indicates the location of the infrared camera. The visual field of view is shown with yellow lines (with black dotting) and the infrared field of view is shown with pink lines. The black contour lines show the seafloor depth in 20 m intervals from the NOAA National Centers for Environmental Information's Southern California Coastal Relief Model with 1 arc-second resolution. Latitude limits are 36.40°–36.45°N and longitude limits are 121.92°–121.97°W.

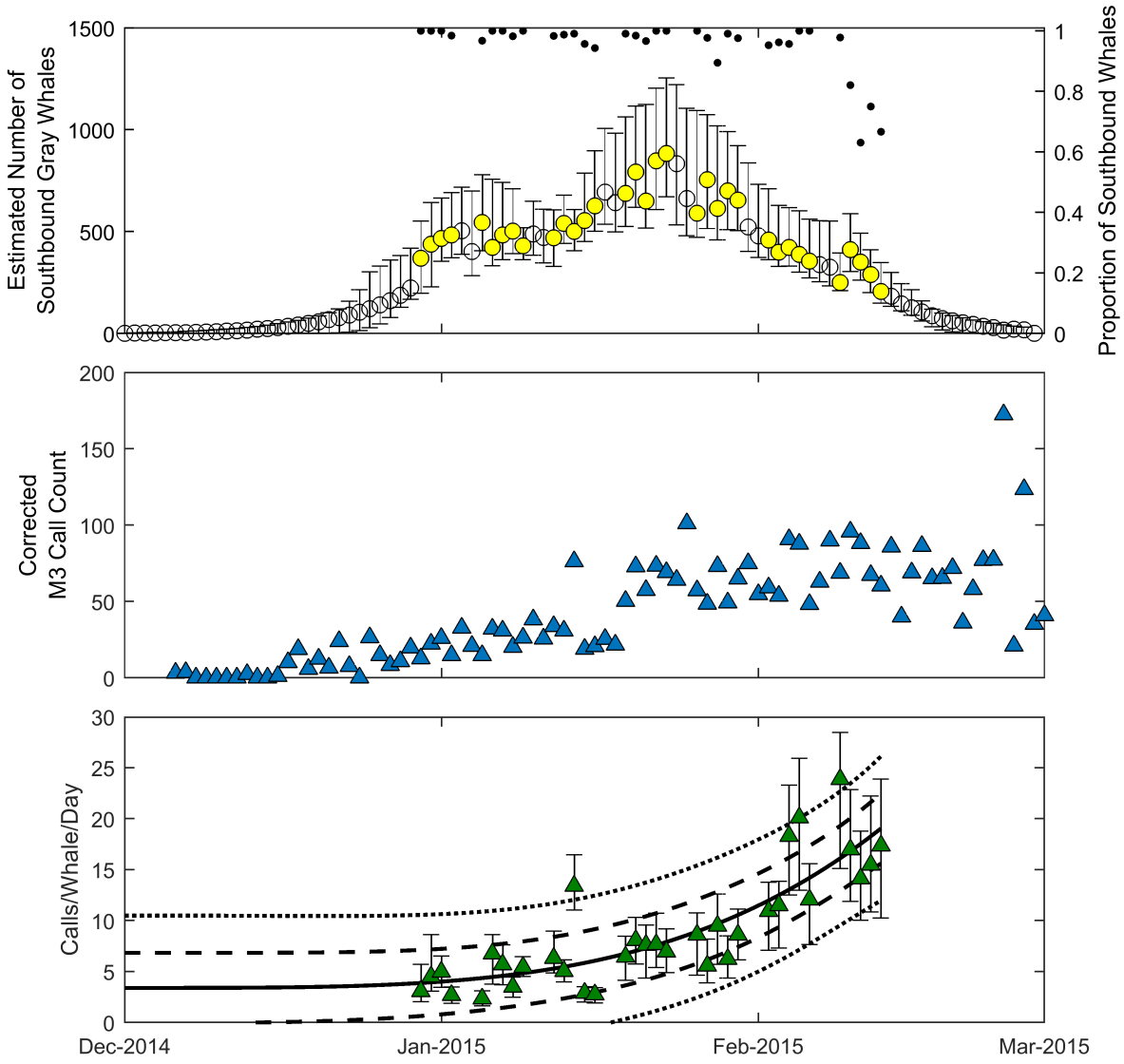

Figure 3.3: Gray Whale Acoustic Recordings and Visual Sightings. The top plot shows the modeled number of southbound gray whales based on visual sightings as circles (left axis) and the proportion of southbound whales sighted each day as dots (right axis). Yellow circles indicate days when visual observers were on-effort. Error bars show the 95% highest posterior density interval of the modeled abundances. The middle plot shows the corrected M3 call count in blue triangles (corrected based on probability of localization). The bottom plot shows the daily calling rate for days when visual observers were on-effort. The solid line is the two-term power model with the dotted line showing the 95% confidence bounds and the dashed line showing the 67% confidence bounds. The coefficients of the two-term power model are $a = 1.22 \times 10^{-6}$, $b = 3.79$, and $c = 3.39$. The 95% confidence bounds for the model are $-1.24 \times 10^{-5} < a < 1.49 \times 10^{-5}$, $1.20 < b < 6.38$, and $0.0385 < c < 6.75$. The error bars show the uncertainty in the calling rate based on the 95% highest posterior density interval of whale abundance for each day.

3.3.2 Infrared Camera Detections and Visual Sightings

The offshore ranges of blows detected using the infrared (IR) camera were between 479 m and 5.8 km, while the ranges of whales sighted by observers were between 185 m and 9.4 km. The IR camera could reliably detect gray whale blows to a range of approximately 2.1 km. An example frame with a blow is shown in Figure 3.4. When cumulative number of blows detected by the camera are plotted as a function of range, the data have two linear slopes, a shallower slope indicating a lower density until 1.2 km range and then a steeper slope from 1.2 km to 2.1 km range (Figure 3.5). Beyond this range, the curve becomes non-linear and appears to approach a horizontal asymptote equal to the total blow count. In contrast, the same plot of visual sightings is linear until about 3 km range, and then becomes non-linear due to the decreasing density of whales from the nearshore gray whale distribution. Similarly, Figure 3.6 shows the number of blows detected and the number of whales counted for daylight hours (upper plot) or estimated for a full 24 hours (lower plot) versus range offshore. Whale counts from visual observers are compared with the number of detected IR blows over the same hours in the top plot and estimated daily abundances from the visual sighting mode (Durban et al., 2017) are compared with the total number of detected IR blows in the bottom plot. If no blows were missed with the IR camera, we would expect the proportion of blows to whales to be constant at all ranges. However, for ranges farther than 2 km, the proportion of blows to whales decreases indicating again that the probability of detection decreases below unity. We set the probability of detection for the IR camera to 1 for ranges less than or equal to 2.1 km and only used blows and animal abundances within this range to estimate blow rate. We did not use detections closer than 500 m due to the very narrow field of view. We estimate that 53% of the gray whales that migrated south on 5–8 January 2015, were between 500 m and 2.1 km from shore.

The infrared blow detections show that the probability of detection is the same at night and day. The number of blows during the 9-hour visual observer watch (07:30–16:30) is approximately 9/24 of the number of blows detected over the full day, which is what is expected

Figure 3.4: Example Frame Showing a Gray Whale Blow Recorded on the Infrared Camera on 05 Jan 2015.

if the probability of blow detection by the camera does not change between night and day. In addition, the Wilcoxon rank sum test did not reject the null hypothesis that the median number of blows per hour were equal when comparing hours in the night with hours in the day (p=0.55), further supporting the observation that the probability of blow detection is the same at night and day.

Using the proportion of gray whales detected visually between 0.5 and 2.1 km from shore yields an average blow rate of 49 blows/whale/hour over these four days (uncertainty bound minimum: 25.5 blows/whale/hour, uncertainty bound maximum: 74.9 blows/whale/hour). In total, 1,427 blows were detected in this range and the mean travel time through the camera field of view is 1.7 min. Results from all four days are summarized in Table 3.1.

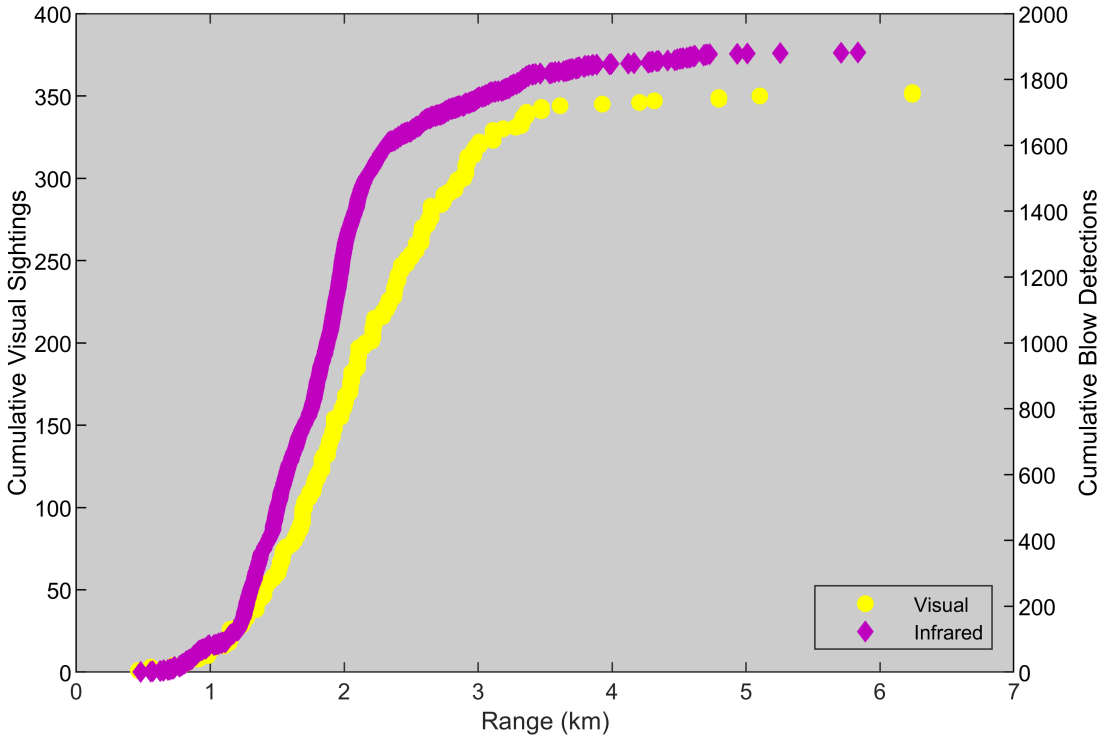

Figure 3.5: Cumulative Visual and Infrared Detections as a Function of Range. Visual sightings (yellow circles) for 5–8 January 2015 are linear until a range of approximately 3 km, while infrared blow detections (pink diamonds) are linear until a range of approximately 2.1 km. Visual sightings do not have a probability of detection that decreases with range (confirmed with aerial sightings), but the probability of detection for blows decreases after 2.1 km.

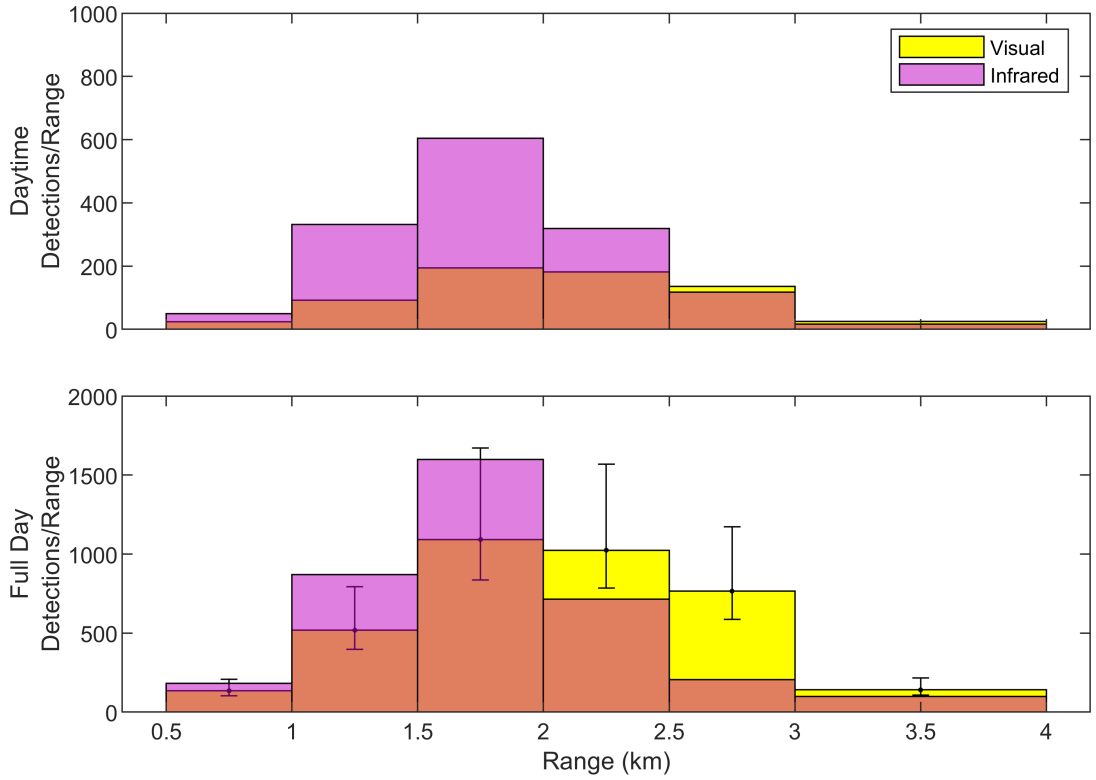

Figure 3.6: Gray Whale Infrared Detections and Visual Sightings. The top histogram shows the number of visually sighted gray whales (yellow) that migrated south past Granite Canyon during 5–8 January 2015 plotted behind the number of infrared blow detections (pink) between 07:30–16:30. Orange shows overlap. The bottom histogram shows the number of modeled gray whales calculated from the visual counts (yellow) and the number of infrared blow detections (pink) for all times on 5–8 January 2015. Error bars for the modeled abundances show the uncertainty as the 95% highest posterior density intervals. All counts are in units of detections/km. Both plots are shown as a function of offshore range and each bar includes the right range bound but not the left bound.

Table 3.1: Summary of Infrared Blow Detections with Ranges Greater Than 0.5 km and Less Than or Equal to 2.1 km. Detected Blows are the total number of whale blows manually detected and Corrected Blows increases the number detected by the fraction of the day with no infrared video assuming 100% probability of detection in this interval of ranges. Median Whales are the modeled median number of whales estimated to migrate south past Granite Canyon from visual sightings. Whales Within Range are the estimated number of those whales that are traveling within 0.5 to 2.1 km from shore based on the offshore distribution from visual sightings. Blow Rate is calculated by dividing the corrected number of blows by the number of whales within the IR camera search area and by the average amount of time it takes for a whale to travel through that search area. Uncertainty Bounds show the blow rates based on the 95% highest posterior density interval for each day. Both Blow Rate and Uncertainty Bounds have units of Blows/Whale/Hour.

Date	Detected Blows	Corrected Blows	Median Whales	Whales Within Range	Blow Rate	Uncertainty Bounds
05 Jan 2015	435	442	544	290	53.5	37.3–71.5
06 Jan 2015	291	294	423	225	45.7	25.5–58.1
07 Jan 2015	407	413	484	258	56.0	36.5–74.9
08 Jan 2015	294	298	502	268	39.1	27.7–49.9

3.4 Discussion

This study combined visual sightings, acoustic call detections, and infrared camera blow detections to calculate the cue rates of migrating eastern North Pacific gray whales. Cue rates are needed to estimate abundance of animals not observed directly. These techniques can be applied to other marine mammals to monitor their abundance over long time periods.

Using visual sightings to model the distribution of gray whales from shore allowed us to document the number of animals in the study area with greater accuracy. We estimate that the average calling rate over the entire migration season is 7.5 calls/whale/day or 0.31 calls/whale/hour, approximately equal to the calling rate measured by Dalheim (1987) in the Baja California lagoons in February.

The acoustic recordings indicate that gray whales have a calling rate that increases by more than a factor of 5 over the duration of the southbound migration. We hypothesize that the

segmented demographic phases of the migration produce this trend. That is, the forerunners of the migration are pregnant females followed then by mature whales and finally juveniles. Juveniles are undertaking their first southbound migration, fully weaned from their mothers, and may call at a higher rate than their mature and more experienced conspecifics. Alternatively, the large increase in calling rate of southbound animals coincides with an influx of gray whales migrating to the north. In contrast, Guazzo et al. (2017) found that the percentage of calls that were part of a track was high at the start of the southbound migration and then decreased toward the middle of the migration. We hypothesize that a small proportion of early gray whales are calling at a high rate, but the overall calling rate is low at this time, while in the middle of the migration, more whales are calling, but not at a high enough rate to be tracked. This positive trend in calling rate over time has important implications for estimating abundance of whales using acoustic methods. An average calling rate will not accurately estimate the number of animals unless the abundance is estimated over the same timescale. Further work should be done to check the predicted trend in calling rate for early segments of the southbound migration and for the northbound migration by increasing visual sighting effort during these times.

Acoustic recordings also can be used to estimate the number of whales that migrate south before visual observers began their effort on 30 December 2014. Using the modeled calling rate, we estimate that 4,340 whales migrated south between 1–29 December 2014 (minimum of 2,248 whales using the upper 67% confidence interval), which is 2,829 more whales than the sum of the daily median values that NOAA estimated traveled past during that time (NOAA median value: 1,511, 95% probability interval: 483–2,982) (Durban et al., 2017). This increase in whale abundance is within the 95% probability interval reported for the gray whale abundance for the entire migration season, but is greater than the 95% probability interval for the 1–29 December, however there is overlap between the two intervals. These results show how cue rates and multiple detection methods can reduce the uncertainty in modeled abundance values derived from a single method.

Infrared cameras have great potential to monitor as effectively at night as during the day and for longer durations than possible for visual observers. The blow rates we measured over the selected four days (49 blows/whale/hour) were similar to those reported by Sumich (1983) from visual observations and the range of blow rates over the four days (39–56 blows/whale/hour) was well within Sumich's measured range. However, the infrared camera had a decreased probability of detecting blows at ranges beyond 2.1 km. Visual observers use handheld binoculars to search for whales, but detecting distant blows from a video is difficult due to decreasing image resolution as range increases. One solution to this problem would be to have multiple cameras optimized to monitor different ranges offshore. In addition an accurate automatic detector system needs to be created to detect blows so that: (1) blow rate can be calculated over the entire migration and (2) a more accurate cue rate can be calculated that can be used to estimate gray whale abundance. We found that a detector system created by Toyon Research Corporation was not consistent in that multiple runs of the detector resulted in different numbers of detections. Zitterbart et al. (2013) developed an automated infrared detector for a ship-based camera so perhaps something similar could be used for the land-based camera. Finally, we chose times when the environmental conditions were ideal to monitor for infrared detections. More effort should be spent to estimate the probability of detection when conditions are not ideal for infrared detection, such as days with high humidity, haze, or choppy seas.

Durban et al. (2017) reported that the 2014–2015 gray whale abundance model did not fit the visual sightings data well. Right-skewed daily abundance distributions pulled the abundance estimations higher and resulted in large probability intervals. We calculated the upper and lower bounds of cue rates using the bounds of the daily abundance values, but we recommend verifying cue rates across multiple years before substituting cue detection methods for visual observations to estimate abundance.

Cue rates are needed to estimate animal abundance from acoustic or infrared detections. In this study, we combined two alternative sensing methods with visual sightings to calculate cue

rates of migrating gray whales. Acoustics-based approaches are advantageous in poor visibility conditions, while infrared blow rates are likely more stable over time than calling rates. Changes in the number of animals that are in our search areas as well as probability of detection would shift our results. Acoustic receivers and infrared cameras have the benefit of being able to monitor at all times of the day and these methods can be automated so that detection algorithm performance can be quantified objectively. Initial effort must be dedicated to developing an automatic detector for cues and designing an appropriate survey, but infrared detectors and acoustic sensors have the potential of greatly improving marine mammal abundance estimates.

3.5 Methods

We combined three methods of sensing and observing gray whales. Visual observers counted whales as they migrated past the study site, hydrophones recorded the whale acoustic calls, and infrared cameras detected the temperature difference between the warmer whale blows and the surrounding water. The observation site was at the NOAA Granite Canyon facility located on Big Sur coast in central California. The continental shelf is about 4 km wide at this location, so it is an ideal place to census gray whales since they stay close to shore to migrate over the shelf. Figure 3.1 shows a map of the survey area.

3.5.1 Visual Sightings

Visual observers from the National Oceanic and Atmospheric Administration (NOAA) counted southbound gray whales from the shore at Granite Canyon during acceptable weather conditions for 34 days from 30 December 2014 to 13 February 2015. The visual observers were 22.3 m above sea level at 36° 26’ 23.61" N 121° 55’ 20.52" W. Raw counts were corrected for the estimated probability of visual detection and the estimated number of whales that passed when the visual observers were off-effort. A model was used to estimate the number of southbound

gray whales that migrated past per day over 90 days starting on 1 December. Durban et al. (2015) described the model used to estimate gray whale abundance from visual counts. Unfortunately the model for this migration season had large probability intervals, so we report uncertainty for cue rates using the 95% highest posterior density interval.

The offshore distribution of gray whales was calculated from visual sightings. For every southbound pod sighted in visibility and Beaufort conditions less than 5, we assumed the group size and direction were the last values recorded and estimated the distance offshore using the mean range for all sightings of that pod. The offshore distribution of gray whales from the visual sightings closely matched the offshore distribution from past aerial surveys (Shelden and Laake, 2002), so we concluded that the visual observers did not miss a greater proportion of whales at far distances.

3.5.2 Acoustic Recordings

Four bottom-moored hydrophones continuously recorded sounds offshore of the NOAA SWFSC visual and infrared survey site from November 2014 until June 2015. This work was completed under the Monterey Bay National Marine Sanctuary Research permit MBNMS-2014-039. Table 1 of Guazzo et al. (2017) lists locations and depths of the hydrophones. A Generalized Power Law Detector (GPL; Helble et al., 2012) detected potential calls in the acoustic data from each of the four hydrophones. All detections were manually verified to be gray whale calls by inspecting spectrograms across the four channels. Detections were localized using the time difference of arrival of the call on each hydrophone compared to the NE hydrophone. Raw call counts were corrected for the estimated probability of detection and localization within the search area based on acoustic propagation properties and background noise. Guazzo et al. (2017) presented a full description of the acoustic methods.

Modeled daily whale abundances from visual sightings (Durban et al., 2017) were combined with acoustic call counts using the calling rate calculations described by Guazzo

et al. (2017) and outlined in the Cue Rate Formulas section below. We did not correct the modeled abundance values for the previously assumed 8% difference in nighttime passage rate since we did not observe a diel change in mean speed or direction for acoustically tracked gray whales (Guazzo et al., 2017). The corrected call count was divided by the estimated number of whales that migrated through the hydrophone array and the time that they spent within the area of the array in order to calculate calling rates. We adjusted the 90% proportion of whales that we previously assumed swam through the array (Guazzo et al., 2017) to 68% using the offshore distribution of whales from the visual sightings. The time that a whale spent in the array is based on the mean measured swimming speed of acoustically tracked animals of 1.6 m/s (Guazzo et al., 2017). The calling rate was estimated every day that visual observers were on-effort. Because visual observers only included southbound whales in their daily estimates but calls may come from whales traveling southbound or northbound, the proportion of visually sighted southbound whales was multiplied with the corrected M3 call count to estimate the number of these calls that were produced by southbound whales. The percentage of southbound whales was above 80% until the last three sighting days when the percentage decreased to between 63–75% (Figure 3.3). This method assumes that southbound and northbound whales are calling at the same rate. A two-term power model of the form $f(x) = ax^b + c$ was fit to the daily calling rates where x=1 is 1 December. This model was selected because the predicted calling rate remained relatively constant for the days prior to the visual census start date, which we decided was the most realistic assumption during this time period. In addition, this model had a low summed square of residuals (SSE). To calculate the number of animals that migrated past Granite Canyon on 1–29 December 2014, we divided the estimated number of calls localized within the area of the array on each day by the modeled daily calling rate, the estimated proportion of animals within the array, and the time spent in the array (see Cue Rate Formulas).

3.5.3 Infrared Camera Detections

Three infrared cameras pointing at different angles offshore recorded video from December 2014 until June 2015 near the visual observers. The coordinates of the infrared cameras were 36° 26' 24.61" N 121° 55' 19.41" W. For the analysis in this paper, we use the data from the middle camera on 5–8 January 2015. These four days had simultaneous visual, acoustic, and infrared observations during good weather conditions with little wind. The center of the lens of the middle camera was 28.1 m above sea level. The camera was an FLIR F-606 model with a lens focal length of 100 mm and 640×480 pixel resolution (http://www.flir.com/security/display/?id=44258). The camera had a long-life, uncooled VOx microbolometer detector which sensed radiation with wavelengths of 7.5 to 13.5μm. The field of view was 6.2° in the horizontal direction and 5° in the vertical direction. The video had a sample rate of approximately 30 frames/s. These images were manually processed using software in which an analyst could watch the video and click on the location of each blow. The software is available on GITHUB (https://github.com/rguazzo/Whale-Blow-Logger). The pixel locations of the blow were converted into latitude and longitude by calculating range and azimuth. Range was computed by finding the angle of the blow from the horizon using linear interpolation of the vertical field of view of the camera and then using the geometry and equations detailed by Gordon (2001) to calculate the distance in meters. Azimuth of the blow was calculated by linear interpolation from the known angles of the edges of the video to the blow. These angles have an error +/-1° due to the potential influence of the metal visual observation shelter on the observer compasses.

In theory, the probability of detection for an infrared camera can be estimated in a similar way as probability of detection for an acoustic system. This probability is affected by the source characteristics or the temperature, size, and shape of a gray whale blow; the noise characteristics or glare from the sun and waves on the ocean; and the transmission loss which is affected by carbon dioxide and humidity since these molecules absorb infrared wavelengths (Baldacci et al., 2005). During the four days that the infrared camera detections were analyzed, visual observers

described calm seas so noise from waves was not a factor. However, accurate physics-based infrared propagation modeling was not possible since we did not have simultaneous sensors over the ocean measuring the aerosol content of the air. Instead, the color of the video frames was used to measure visibility. The RGB matrix of each video frame was converted into grayscale and the average color value for each row of pixels was calculated over the length of each video. The ability to detect a whale blow depends on the contrast of the light blow and the dark water which was quantified as the color variance across the vertical axis. During times of lower visibility, the water had a lighter color in the IR image and the variance across the vertical axis of the video frame was lower. We measured blows per second as a function of color variance across the vertical axis of the video frame to assess if the observed changes in variance affected the detectability of blows. The color variance was not a function of the number of blows detected, so we concluded that for these days, probability of detection was not impacted by visibility.

Probability of detection of a gray whale blow using the IR camera was, however, impacted by distance offshore. We plotted the cumulative number of blows versus range to evaluate the impact of range on detectability (Figure 3.5). If whales were randomly distributed and every blow was detected, the function should be linear with a positive slope equal to the density of blows. Since the probability of detection of visual sightings did not decrease with range, we compared the ranges at which the IR camera blow detections and the visual sightings became non-linear indicating that probability of detection after that point decreased due to range.

The number of detected blows from the infrared camera video were compared with the estimated number of whales from the visual sightings. This comparison was done on two different timescales. First, we compared the number of blows detected from 07:30–16:30 each day, the same time visual observers were on effort. We corrected these counts for the brief periods of time in between adjacent video files and compared these blow counts with the raw visual counts in several offshore range bins. We also compared full day blow counts with modeled median whale abundances and their associated uncertainties (95% highest posterior density intervals;

Durban et al., 2017). Infrared camera blow counts were divided by the area of each bin and then multiplied by the average arc length for whales traveling through that bin. Visual counts and modeled abundances were divided by the width of each offshore range bin. In this way, all counts were in units of detections per distance offshore. We multiplied the estimated number of whales for each day (and its associated uncertainties) by the proportion of whales seen migrating in each range bin. This method assumes that whales were not changing their distribution at nighttime, which we confirmed using acoustically tracked gray whales (Guazzo et al., 2017).

Gray whale blow rate was calculated in a similar way as call rate. The number of blows within the search area was divided by the number of whales estimated to migrate through that search area and the average time it takes to travel through the area. We used the visually-determined distribution of whales on the same four days as the infrared camera videos to estimate the proportion of whales within the search area. To calculate the time spent in the search area, we used the range of sighted whales and calculated the arc length within the camera field of view. We divided the arc length by the average swimming speed calculated by Guazzo et al. (2017) to estimate average time within the field of view. The Cue Rates Formulas section presents the equations used in these calculations in detail.

3.5.4 Cue Rate Formulas

Cue rate (for both call rate and blow rate) was estimated as

$$\widehat{r}(t) = \frac{\widehat{N}_C(t)}{\widehat{N}_W(t)\ \widehat{P}_{SA}\ \widehat{\overline{t}}_{SA}} \tag{3.1}$$

where $\widehat{N}_C(t)$ is the estimated number of cues that occur in the search area during a certain time period (usually 1 day) as a function of time, $\widehat{N}_W(t)$ is the estimated number of whales present from the abundance model during this same time period as a function of time, $\widehat{P}_{SA}$ is the estimated proportion of whales that are in the search area based on visual sightings, and $\widehat{\overline{t}}_{SA}$ is

the estimated average amount of time a whale spends in the search area, . The units for cue rate are cues/whale/unit time.

The number of cues $\hat{N}_C(t)$ was estimated using the number of raw cues detected and the probability of detection. For acoustic calls and using nomenclature very similar to that used by Marques et al. (2009)

$$\widehat{N}_C(t) = n_c(t)\frac{1 - \widehat{c}_N(t)}{\widehat{P}_L(t)\,(1 - P_{NE})} \tag{3.2}$$

where $n_c(t)$ is the number of raw calls detected and localized, $\hat{c}_N(t)$ is the estimated proportion of northbound and milling whales, $\widehat{P}_L(t)$ is the estimated probability of localization, and P_{NE} is the proportion of time with no effort. Since only southbound whales were included in the visually estimated daily abundance, calls from whales swimming northbound or milling represent false alarms. The estimated proportion of northbound and milling whales, $\hat{c}_N(t)$, was determined from visual records of the bearing of all sighted gray whales. Guazzo et al. (2017) described methods used to estimate probability of localization $\widehat{P}_L(t)$. To summarize, 100 source level realizations were randomly selected from the probability distribution of source levels estimated in the paper. For each of these source levels, transmission loss was calculated across an (x,y) grid of source locations to each hydrophone (Guazzo et al., 2017), noise level was calculated for each hydrophone for each minute of recording, and the received signal to noise ratio (SNR) was calculated for the i-th hydrophone as

$$SNR_{dB}(x, y, i, t) = SL_{dB} - TL_{dB}(x, y, i) - NL_{dB}(i, t) \tag{3.3}$$

We took the minimum SNR across the four hydrophones and calculated the proportion of the 100 source level realizations with SNRs greater than the 0.5 dB detection threshold to get $\widehat{P}_L(x, y, t)$. We then averaged over the search area to get $\widehat{P}_L(t)$. If $\widehat{P}_L(t)$ <0.5, any calls detected in that minute were not included in the total $n_c(t)$ and that minute had no effort. The proportion of minutes in a day with no effort was P_{NE}.

Durban et al. (2015, 2017) derived the estimated number of whales per day $\widehat{N}_W(t)$. The daily abundance estimates were not corrected for a different nighttime passage rate since acoustic tracks for this migration season indicated the migration rate was the same at night and day (Guazzo et al., 2017).

The average amount of time for a whale to travel through the acoustic search area $\widehat{\bar{t}}_{SA}$ was estimated by dividing the average distance traveled through the search area by 1.6 m/s, the mean speed estimated from acoustic tracks (Guazzo et al., 2017). For the acoustic recordings, $\widehat{\bar{t}}_{SA}$ = 23.75 min (Guazzo et al., 2017).

The number of estimated blows was calculated using

$$\widehat{N}_C(t) = n_b(t)\frac{1}{\widehat{P}_D(t)\,(1 - P_{NE})} \tag{3.4}$$

where $n_b(t)$ is the raw number of blows detected, $\widehat{P}_D(t)$ is the estimated probability of detection, and as before, P_{NE} is the proportion of time with no effort. Since the blows were detected in the infrared video by a human operator and these four days with infrared detections are well before the northbound migration, the probability of false detection, $\hat{c}$, was zero. Also, for whales with ranges $\leq$ 2.1 km, $\widehat{P}_D(t) = 1$. No blow detections less than 500 m or farther than 2.1 km were included in $n_b(t)$. Short time gaps existed between adjacent video files, resulting in a total proportion of minutes with no video data, P_{NE}. The average amount of time for a whale to travel through the IR search area $\bar{t}_{SA}$ was estimated using the range (r) distribution of visually sighted whales, $n_W(r_j)/\sum_j n_W(r_j)$, and the IR camera's 6.2° horizontal field of view

$$\widehat{\bar{t}}_{SA} = 2\pi\frac{6.2^\circ}{360^\circ}\sum_j\left(\frac{n_W(r_j)}{\sum_j n_W(r_j)}\,\frac{r_j}{s}\right) \tag{3.5}$$

where s=1.6 m/s. For the IR camera recordings, $\widehat{\bar{t}}_{SA}$ = 1.7 min.

Finally cue rates (calling rates in this paper) were used to estimate the number of whales

using

$$\widehat{N}_W(t) = \frac{\widehat{N}_C(t)}{\widehat{r}(t)\ \widehat{P}_{SA}\ \widehat{\bar{t}}_{SA}} \tag{3.6}$$

3.6 Acknowledgements

R.G. was awarded the SMART Scholarship, funded by USD/R&E (The Under Secretary of Defense-Research and Engineering), National Defense Education Program (NDEP) / BA-1, Basic Research. J.H. received support for the acoustic array from the U.S. Army Corps of Engineers using funds provided by the U.S. Navy's Pacific Fleet through the Cooperative Ecosystem Studies Units (Grant Number W9126G-15-2-003; http://www.cesu.psu.edu/). The authors would specifically like to thank Chip Johnson from Pacific Fleet. This work would not have been possible without the efforts of the NOAA visual observers from Southwest Fisheries Science Center (Lisa Ballance, Bob Brownell, Susan Chivers, Paul Fiedler, Aimee Lang, Morgan Lynn, Vicki Pease, Wayne Perryman, Jeremy Rusin, and Mridula Srinivasan). Kevin Sullivan of Toyon Research Corporation helped design, deploy, and troubleshoot the IR camera system and provided information about the camera system specifications. Funding to Toyon Research Corporation for the development and deployment of the IR camera system was provided by the National Oceanic and Atmospheric Administration (NOAA) Program for Small Business Innovation Research (SBIR). Wayne Perryman, Kelly Jacovino, and Morgan Lynn were instrumental in all aspects of running and maintaining the IR camera system during field operations. We thank Sean Wiggins, Ryan Griswold, and the other members of the Scripps Whale Acoustics Lab for designing, building, deploying, and recovering the hydrophone-recorder packages. Jay Barlow, Sarah Creel, Tyler Helble, James Nieh, Joel Norris, Mark Ohman, Lynn Russell, and members of the Scripps Whale Acoustics Lab provided useful feedback about the data analysis.

Chapter 3, in full, has been submitted for publication in *Scientific Reports*, Regina A. Guazzo, David W. Weller, Hollis M. Europe, John W. Durban, Gerald L. D'Spain, and John

A. Hildebrand, "Migrating eastern North Pacific gray whale cue rates estimated from acoustic recordings, infrared camera images, and visual sightings." The dissertation author was the primary investigator and author of this paper.

Chapter 4

Gray Whale Migration Patterns Through the Southern California Bight from Multi-Year Visual and Acoustic Monitoring

4.1 Abstract

Eastern North Pacific gray whale (*Eschrichtius robustus*) sightings and acoustic recordings from the Southern California Bight during seven migration seasons were analyzed for interannual changes and compared with concurrent environmental measurements. Acoustic call counts did not follow a clear trend over these years. Using a calling rate of 7.5 calls/whale/day, in most years, less than 10% of the population migrated within the 20-km detection range of the offshore hydrophone. Estimated number of gray whales migrating off Santa Barbara and Los Angeles exponentially grew at a greater rate (0.11 and 0.26, respectively) than the population size growth rate (0.05). This finding indicates that over these migration seasons, an increasing proportion

of the population was using the nearshore migration corridor in the Southern California Bight, especially near Los Angeles, which could increase the negative anthropogenic impact on this species. Although several climatic events including El Niño and La Niña occurred between 2008 and 2016, neither water temperature in the Southern California Bight nor sea ice freeze and melt timing in the gray whale Arctic feeding area improved generalized additive models of gray whale presence or numbers at the acoustic or visual monitoring sites. Over these times, the gray whale migration timing appears to be driven more by their biological clock and instinct than by the extrinsic factors accounted for in the present analysis. Future work should test other potential influencers on the gray whale migration over longer timescales.

4.2 Introduction

Eastern North Pacific gray whales (*Eschrichtius robustus* Lilljeborg) annually migrate from the Arctic and subarctic waters of the Bering, Chukchi, and Beaufort Seas where they feed in the summer to the subtropical waters of the Pacific lagoons of the Baja California Peninsula, Mexico where they spend the winter. Their migration path is along the continental shelf for most of the route, but in the Southern California Bight many gray whales move offshore and travel through the Channel Islands (Carretta et al., 2000; Sumich and Show, 2011). Gray whales are dependent on the high latitude benthic-dominated ecosystem for feeding and low latitude warm lagoons for nursing calves and mating and as a result may be especially sensitive to environmental change and variation across their range.

Arctic amplification of climate change, or the greater temperature increase at high latitudes compared to low latitudes, could especially impact gray whales. Gray whales primarily eat benthic, tube-dwelling amphipods, which had high population densities in the Chirikov Basin in the northern Bering Sea between at least the 19th-century whaling period and the 1980s (Highsmith and Coyle, 1991). *Ampelisca macrocephala* (Liljeborg) is the dominant species

in this area and in the gray whale diet (Rice and Wolman, 1971; Highsmith and Coyle, 1991). These amphipods live 5–6 years and females begin producing one brood per year at 4–5 years old, so fewer, larger individuals make up most of the production (Highsmith and Coyle, 1991). The female amphipods brood their young and release juveniles directly into the adult habitat with no larval stage (Highsmith and Coyle, 1991). *A. macrocephala* primarily eat diatoms that sink from the phytoplankton bloom and opportunistically consume larvae of sand dollars which compete for their habitat (Highsmith and Coyle, 1991). The number of eggs produced by a mature female is positively related to the female size and female size at maturity is negatively related to water temperature (Highsmith and Coyle, 1991). *Ampelisca spp.* biomass in the Chirikov Basin declined by almost 50% between the 1980s and 2002–2003 due to fewer large animals in the population (Coyle et al., 2007). This amphipod decline could have been because of top-down control by more gray whale predators and/or climate change affecting the organic carbon flux to the benthos (Coyle et al., 2007).

Arctic sea ice is decreasing and the decrease is accelerating. Monthly anomalies of sea ice extent decreased by 4% per decade from 1978–2010 and over 8% per decade from 1996–2010 (Comiso, 2012). September, the middle of the gray whale summer feeding period, is the month with the least sea ice cover and the most dramatic decrease over this observation period (Comiso, 2012). Although the rest of the Arctic is losing sea ice, the Bering Sea, where gray whales travel through and may feed, is gaining ice (Comiso, 2012). Sea ice is also impacted by shorter timescale variation. A positive phase of the Arctic Oscillation (AO) index corresponds with increased sea ice in the Bering, southern Chukchi, and Beaufort Seas, while a positive phase of the El Niño Southern Oscillation (ENSO) index corresponds with decreased sea ice in the Chukchi and southern Beaufort Seas (Liu et al., 2004). Both of these climate oscillations are higher frequency trends compared to the lower frequency and declining trend of Arctic sea ice (Liu et al., 2004).

A reduction in Arctic sea ice will likely result in an ecosystem shift. Sea ice cover

influences the strength of pelago-benthic coupling, which has resulted in highly productive benthic biomass regions (Piepenburg, 2005). When sea ice lasts into spring, an ice-associated phytoplankton bloom quickly sinks due to low zooplankton abundance. When sea ice melts earlier, the phytoplankton bloom occurs later when zooplankton are abundant and consume the bloom (Overland and Stabeno, 2004). Decreased sea ice may cause the Arctic to shift from a benthic-dominated ecosystem to a pelagic-dominated ecosystem (Overland and Stabeno, 2004; Piepenburg, 2005). Since Arctic amphipods have relatively long-lifespans, their populations may not be as impacted by interannual variations in sea ice, but more impacted by long-term negative trends in sea ice and positive trends in temperature, affecting the number of individuals that survive to maturity and the size of annual broods. Over time, decreased sea ice, warmer temperatures, and an Arctic ecosystem shift have the potential to negatively affect the gray whale population if they are not able to switch to a different prey source.

The gray whale migration has been monitored since the 1960s as the population has recovered from over-exploitation. Most monitoring has been in the form of shore-based visual censuses along their migration route. The most long-term studies have been at Granite Canyon (e.g. Buckland et al., 1993; Durban et al., 2015), Piedras Blancas (e.g. Perryman et al., 2010), Santa Barbara (www.graywhalescount.org), and Point Vicente (https://acs-la.org/GWCensus.htm), all in central and southern California. Aerial surveys have also been conducted over parts of the migration route, with two sets of surveys of the migration through the Southern California Bight in 1988–1990 by Sumich and Show (2011) and 1998–1999 by Carretta et al. (2000). In the Southern California Bight, some of the gray whale population maintains a coastal migration route, while the majority of the population migrates through the Channel Islands according to aerial surveys, using routes around the western sides of Santa Catalina and San Clemente Islands (Sumich and Show, 2011). Around San Clemente Island, daily averages of over 400 animals migrating in both directions were estimated between January and April in 1999 (Carretta et al., 2000). However, high interannual variability exists in the numbers of whales on each migration

route (Sumich and Show, 2011) and so population size estimates are challenging using data from sites in southern California alone.

Passive acoustic monitoring can be used to measure marine mammal presence in remote locations for many years with lower effort than visual surveys. While migrating, gray whales primarily make M3 calls. These calls are 1.8 s in duration with a mean frequency of 48 Hz and a root mean square source level of 157 dB re : 1μPa at 1 m (Guazzo et al., 2017). By quantifying the number of calls produced as a function of time, we can understand the seasonal cycle of the gray whale migration.

Gray whale mortality may be linked to environmental change. One of the most notable examples occurred in 1999 and 2000 when there was an unusual mortality event of gray whales, many of which were emaciated (Gulland et al., 2005). In 1998 and 1999, the fewest female-calf pairs were counted in the Mexico wintering lagoons compared to other visual surveys conducted (1978–1982, 1996–1999) (Urbán-Ramírez et al., 2003). It is unclear whether the unusual mortality event was due to the strong El Niño Southern Oscillation (ENSO) event, sea ice conditions, high population density of gray whales, or a combination of factors (Gulland et al., 2005). Coincidental with this mortality event, in 2000 and 2001, gray whale sightings around Kodiak Island, Alaska were significantly higher than other years in a five-year aerial survey (Moore et al., 2007). Gray whales may have altered their migration and foraging pattern in response to a low food supply and opportunistically foraged along their migration route on lower-quality prey (Moore et al., 2007).

Gray whales may shift the timing and spatial distribution of their migration as a result of climatic change. The Pacific Decadal Oscillation (PDO) changed phases in the late 1970s from a negative phase to a positive phase (Mantua and Hare, 2002). Concurrent with this phase change, the median date of the southbound migration shifted about a week later for sightings after 1987/1988 compared to those before 1980 (Rugh et al., 2001). This change in migration timing could be due to a decrease in benthic amphipod biomass in the gray whale foraging areas of the

Chirikov Basin from the 1980s to 2000s causing the gray whale foraging range to expand north (Moore et al., 2003; Coyle et al., 2007). Currently the central feeding area for the eastern North Pacific gray whales is in the Chukchi Sea along the continental shelf between Point Lay and Point Barrow where their presence is correlated with high abundances of amphipods (Schonberg et al., 2014; Brower et al., 2017). If gray whales swim farther north to find suitable prey, they will also need to consume more calories to sustain their journey to and from the southern wintering areas.

Fecundity of gray whales is particularly affected by the availability of important feeding areas during the previous summer. More calves are born after summers with more ice-free days and fewer calves after summers with fewer ice-free days indicating that females may be less likely to carry their pregnancy to term when they have less time to feed (Perryman et al., 2002; Salvadeo et al., 2015). These studies measured interannual fluctuations in sea ice, but it is unknown how gray whales will be affected by long-term negative trends in sea ice. Once pregnant females reach Mexico, the oceanic conditions may impact which breeding lagoon gray whales choose. When the sea surface temperature was warmer during an El Niño, more females with calves were in the northernmost lagoon, but when the temperature was cooler during a La Niña, more females with calves were in the southernmost lagoon (Gardner and Chávez-Rosales, 2000; Salvadeo et al., 2015). Additionally, since 1980, more gray whale calves have been sighted during the southbound migration north of the Mexican lagoons (Shelden et al., 2004). This northward shift in birthing location could be due to warmer temperatures forcing gray whales to travel farther north to feed, increasing the length of their migration, and forcing pregnant gray whales to give birth before they reach Mexico (Shelden et al., 2004). PDO and ENSO climatic cycles as well as sea ice cover affect the timing and distribution of the gray whale annual migration and the population health.

The eastern North Pacific population of gray whales had an abundance of 26,960 in 2015–2016 (Durban et al., 2017) and is no longer considered endangered under the U.S. Endangered Species Act. However, it is uncertain how these migratory whales, which are so dependent on the

Arctic benthos and Mexican lagoons, will respond to climate change. To investigate the effects of climate on the annual variations in the migration and to understand the gray whale migration around the Channel Islands, we analyzed seven migration seasons of acoustic data recorded north of San Clemente Island and visual sightings from Los Angeles and Santa Barbara in southern California. This paper describes the timing and variability of the acoustic and visual records of the gray whale migration through the Southern California Bight and evaluates various signals that may influence the migration.

4.3 Materials and Methods

4.3.1 Passive Acoustic Call Detections

Single-hydrophone, high-frequency acoustic recording packages (HARPs) (Wiggins and Hildebrand, 2007) were deployed at approximately 33.5° N and 119.25° W (Figure 4.1) and recorded continuously. These bottom-moored devices were about 900 m deep, 90 km southwest of Los Angeles and 80 km northwest of San Clemente Island. For this analysis, we used data from deployments from each gray whale migration season from 2008–2009 through 2014–2015. Dates, positions, and seafloor depths for each deployment are listed in Table 4.1. The HARPs recorded with a sampling rate of 200 kHz and we decimated the data to a sampling rate of 2 kHz for an effective bandwidth of 10 to 1,000 Hz. A Generalized Power Law (GPL) detector (Helble et al., 2012) with parameters optimized for gray whale M3 calls (Guazzo et al., 2017) identified potential calls in the fast Fourier transformed data (1024 sample FFT length, 95% overlap). M3 call spectrograms were then visually verified by an experienced analyst (RAG).

To estimate probability of detection for the HARPs, we modeled transmission loss using the Peregrine parabolic equation propagation model (Heaney and Campbell, 2016; Heaney et al., 2017). Sediment thickness at the HARP location is about 300 m (5-arc minute resolution; Whittaker et al., 2013), but a sediment thickness of 200 m was used in the Peregrine model, which

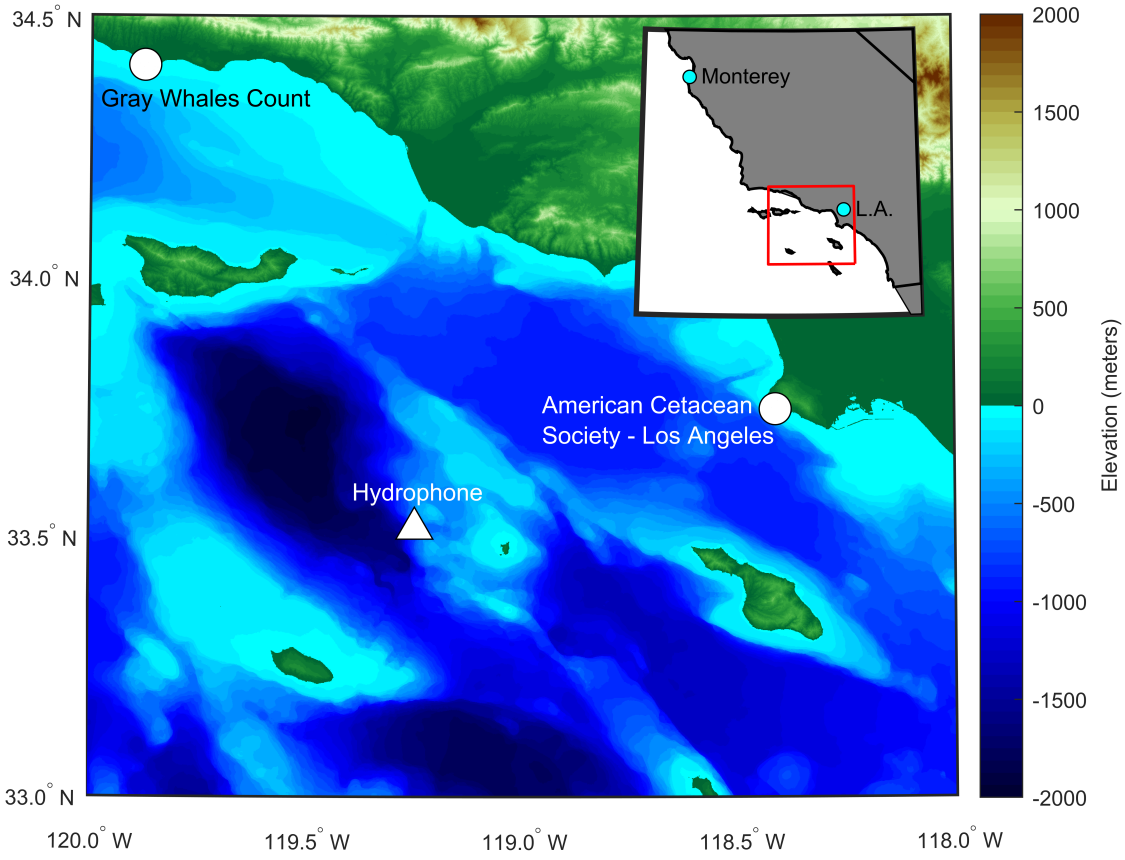

Figure 4.1: Map of Gray Whale Monitoring Locations. The study area is in the Southern California Bight as denoted by the red box in the inset map. The acoustic recording location is marked with a white triangle and the visual census locations are marked with white circles. For reference, Santa Barbara Island, the small island east of the hydrophone, is about 20 km from the hydrophone. Variations in hydrophone deployment locations are too close to be seen on this map. Colors indicate land elevation and seafloor depth with respect to sea level (NOAA National Centers for Environmental Information's Southern California Coastal Relief Model, 3 arc-second resolution).

Table 4.1: Deployment Locations of High-Frequency Acoustic Recording Packages. Although each deployment was intended to be in the same location, there was some variability. Seafloor depths are in meters.

Migration Season	Dates	Latitude	Longitude	Depth
2008–2009	Jan 2009–Mar 2009	33°30.582′ N	119°15.282′ W	895
2008–2009	Mar 2009–May 2009	33°30.579′ N	119°15.280′ W	1,123
2009–2010	Dec 2009–Jan 2010	33°30.937′ N	119°14.798′ W	912
2009–2010	Jan 2010–Mar 2010	33°30.915′ N	119°14.690′ W	891
2010–2011	Dec 2010–Apr 2011	33°30.897′ N	119°14.888′ W	919
2011–2012	Nov 2011–Mar 2012	33°30.886′ N	119°14.869′ W	927
2012–2013	Dec 2012–Apr 2013	33°30.599′ N	119°15.305′ W	907
2013–2014	Sep 2013–Jan 2014	33°30.584′ N	119°15.252′ W	917
2013–2014	Jan 2014–Apr 2014	33°30.577′ N	119°15.251′ W	877
2014–2015	Nov 2014–Feb 2015	33°30.837′ N	119°14.943′ W	900

is valid since the longest wavelengths of gray whale calls are much less than the sediment thickness. The winter sound speed profile was created from an average of typical winter conditions. The sound speed at the surface was about 1500 m/s and decreased to 1490 m/s at depths below 40 m.

We used a Monte Carlo method to insert a high signal-to-noise ratio (SNR) M3 call, which was assumed to have the characteristics of a source call, into 272 randomly selected 75-s samples of background noise from the December 2012–April 2013 deployment. Using the transmission loss calculated by the Peregrine propagation model, we modeled calls received by the HARP for source depths of 10 m and ranges out to 50 km. Bearing increments were 5° and range increments were 450 m. We determined probability of detection over the search area as a function of range and noise level by comparing GPL detections from random noise samples with and without the modeled received call. Probability of detection of gray whale M3 calls was approximately zero at ranges beyond 20 km, so we assume a search area radius of 20 km and all probability of detection versus noise level values are for this search area. A power model

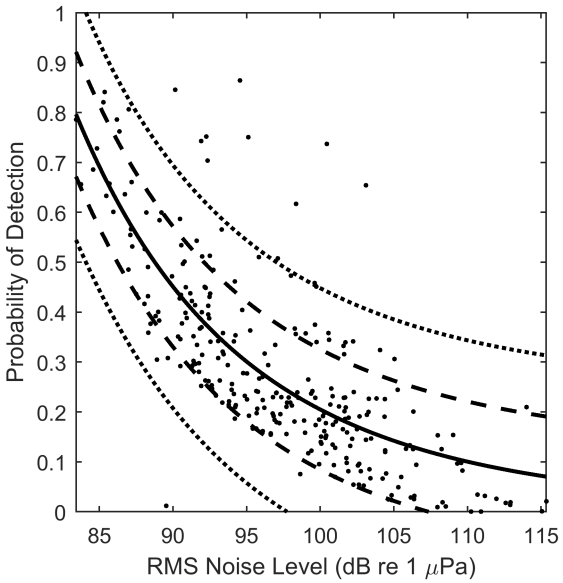

Figure 4.2: Monte Carlo-Generated Samples of Probability of Detection Versus Noise Level. 272 75-s noise samples were randomly selected from the December 2012–April 2013 deployment. Noise level was integrated over the 20–100 Hz band. The y-axis represents the proportion of source locations within a 20 km range at which an M3 call generated was successfully detected by the generalized power law (GPL) detector. A power model was fit to these data points. 67% (dashed lines) and 95% (dotted lines) prediction intervals are shown (non-simultaneous observation bounds).

($y = ax^b$) was fit to the Monte Carlo-generated samples of probability of detection as a function of root mean square (RMS) noise level integrated over the 20–100 Hz band (Figure 4.2).

RMS Noise Level was calculated for every 75-s period of recording and was used to estimate probability of detection during that time period. Numbers of M3 calls detected in each 75-s period were divided by the probability of detection to generate estimated number of calls in that period. Time periods with noise levels greater than 100 dB re re : 1μPa were excluded from analysis and daily counts were adjusted for total time without effort. If noise levels were less than or equal to 100 dB re re : 1μPa, effort was zero for 7 seconds out of every 75 to account for periods of HARP disk write noise. Estimated total number of M3 calls for each day was then

$$N_C(t) = \sum_j \left(\frac{n_c(t_j)}{\widehat{P}_D(t_j)} \right) \frac{1}{(1 - P_{NE}(t))} \tag{4.1}$$

where j is the number of 75-s periods with noise levels less than or equal to 100 dB re : 1μPa, n_c is the number of detected calls in each 75-s period, $\widehat{P}_D$ is the estimated probability of detection in that 75-s period, and P_{NE} is the proportion of time in a day with no effort. The 100 dB threshold was chosen since calls detected above this threshold would most likely have been produced in the near-field and transmission loss may not be accurately predicted for this range. Probability of false alarm was assumed to be zero since all calls were manually verified to be gray whale M3 calls, however, if any calls were detected from outside of the 20 km search area, these calls would represent false alarms.

Acoustic hourly presence or absence can also quantify calling periods and is less influenced by calling rate. Guazzo et al. (In Review) showed that gray whale calling rate varies substantially over a migration season. Presence or absence of gray whale M3 calls for every hour of recording was saved together with the mean probability of detection during that hour.

4.3.2 Sightings

Visual censuses were completed annually by two organizations in southern California (Figure 4.1). The American Cetacean Society - Los Angeles Chapter Gray Whale Census and Behavior Project (ACS/LA census) is located on the Palos Verdes Peninsula in Los Angeles County, California (33°44.688' N 118°42.709' W), 41.8 m above sea level. Gray Whales Count (GWC census) is located on Counter Point (or Coal Oil Point) part of the University of California Natural Reserve System in Santa Barbara County, California (34°24.432' N 119°52.701' W), 14.2 m above sea level.

ACS/LA census observers counted both southbound and northbound gray whales from 1 December until the middle or end of May for approximately 12 hours each day, sunrise to sunset (up to 1800). Whales from the coast to about 8.6 km were tracked over a 145° field of view. Total number of whales as well as number of hours on-effort were reported for each day. Single whales were differentiated from female-calf pairs. Whales were differentiated by direction and

calves were noted migrating in both directions. Visual observations continued regardless of environmental conditions (however, some days ended early due to poor conditions) and all times with observations were on-effort. During each watch period, a minimum of 2 and a maximum of 6 observers, including the project coordinator (ASJ) or a seasoned observer, were on-effort.

GWC census observers recorded sightings of all northbound gray whales from the beginning of February until the end of May from 0900 to 1700 daily. Whales from the coast to about 5.6 km were tracked over a 200° field of view. The total number of northbound whales as well as number of hours on-effort were reported for each day. Single northbound whales were differentiated from female-calf pairs. Only times with adequate visibility and sea conditions (<5 Beaufort Sea State) were included as on-effort. During each watch period, a minimum of 2 and a maximum of 5 observers, including the project coordinator (MHS), were on-effort.

To estimate daily (24-hour) numbers of whales at each site and assess the patterns in each year's data, gray whale daily counts were divided by the proportion of the day on-effort.

$$N_W(t) = n_w(t)\frac{1}{(1 - P_{NE}(t))} \tag{4.2}$$

Because perfect detection during on-effort times is unrealistic, all visual daily counts of whales are minimum counts. GWC annual northbound counts were separately corrected to account for probability of detection in the same way as described by Durban et al. (2015). These corrections result in an annual single gray whale estimate and an annual mother-calf estimate that migrated past Santa Barbara. The annual modeled counts were used to analyze interannual changes in numbers of whales, which is described further in the Interannual Comparison section.

In addition to these southern California survey efforts, we incorporated population abundance estimates from the National Oceanic and Atmospheric Administration's (NOAA's) Granite Canyon gray whale census. These estimates have been published by Durban et al. (2015) and Durban et al. (2017). In this way, we were able to compare count trends at each southern

California site with the overall population trends. These methods are described further in the Interannual Comparison section.

4.3.3 Environmental Measurements

Satellites use microwave radiation to measure the percent of a given area covered by sea ice. The Advanced Microwave Scanning Radiometer (AMSR) instruments sense microwave emission from the earth's surface and are not affected by cloud cover (Kawanishi et al., 2003). Daily measurements of 89 GHz center frequency were converted into sea ice concentration using the ARTIST Sea Ice (ASI) algorithm with 6.25-km grid resolution (Spreen et al., 2008). The AMSR-E instrument transmitted data from May 2002–October 2011 and the AMSR-2 instrument has been transmitting data since May 2012.

To calculate mean daily sea ice concentrations over the gray whale feeding area, we used Windows Image Manager (WIM) and WIM Automation Module (WAM) (Kahru, 2001). We averaged the daily sea ice concentrations over the feeding area from Dease Inlet, east of Point Barrow, to Cape Lisburne covering the area from about 20–120 km from shore. This area was chosen based on gray whale aerial sighting data reported by Brower et al. (2017). We estimated the melt date as the date in the spring when the average sea ice concentration dropped below 90% and the ice-over date as the date in the fall when the average sea ice concentration across the feeding area increased above 10%. The length of the ice-free season was

$$L_{IF} = D_F - D_M \tag{4.3}$$

where D_F is the calendar date of the fall freeze and D_M is the calendar date of the spring melt. The freeze and melt dates are not necessarily cut-offs for gray whale feeding, instead they are markers for when the spring melt and fall freeze began.

The California Cooperative Oceanic Fisheries Investigations (CalCOFI) collect

oceanographic measurements and samples on quarterly cruises along transects that are perpendicular to the coast (http://calcofi.org/). We averaged the temperatures of the upper 10 m of the water column from the winter cruises of 2009–2015 to estimate temperatures that gray whales experienced while migrating. "Offshore" temperature was measured less than 10 km from the hydrophone at station 86.7/45 (33.48953°N 119.31910°W), "Nearshore" temperature was measured along the northern edge of the Palos Verdes Peninsula at station 86.7/33 (33.88953°N 118.49033°W), and "Point Conception" temperature was measured at station 80/50.5 (34.46667°N 120.48906°W) (station 80/51.0 at 34.45000°N 120.52390°W for the 2015 cruise) where southbound migrating gray whales select either an offshore route through the Channel Islands or a nearshore route. No temperature measurements were available at or near Point Conception in 2014.

4.3.4 Interannual Comparison

To test if the same proportion of gray whales use the different southern California migration routes annually, we compared the growth rate observed at sites in southern California with that estimated from NOAA's gray whale population census. If a constant proportion of gray whales was using the nearshore route, the growth rate of estimated nearshore whales should equal the population size growth rate. However, if the proportion of gray whales using the nearshore route was increasing over time, the growth rate for sightings off the nearshore sites would be greater than the population growth rates, but if the proportion of gray whales using the nearshore route was decreasing, the growth rate for sightings would be less than the population growth rate.

The eastern North Pacific gray whale population size was estimated by NOAA several times over this study period (Durban et al., 2015, 2017). Observers counted southbound migrating gray whales at Granite Canyon in central California in 2009–2010, 2010–2011, 2014–2015, and 2015–2016. Counts were later converted into estimated population sizes based on probability of detection and effort parameters (Durban et al., 2015). Although the 2015–2016 migration was

not included in our Southern California Bight analysis, we included this year in our population trend estimate to increase the sample size and precision of the trend due to lower precision of the 2014–2015 estimate.

We fit the population size and Southern California Bight observations with an exponential model

$$dN/dt = rN \tag{4.4}$$

$$N = N_0\, e^{rt} \tag{4.5}$$

where N is the annual counts, r is the growth rate, t is the start year of the migration, and N_0 is the count for t=0. To test if the differences between growth rates were significant, we used Analysis of Covariance (ANCOVA) of the linear form of the exponential model

$$\ln N = rt + C \tag{4.6}$$

where C is lnN_0.

For the acoustic hydrophone detections and visual sightings off Los Angeles, annual counts were calculated from the same days across all years so that a change in number was not due to effort. The days were chosen based on the first and last dates that all years had in common. The number of calls or sightings during gaps in effort within these days were estimated using shape-preserving piece-wise cubic interpolation. Raw daily gray whale ACS/LA census sightings were corrected by dividing the counts by the proportion of the day on-effort. Acoustic call counts were corrected for probability of detection based on the Peregrine propagation model (Figure 4.2). Confidence intervals were estimated using the 67% prediction interval bounds for the noise level versus probability of detection data. We used the upper and lower bounds of probability of detection for each noise level measurement to calculate the estimated number of calls. Annual sightings of gray whales off Santa Barbara used similar methods as the NOAA census at Granite

Canyon and were corrected for probability of detection using the model described by (Durban et al., 2015). This model corrects for probability of detection, primarily influenced by visibility and number of whales passing at a time, and makes assumptions about the number of whales passing during off-effort times.

Acoustic calling rate may be more variable between years than cues used to recognize gray whales visually. It is unknown if or how gray whale calling rate changes over time, but humpback whales migrating off the coast of Australia have decreased their singing rate as their population size has increased (Noad et al., 2017). Gray whale calling rate was estimated by Guazzo et al. (In Review) to be 7.5 calls/whale/day at Granite Canyon averaged over the entire migration season. If we assume this calling rate for all years, we can estimate the number of gray whales that migrated within a 20 km radius of the hydrophone.

$$\widehat{N}_W = \frac{\widehat{N}_C}{\widehat{r}\,\widehat{\bar{t}}_{SA}} \tag{4.7}$$

where $\widehat{r}$ is the calling rate and $\widehat{\bar{t}}_{SA}$ is the estimated amount of time spent in the search area estimated as the average distance through the search area divided by the mean speed. Using the Mean Value Theorem, the average distance through search area is

$$\frac{\int_0^{2\pi} 2R\,\sin\frac{\theta}{2}\,d\theta}{2\pi} \tag{4.8}$$

which is $80/\pi$ km for R=20 km. Acoustically tracked gray whales migrate with an average speed of 1.6 m/s (Guazzo et al., 2017), so we estimate that migrating whales spent on average about 4.4 hours within the detection range of the instrument.

Finally, we compared observed changes in sea ice melt and freeze timing in the gray whale feeding area and changes in ocean temperature in southern California with known climate patterns observed over the same time.

4.3.5 Generalized Additive Model Regression Analysis

We hypothesized that interannual changes in sea ice in the Arctic feeding areas and local temperature along the gray whale migration route may affect the gray whale migration through the Southern California Bight. To test this hypothesis, we used Generalized Additive Models (GAMs; Hastie and Tibshirani, 1990) which model a link function of the response variable (y) as the sum of non-linear functions of the predictor variables (x)

$$link(y_i) = \alpha + \sum_j f_j(x_j) + \epsilon_i \tag{4.9}$$

We used the R GAM package 'mgcv' with gamma=1.4 to avoid over-fitting (Wood, 2006) and evaluated potential models with Akaike's information criterion (AIC).

Acoustic M3 call hourly presence and visual daily gray whale counts were tested as response variables (Table 4.2). These response variables were tested using several different temporal groupings in case the predictor variables impacted one phase of the migration more than the other. Since migration direction cannot be determined from single hydrophone acoustic data, acoustic models tested predictor variable effects on the full migration season, the first half of the migration (mostly southbound migrators), and the second half the migration (mostly northbound migrators, acoustic data not available for 2014–2015). The date that started the second half of the migration was determined using the ACS/LA census visual counts and was defined as the first day when the northbound count exceeded the southbound count for at least two days in a row. Models with visual daily counts as the response variable were fit separately for the two different sighting efforts (ACS/LA and GWC censuses). The ACS/LA census monitored both the southbound and northbound migrations so models tested predictor variable effects on the full migration, southbound whales, northbound whales, and northbound calves. The GWC census only monitored the northbound migration so models tested predictor variable effects on the full northbound migration, northbound single adults, and northbound calf counts. Counts and hourly

presence or absence were not corrected for effort or probability of detection and instead these values were included as predictor variables.

Table 4.2: Response Variables Used in Generalized Additive Models.

Method	Variable	Family	Link Function
Acoustic M3 Call Detections	Hourly Presence	Binomial	Logit: $\log \frac{\mu}{1-\mu}$
Gray Whale Sightings	Daily Count	Poisson	Log: $\log \mu$

Several predictor variables were chosen that we hypothesized might influence observations of the gray whale migration (Table 4.3). The null hypothesis was that the environmental variables did not affect the gray whale migration, so models were compared with and without environmental variables. The non-environmental variables were temporal (year, day, hour, time of day) or due to the limitations of the monitoring systems (probability of detection or effort). One null hypothesis tested if there was an interaction effect between year and day suggesting a change in seasonality with year. Environmental variables included temperature near the monitoring locations, temperature at Point Conception where the whale southbound migration paths split, and timing of the ice melt and freeze during the most recent feeding season. Some environmental variables only changed once per year (listed as Year-Specific in Table 4.3). When these variables were tested, the year and year-specific variable were not used in the same model to avoid correlation. For the same reason, the day variable was replaced with days since fall ice-over to test if the date of the fall freeze was a better predictor of the migration than calendar date. To test if day and ice-over date estimated the migration better than day and year, the annual difference from the mean ice-over date was included as a year-specific variable. Since Point Conception is north of the monitoring sites in the Southern California Bight, Point Conception temperature was only used as a predictor in full migration and southbound-only models.

Table 4.3: Predictor Variables Used in Generalized Additive Models. All variables below the dashed line are environmental variables and variables above the dashed line are used in the null hypothesis models. [a]Used instead of Year [b]Used instead of Day [c]Not used for northbound-only models

Description	Method	Type	Migration Seasons
Start year of the migration season	Acoustic, Visual	Categorical	All
Day with 1-Dec=1	Acoustic, Visual	Continuous	All
Hour of the day (0–23)	Acoustic	Continuous, Cyclic	All
Time of day (day or night)	Acoustic	Categorical	All
Mean hourly probability of detection	Acoustic	Continuous	All
Proportion of day with effort	Visual	Continuous	All
Offshore temperature[a]	Acoustic	Continuous (Year-Specific)	All
Nearshore temperature[a]	Visual	Continuous (Year-Specific)	All
Point Conception temperature[a,c]	Acoustic, Visual	Continuous (Year-Specific)	Not 2013–2014
Days since fall ice-over[b]	Acoustic, Visual	Continuous	Not 2011–2012
Difference from mean ice-over date[a]	Acoustic, Visual	Continuous (Year-Specific)	Not 2011–2012
Length of the ice-free season[a]	Acoustic, Visual	Continuous (Year-Specific)	Not 2011–2012, 2012–2013

4.4 Results

Acoustic recordings and sightings allowed monitoring of the gray whale migration along both major routes through the Southern California Bight for seven consecutive migration seasons

with very few gaps in coverage (Figures 4.3 to 4.6). The acoustic data contained short gaps (less than 1 week) in between subsequent HARP deployments and a few longer gaps due to processing errors, but all the longer gaps were during times when no or very few calls were detected. Other periods of no-effort were due to noise masking of calls, but all daily counts were corrected based on the proportion of the day with effort. Most of the gaps in the visual data were due to visual observers being unable to work at night or in rain, fog, or high wind, but, like acoustic counts, total daily visual counts were corrected for proportion of the day with effort.

Pulses of whales migrating during different phases of the migration were apparent in the visual time series. The southbound migration consisted of a steady stream of whales from December to February, but no clear peak (Figure 4.5), but the northbound migration had a peak in March of northbound whales primarily without calves (Phase A) and then another peak at the end of April or beginning of May of northbound presumably female whales with calves (Phase B) (Figures 4.5 and 4.6). Acoustic calls were recorded from December or January until the beginning of April, but very few or no calls were recorded after the start of April in years with effort. Three migration seasons, 2008–2009, 2009–2010, and 2011–2012, contained peaks in number and presence of calls at the beginning of March, but most years had more steady numbers or presence of calls over time with scattered days of high estimated total calls (Figures 4.3 and 4.4).

4.4.1 Interannual Comparison

The eastern North Pacific gray whale population size increased with a growth rate of 0.0520 (95% Confidence Interval: -0.00523–0.109) from of the reported population sizes for the 2009–2010, 2010–2011, 2014–2015, and 2015-2016 migration seasons (Durban et al., 2015, 2017) (Table 4.4 and Figure 4.7). Acoustic and visual ACS/LA counts were only included between the start and end days that were common to all the migration seasons. For acoustic recordings, days 44–108 (13 January–18 March, 17 March in 2012 due to leap year) were included and for ACS/LA visual sightings, days 1–166 (1 December–15 May, 14 May on leap years) were

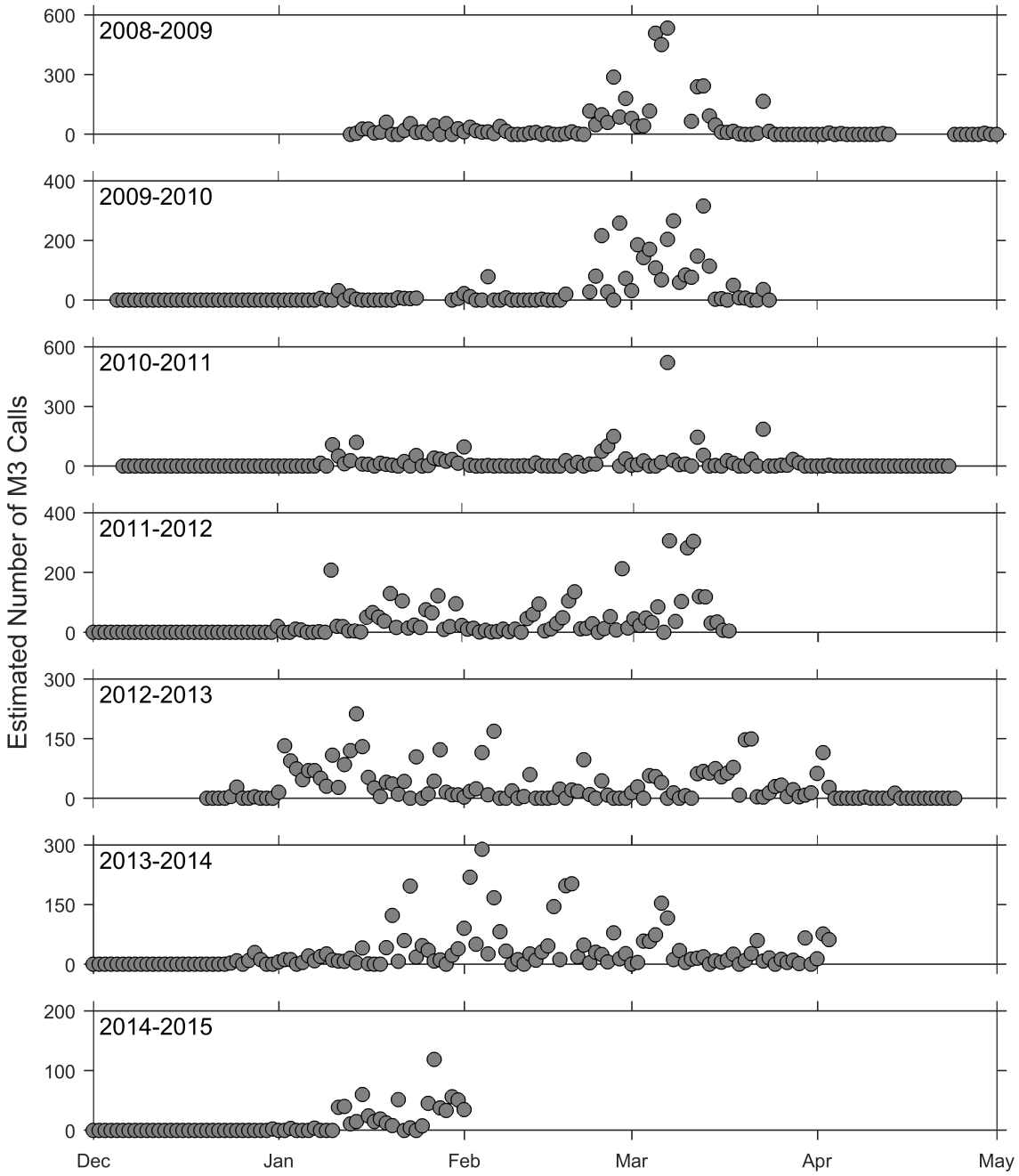

Figure 4.3: Daily Estimated Number of Gray Whale M3 Calls. Estimated calls are calculated using total detections, probability of detection, and effort (Equation (4.1)). Each point represents one day. Days without points did not have effort. Note the differences in the y-axes for each migration season. Dates on x-axes extend from 1 December to 1 May.

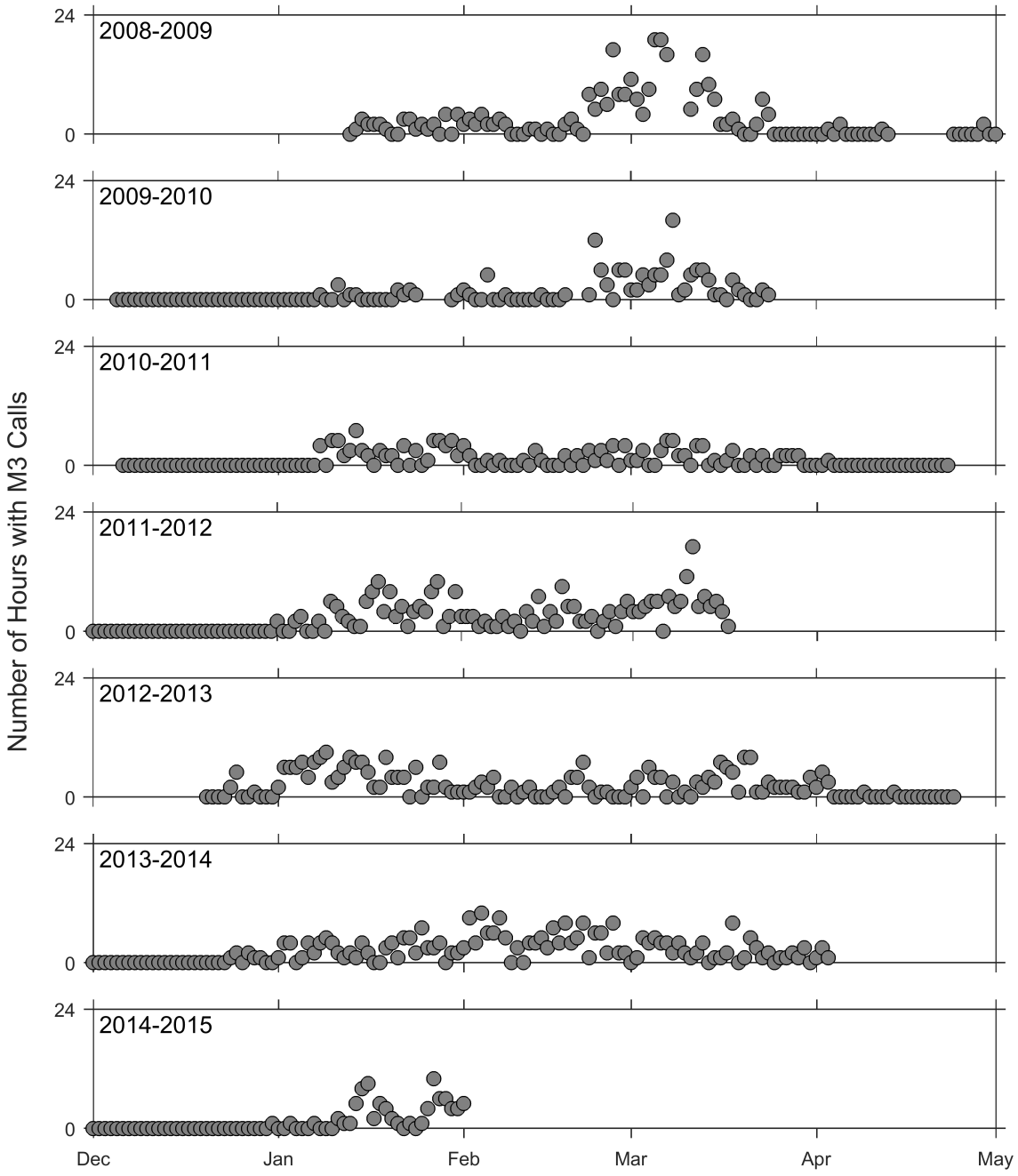

Figure 4.4: Daily Number of Hours with Gray Whale M3 Calls. Each point represents one day. Days without points did not have effort. Dates on x-axes extend from 1 December to 1 May.

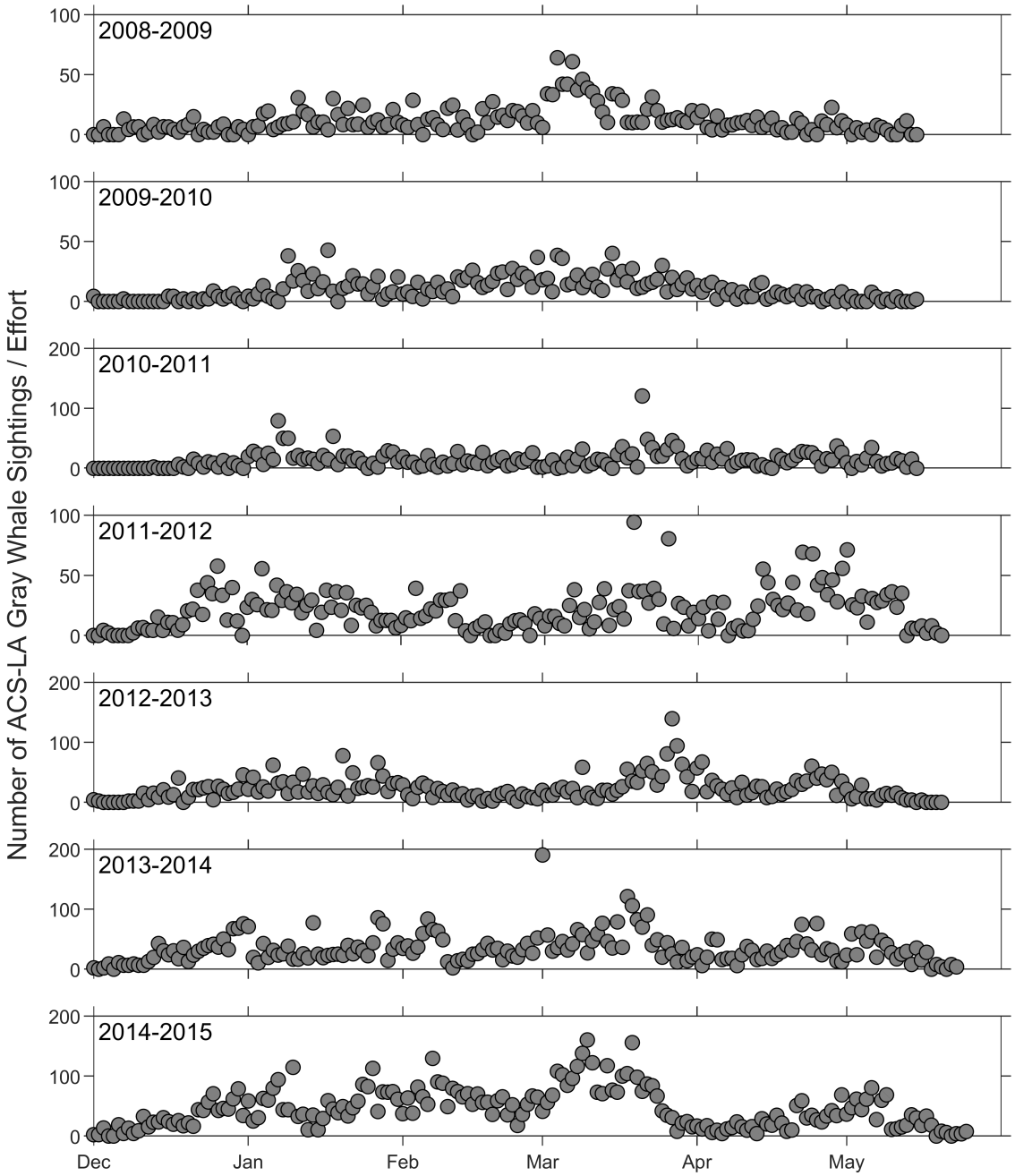

Figure 4.5: Daily Estimated Number of Gray Whale Sightings off Los Angeles from the American Cetacean Society - Los Angeles (ACS/LA) census. Values were calculated by dividing the daily counts by the proportion of the day with effort (Equation (4.2)). Each point represents one day. Days without points did not have effort. Note the differences in the y-axes for each migration season. Dates on x-axes extend from 1 December to 1 June.

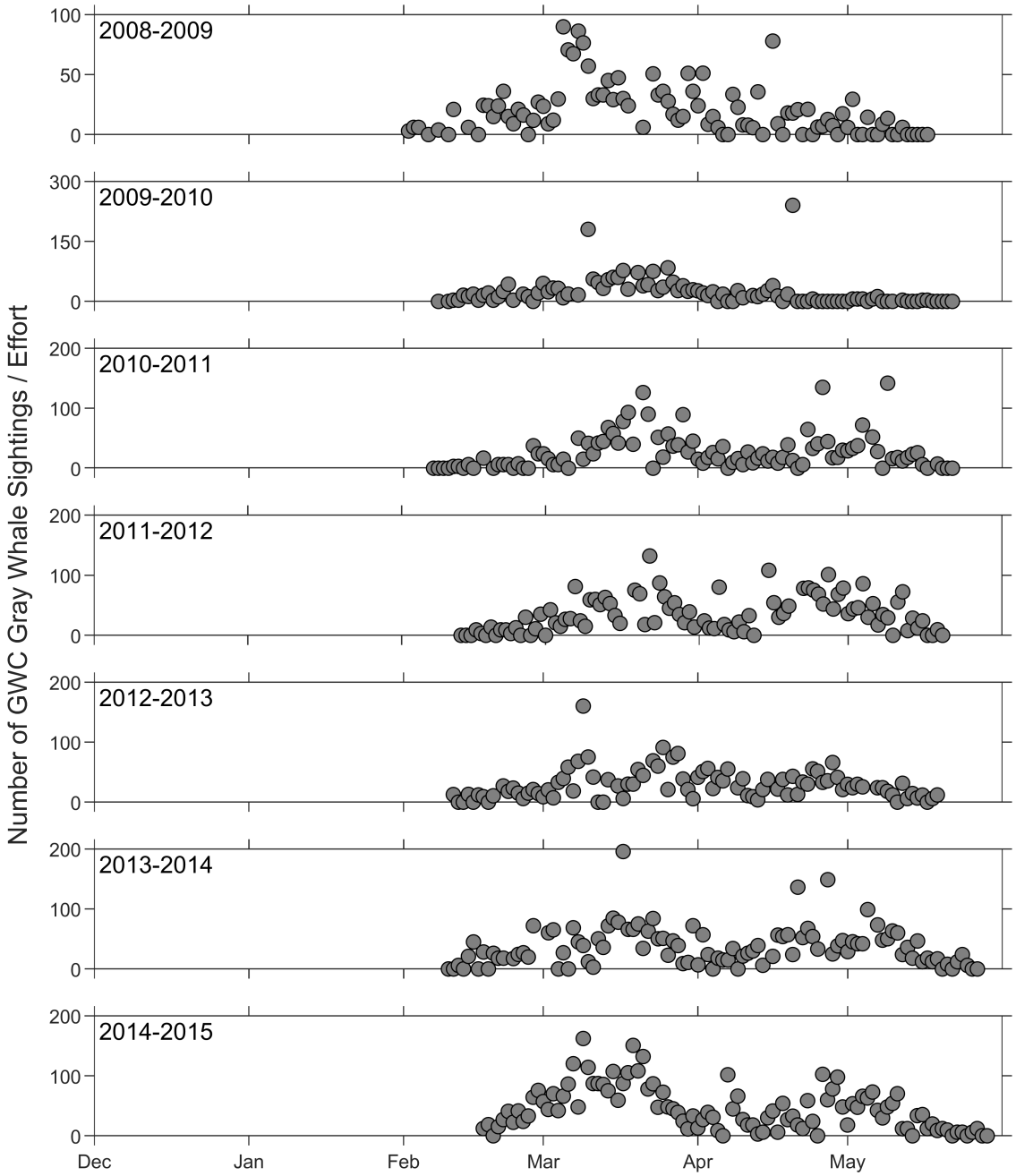

Figure 4.6: Daily Estimated Number of Northbound Gray Whale Sightings off Santa Barbara from the Gray Whales Count (GWC) census. Values were calculated by dividing the daily counts by the proportion of the day with effort (Equation (4.2)). Each point represents one day. Days without points did not have effort. Note the differences in the y-axes for each migration season. Dates on x-axes extend from 1 December to 1 June.

included (counted starting with 1 December). Annual acoustic M3 call counts did not follow a clear trend, so a model was not fit to these data (Table 4.5). Because the estimated number of calls exponentially increases as probability of detection decreases, the confidence intervals for estimated number of calls are more sensitive to changes in probability of detection as the values approach zero. The number of estimated whales by ACS/LA increased the most over this time period with a growth rate of 0.256 (95% Confidence Interval: 0.177–0.335). The growth rate was 0.311 for southbound whales only and 0.219 for northbound whales only. The northbound GWC modeled estimates increased by a growth rate of 0.107 (95% Confidence Interval: 0.0606–0.154) (0.0880 for adults only). When comparing these growth rates to those of the population size growth rate, the ACS/LA sightings growth rate was significantly greater than the population size growth rate (p=0.0012 for full migration, p=$p = 6.9 \times 10^{-5}$ for southbound only, p=0.0063 for northbound only). The growth rate for estimated northbound whales off Santa Barbara was also greater than the population size growth rate (p=0.056 for all whales, p=0.092 for adults only).

We estimated the number of whales that migrated through the 20 km radius search area surrounding the HARP between days 44–108 (13 January–18 March, 17 March in 2012) of each migration season using an estimated calling rate of 7.5 calls/whale/hour (Table 4.5). This method assumes that gray whales call at the same rate in the Southern California Bight as they do farther north at Granite Canyon and that calling rate is constant from year to year. The estimated number of whales migrating through the search area over these days is less than 10% of the population in most years.

The gray whale feeding area was essentially ice-free from the beginning of August until the beginning of November every year, but the timing of the spring melt and the length of the ice-free season varied considerably (Figure 4.8). The mean spring melt day was approximately 22 May but ranged from 3 May (2008) to 12 June (2009). In most years, the amount of time between the "melt day" and when the feeding area was ice free was less than 2 months, but in 2008 and 2010, the melt took about 3 months. The fall ice-over occurred much more rapidly

Table 4.4: Interannual Changes in Population Size and Nearshore Sightings. NOAA's Population Size estimates are published by Durban et al. (2015) and Durban et al. (2017). American Cetacean Society - Los Angeles (ACS/LA) raw sightings between days 1–166 (counted starting with 1 December) were corrected for proportion of the day on-effort, but these sightings were not corrected for probability of detection and so values are relative for this site and should not be compared between sites. Raw counts off Santa Barbara (GWC) were corrected using a probability of detection model (Durban et al., 2015). All values are estimates. The growth rate is an exponential growth rate (Equation (4.5)).

Migration Season	NOAA's Population Size	Los Angeles Full Migration	Santa Barbara Northbound Model
2008–2009	—	1,991	2,726
2009–2010	21,210	1,687	2,734
2010–2011	20,990	2,338	3,273
2011–2012	—	3,574	4,171
2012–2013	—	3,841	3,515
2013–2014	—	5,880	4,628
2014–2015	28,790	7,999	5,094
2015–2016	26,960	—	—
Growth Rate	**0.0520**	**0.256**	**0.107**

and the gray whale feeding area was covered in ice within a month after the freeze started. The mean ice-over day was approximately 2 November and was much more consistent between years than melt day. The earliest ice-over occurred on 28 October (2010) and the latest on 6 November (2009). The mean length of the ice-free season was 161.2 days with a minimum of 145 days in 2013 and a maximum of 183 days in 2008.

The mean temperature of the upper 10 m of the water column was 14.43°C at the nearshore site and 14.45°C at the offshore site (Table 4.6). Point Conception was usually slightly cooler and had a mean temperature of 13.82°C. The nearshore and the offshore sites were always within 0.4°C of each other with the nearshore site warmer than the offshore site in 2009, 2012, and 2015,

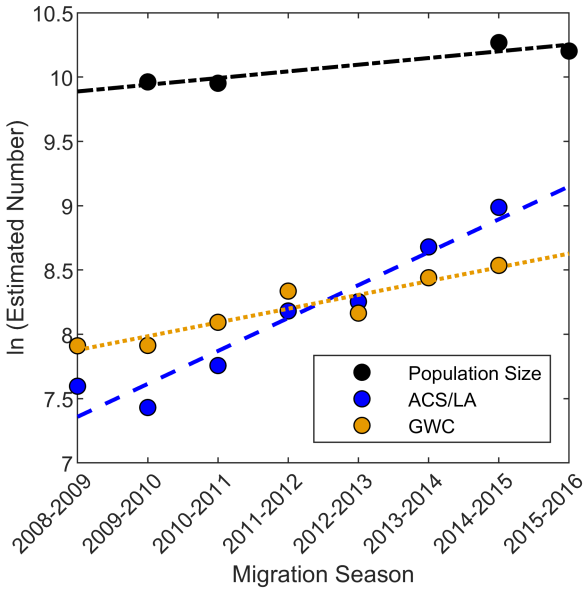

Figure 4.7: Log-Transformed Interannual Changes in Population Size and Nearshore Sightings. This plot shows the same data as Table 4.4, but with log-transformed estimated population size or nearshore sightings. The lines of best fit have a slope equal to the exponential growth rate (0.0520 for NOAA's population size, 0.256 for sightings off Los Angeles (ACS/LA), and 0.107 for sightings off Santa Barbara (GWC).

Table 4.5: Estimated Number of Whales Based on Call Counts for Days 44–108. Days are counted starting with 1 December. Day bounds were selected based on the days that all years had in common. Acoustic M3 Calls have been corrected for probability of detection and proportion of the day with effort. Counts for days between recordings were interpolated. Confidence intervals were calculated using the 67% prediction interval of the observations from noise level versus probability of detection. See methods section for formulas.

Migration Season	Acoustic M3 Calls	Confidence Interval	Estimated Number of Whales
2008–2009	4,812	3,812–17,931	3,483
2009–2010	3,006	2,176–6,025	2,175
2010–2011	1,863	1,449–3,061	1,348
2011–2012	3,480	2,806–4,972	2,519
2012–2013	2,312	1,791–3,816	1,673
2013–2014	3,178	2,479–5,070	2,300

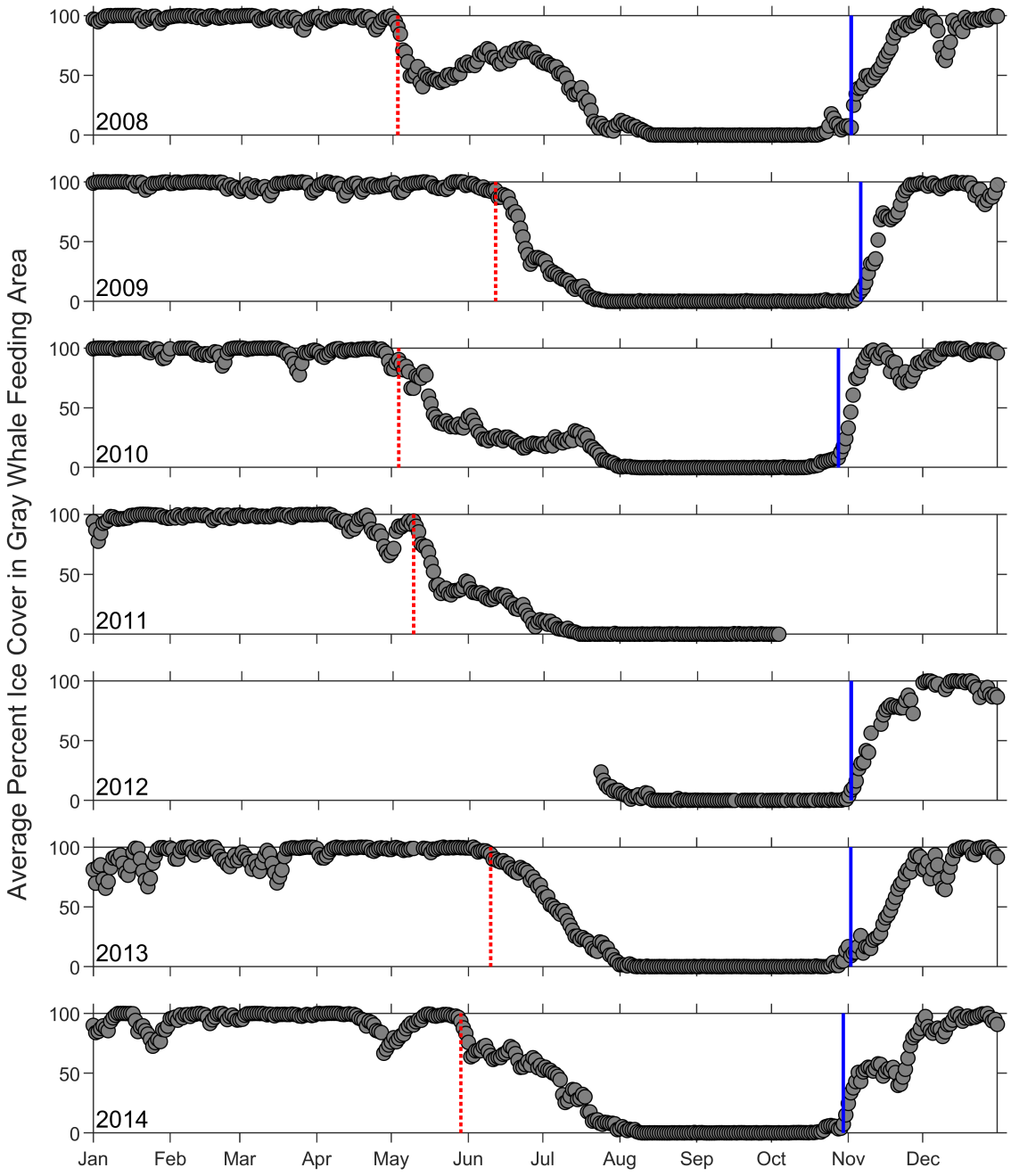

Figure 4.8: Average Sea Ice Concentration in the Gray Whale Feeding Area. The spring melt date is the date when the average sea ice concentration dropped below 90% (red dashed line) and the fall ice-over date is the date when the average sea ice concentration increased above 10% (blue solid line). Sea ice concentration was measured on 6.25-km square grids.

and the offshore site warmer than the nearshore site in the other years. The standard deviation across all three sites was the least in 2009 and 2013 and these were the only two years when the temperature at Point Conception was greater than one of the more southerly sites. The standard deviation across all three sites was the greatest in 2011. The coldest year across all three sites was 2013 and the warmest year was 2015.

Table 4.6: CalCOFI Temperature Measurements During Winter Cruises 2009–2015. Measurements are an average across the two temperature sensors and across depth from 0–10 m.

Year	Nearshore	Offshore	Point Conception
2009	13.80°C	13.55°C	13.70°C
2010	14.90°C	14.96°C	14.30°C
2011	14.32°C	14.62°C	12.90°C
2012	14.32°C	14.11°C	13.61°C
2013	12.37°C	12.76°C	12.50°C
2014	14.66°C	14.86°C	—
2015	16.65°C	16.34°C	15.89°C

4.4.2 Generalized Additive Model Regression Analysis

In all comparisons, the null model with no environmental variables had an AIC equivalent to the best model with environmental variables indicating that including environmental variables did not improve the fit of the generalized additive model. The best null models included all the temporal variables as well as the probability of detection (for acoustic call presence or absence) or proportion of the day with effort (for visual sightings) variables.

In every case, including calendar day in the model resulted in a significantly better model (lower AIC) than including number of days since ice-over (other variables included were year, hour, daytime, and probability of detection or effort). Including day with difference from the mean ice-over date instead of year did not improve the model and in most cases, the model with

year, day, hour, daytime, and probability of detection or effort still had a significantly lower AIC value.

The best acoustic hourly call presence model included year, day, hour, time of day, and probability of detection (Figure 4.9). Year did not show a clear trend with acoustic presence and the pattern appears cyclical. Acoustic presence as a function of day is similar to what was observed in the acoustic time series. The function increased rapidly for the first month and then remained fairly constant with a small peak just before day 100 (early March) and then decreased after that. Acoustic presence as a function of hour reached its maximum in the early morning hours before sunrise and its minimum around sunset. In addition, acoustic presence was greater at night than during the day. Acoustic presence as a function of probability of detection had a decreasing positive slope as probability of detection increased, possibly because presence or absence was not as strongly affected by probability of detection as total call count.

Both models based on visual data showed similar trends for number of sightings (Figures 4.10 and 4.11). Daily visual counts increased as a function of year as observed when comparing the number of sightings across years in Table 4.4. For the ACS/LA census, sightings increased rapidly during the first month, similar to the acoustic presence model, but the peak slightly after day 100 (mid-March) was much more pronounced and there was a second peak around day 150 (end of April). These two later peaks were also observed in the GWC census northbound sightings model. Daily visual counts were positively correlated with proportion of the day with effort, but the relationship was modeled significantly better by a non-linear function than by forcing the function to be linear.

4.5 Discussion

The gray whale Southern California Bight migration route choice contains a complicated trade-off. The coastal route may provide more protection from predators and opportunistic

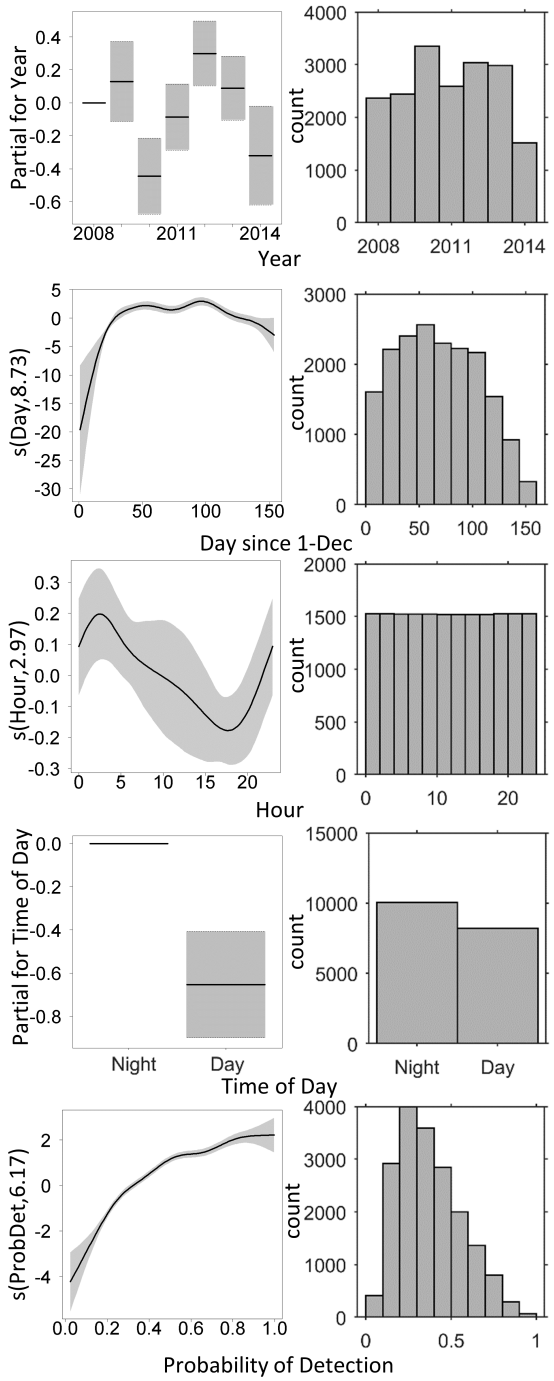

Figure 4.9: Generalized Additive Model Results for Acoustic Data. Hourly presence of gray whale M3 calls modeled as a function of year, day, hour, time of day, and probability of detection (left) and histograms of these variables (right). Day, hour, and probability of detection were fit with a spline fit and 8.73, 2.97, and 6.17 estimated degrees of freedom respectively. Year and time of day were modeled as factors with 6 and 1 degrees of freedom respectively. Shading indicates 2 standard error bounds.

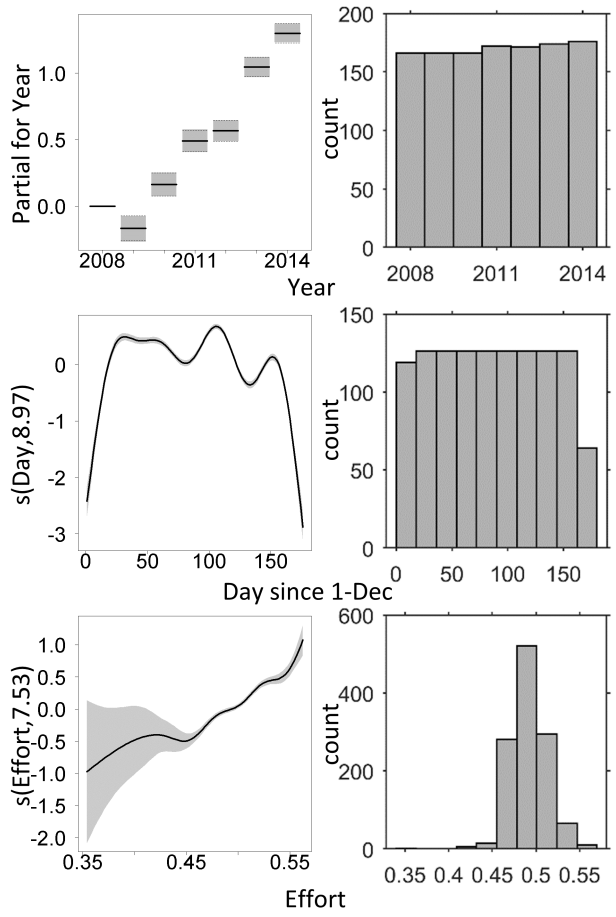

Figure 4.10: Generalized Additive Model Results for Visual ACS/LA Census Data. Daily counts of sighted gray whales modeled as a function of year, day, and proportion of the day with effort (left) and histograms of these variables (right). Day and effort were fit with a spline fit with 8.97 and 7.53 estimated degrees of freedom respectively. Year was modeled as a factor with 6 degrees of freedom. Shading indicates 2 standard error bounds.

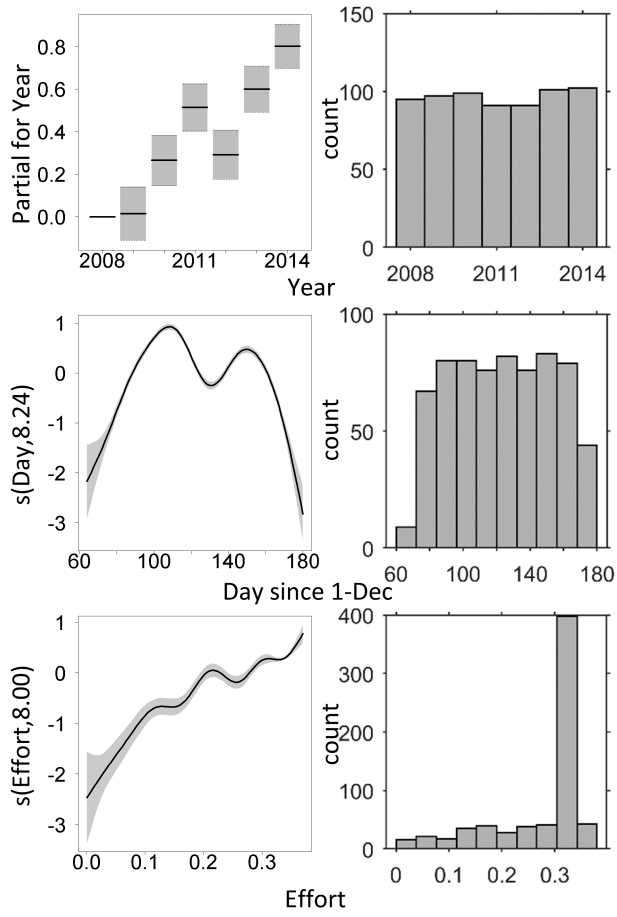

Figure 4.11: Generalized Additive Model Results for Visual GWC Census Data. Daily counts of sighted northbound gray whales modeled as a function of year, day, and proportion of the day with effort (left) and histograms of these variables (right). Day and effort were fit with a spline fit with 8.24 and 8.00 estimated degrees of freedom respectively. Year was modeled as a factor with 6 degrees of freedom. Shading indicates 2 standard error bounds.

foraging, but also has a greater risk of negative interactions with humans through entanglements, ship strikes, and background noise. Based on mapping of probable routes identified by Sumich and Show (2011), offshore routes save about 20–25 km each way, but the deeper water and reduced cover may deter some whales. In addition, whales traveling along the offshore route by San Clemente may be impacted by U.S. Navy activities.

Although variability existed in the acoustic M3 call time series and the visual sightings time series, the annual migration pattern through the Southern California Bight was consistent with observations from other locations along the eastern North Pacific gray whale migration route. The acoustic time series were less consistent than the visual time series possibly because gray whales do not have to vocalize while migrating and producing sound may make them more at risk for predators. Notably, acoustic calls along the offshore route started later than visual sightings along the nearshore route and offshore acoustic calls ended earlier than nearshore visual sightings. This difference could be due to low calling rates and different behavior of different demographics of whales. As Guazzo et al. (In Review) showed, gray whales migrating toward the start of the southbound migration had the lowest calling rate of the southbound migrators. Even though all migrating gray whales traveled close to shore by Granite Canyon, very few calls were detected until the middle of December 2014 and no calls were recorded after the beginning of April 2015 (Guazzo et al., 2017). These times with low calls correspond to times when pregnant females migrate south and females with calves migrate north. Acoustic detection may not be the best way of assessing presence of this demographic segment of the gray whale population. In addition, the GAM model showed a greater proportion of nighttime hours with calls compared to daytime hours. This diel change in calling behavior aligns with observations at Granite Canyon where over twice as many calls were recorded at night compared to the day (Guazzo et al., 2017).

Sumich and Show (2011) reported high interannual variability in the number of whales taking an offshore route. We also found high interannual variability in the number of calls recorded, which could indicate interannual changes in the number of whales taking an offshore

route near the hydrophone and/or changes in the calling rate of gray whales. Over the seven migration seasons between 2008–2009 and 2014–2015, an increasing proportion of gray whales used the nearshore route, as indicated by a greater growth rate of estimated whales off of Santa Barbara and Los Angeles than the population size growth rate. The growth rate at the ACS/LA census site was about 5 times the population growth rate. This high rate of change could indicate that an increased proportion of gray whales migrated past Los Angeles that may have bypassed it in the past in a more offshore route, but still intercepted the coast before Santa Barbara on their journey north. An increase in sightings due to increased probability of detection seems unlikely given that the same experienced observers anchored each shift across these years, local whale watching boats anecdotally reported a similar increase in sightings, and the GWC census also observed a growth rate in estimated number of northbound gray whales greater than the population growth rate. In addition, at the ACS/LA census location, fewer days had compromised visibility due to fog between 2008–2009 and 2010–2011 than between 2011–2012 and 2014–2015 indicating that the increase in sightings was not due to an increase in visibility. An increase in sightings along the coast could be explained by an increasing population size and the tendency for younger whales to prefer a coastal route (Sumich and Show, 2011). Solving for for the growth rate, r, in the exponential growth equation (Equation (4.5)), results in

$$r = \frac{1}{t} \ln \frac{N}{N_0} \tag{4.10}$$

According to Table 4.4, the growth rate of the population (r_{pop}) was 0.052/year. Let M_0 and N_0 equal the number of gray whales in the full population and the number migrating past Los Angeles respectively at the start of this timeseries. If the increase in sightings off Los Angeles is due entirely to a population size increase, the number of whales migrating off Los Angeles would be

$$M = M_0 + (N - N_0) \tag{4.11}$$

Subtracting N_0 from both sides of Equation (4.5), gives an equation for the change in population size

$$N - N_0 = N_0(e^{r_{pop}t} - 1) \tag{4.12}$$

which can be substituted into Equation (4.11)

$$M = M_0 + (N_0(e^{r_{pop}t} - 1)) \tag{4.13}$$

The growth rate of sightings off Los Angeles is

$$r_{LA} = \frac{1}{t} \ln \frac{M}{M_0} \tag{4.14}$$

Substituting Equation (4.13) for M results in

$$r_{LA} = \frac{1}{t} \ln \frac{M_0 + (N_0(e^{r_{pop}t} - 1))}{M_0} \tag{4.15}$$

If we assume 1/10 of the population migrates along the coast at Los Angeles for $t = 0$ or $M_0/N_0 = 0.1$ and let $t = 7$ years and $r_{pop} = 0.052$/year, then the $r_{LA} = 0.24$, which is similar to the measured growth rate of sightings off Los Angeles. The fraction of the population using the coastal route seems reasonable based on aerial surveys (Carretta et al., 2000), but could be estimated more precisely after probability of detection corrections for the ACS/LA census sightings.

Assuming that offshore gray whale calling rate was constant between years and equal to the calling rate estimated farther north at Granite Canyon, in most years, less than 10% of the population migrated through the area within 20 km of the hydrophone during days 44–108 when an average of 45% of ACS/LA census sightings were during these days (range: 30–63%). This 10% value is lower than expected based on the estimate by Carretta et al. (2000) that an average of over 400 whales were migrating through the offshore area every day between January and

April, which corresponds to almost the entire population migrating offshore through the Southern California Bight. Precise migration routes through the Southern California Bight are unknown and a low number of whales may swim through the hydrophone search area because gray whales may be more dispersed or they may follow a different route, perhaps swimming along bathymetric ridges. Alternatively, gray whales may call at a lower rate in the Southern California Bight. Gray whales often flee to shallow water when they are attacked by killer whales, so it is possible that gray whales feel more at risk in the deeper water offshore and call less often to avoid attracting predators, even though killer whales are less common in the Southern California Bight than farther north in Monterey Bay. Additionally, offshore waters are likely clearer than nearshore waters, increasing visibility and possibly decreasing the need for acoustic communication. These hypotheses could be tested by deploying a hydrophone "toll-gate" perpendicular to the coast, spaced at intervals that allow for all migrating gray whales to be within the search area of one hydrophone. This method would allow us to compare the number of calls as a function of distance from shore and calculate the calling rate through the Southern California Bight.

Several climatic events occurred between 2008 and 2015, but most notable was the warm Blob of high ocean temperatures that was first detected at the end of 2013 and led into a strong El Niño in 2015–2016 (Bond et al., 2015; Jacox et al., 2016; Hu et al., 2017). Other ENSO events occurred in 2009–2010 (moderate El Niño), 2010–2011 (strong La Niña) and 2011–2012 (moderate La Niña) (Boening et al., 2012). The temperature difference across the three CalCOFI sites was the greatest in 2011 during the strong La Niña. The temperature of the upper 10 m at Point Conception was about 1.6°C less than the mean temperature of the Nearshore and Offshore sites. The temperature was greatest across the three sites in 2015, during the Blob and the strong El Niño. Unfortunately ice data was only available for part of the years in 2011 and 2012 during the strong La Niña and the time series does not last long enough to see any effects on sea ice by the Blob and the strong El Niño.

The results of the GAM analysis suggest that over these years the gray whale migration

may be cued by more intrinsic than the extrinsic factors included in this study. Including sea ice variables did not result in a better model (based on AIC values) than temporal and probability of detection or effort variables. Possibly the need to give birth and mate drives the migration more than the surrounding environmental conditions. In addition, including temperature measurements in the GAM analysis did not result in a better model. Ocean temperature does not seem to affect which migration route the gray whales choose and this choice may be affected more by instinct or demographic. Further modeling should be done using acoustic and visual data from especially anomalous years in the environment and in the gray whale migration to assess if there are external factors that do sometimes affect the migration. Rugh et al. (2001) reported a shift in the timing of the gray whale migration coinciding with a change in PDO. Perhaps the gray whales are cued by certain changes in the environment on longer timescales. A major factor in the observed migration timing is how far the whales have had to swim from their feeding areas and since the 1980s, the primary gray whale feeding area has moved farther north (Moore et al., 2003; Coyle et al., 2007). Over longer time periods, reductions in sea ice may result in the feeding area moving again, the migration route expanding, and the timing of the migration through California shifting even later.

4.6 Conclusions

By combining multiple methods of observation over several locations, we were able to better understand the gray whale migration in the Southern California Bight over seven migration seasons. If the gray whale calling rate is the same as it is farther north, the proportion of the population that travels offshore through the 20 km hydrophone detection range is small. Analysis of acoustic data from a hydrophone "toll-gate" in the Southern California Bight would help to determine if the relatively low number of calls is due to a lower calling rate or gray whales migrating through different parts of the Southern California Bight. Understanding migration

routes through Southern California is necessary to define the anthropogenic impact on this population. Over these seven migration seasons, the proportion of the population migrating along a nearshore route, within sighting range of visual observers, increased substantially, with the proportion migrating off Los Angeles increasing the most. Since the San Pedro Bay port complex (ports of Los Angeles and Long Beach) is the 9th busiest container port complex in the world (https://www.portoflosangeles.org/about/facts.asp) and Los Angeles is the second largest metropolitan area in the U.S., an increasing proportion of gray whales migrating along the coast will result in increased negative impacts from ship strikes, chemical and noise pollution, and fishing gear entanglements. It is thought that younger gray whales tend to favor more nearshore routes while older whales migrate more offshore (Sumich and Show, 2011). Perhaps an increasing proportion of gray whales are using the nearshore route due to an increased population with a larger proportion of younger whales. To account for changing visibility and effort and to compare numbers of gray whales migrating past the different sites, probability of detection analysis should be used to correct the number of sightings off Los Angeles.

This analysis is a retrospective study of available data. Future work assessing how the migration patterns of gray whales may be affected by climate change should design a study to reduce the number of variables. Ideally, this study should take place at a location like Granite Canyon where the entire population migrates within a defined area in order to reduce confounding variables related to unknown calling rates and distribution of whales. Acoustic data should be collected for 10–15 migration seasons to capture several climatic events and changes in prey abundance that may affect the migration. In years with population size estimates, these values could be used to compare calling rate between years. Finally, other variables that may impact gray whales should be measured. For example, benthic prey abundance could be measured in the gray whale feeding area at the same sampling locations for the duration of the study. Benthic amphipod abundance has been measured as a function of location in the Arctic feeding areas (Brower et al., 2017), but has not been measured as a function of time on fine (less than decadal)

scales.

Generalized additive models of both acoustic and visual data led to the conclusion that the gray whale migration may be cued and influenced more by the whales' biological clock and instincts than by the environment. Modeling over longer duration time series will help to assess and predict how the gray whale migration will be affected by future environmental changes. Generalized additive modeling of acoustic data is a useful tool to determine the influence of several variables on the detection and presence of marine mammals in areas that are difficult to monitor visually.

4.7 Acknowledgments

Acoustic data collection was supported by grants from the U.S. Army Corps of Engineers using funds provided by the U.S. Navy's Pacific Fleet through the Cooperative Ecosystem Studies Units. The authors would specifically like to thank Chip Johnson from Pacific Fleet. RAG was awarded the Science, Mathematics & Research for Transformation (SMART) Scholarship, funded by the USD/R&E (Under Secretary of Defense/Research & Engineering) National Defense Education Program (NDEP) / BA-1, Basic Research. ASJ thanks the scores of dedicated citizen scientists, trained volunteers who have helped collect and record data for the ACS/LA Gray Whale Census and Behavior Project, as well as the Point Vicente Interpretive Center staff who have gone out of their way to provide a terrific observation platform. Collaborators for the ACS/LA census include Dave Rugh, Kim Sheldon, and Wayne Perryman (NOAA AFSC and SWFSC) and Dave Janiger (NHMLAC). MHS thanks the Counters, a team of diverse, passionate individuals who make GWC possible. GWC collaborators include Dave Weller, John Durban, and Wayne Perryman (NOAA SWFSC), John Calambokidis (Cascadia Research Collective), Sean Wiggins (Scripps Whale Acoustics Lab), and Cris Sandoval (Coal Oil Point Reserve). GWC is supported by generous and committed foundations and organizations, including an anonymous foundation

administered by the Orange County Community Foundation and the Pacific Life Foundation. Dennis Rimington provided assistance with the Monte Carlo code used to estimate acoustic probability of detection. We are grateful for Wayne Perryman and Trevor Joyce for sharing what they have learned about the effects of sea ice on gray whale calf production. We thank Josh Jones for retrieving the sea ice data and Mati Kahru for help with the WIM/WAM software used to process the sea ice data. Sarah Creel, Tyler Helble, Mark Ohman, and Dave Weller provided feedback that improved this study.

Chapter 4, in full, is currently being prepared for submission for publication. Regina A. Guazzo, Alisa Schulman-Janiger, Michael H. Smith, Jay Barlow, Gerald L. D'Spain, and John A. Hildebrand, "Gray whale migration patterns through the Southern California Bight from multi-year visual and acoustic monitoring." The dissertation author was the primary investigator and author of this paper.

Chapter 5

Conclusions

In this dissertation, I described the calls produced by migrating gray whales, I analyzed how gray whale behavior changes over different timescales, and I proposed recommendations for future studies using similar methodology. These findings will help improve abundance estimates and are the start to understanding how gray whales may be impacted by anthropogenic activities and climate change.

5.1 Migrating Gray Whale Call Characteristics

In Chapter 2, I used multiple detections of the same calls on different hydrophones to calculate call characteristics and describe which characteristics are most robust to environmental propagation. I estimated gray whale M3 call source levels and compared the values across three different calculation methods. Many past peer-reviewed publications that report source level have not described calculation methods or transmission loss assumptions. By showing a 65-fold difference in pressure amplitudes squared between the root mean square and peak-to-peak source levels, I stress the importance of describing all methods and assumptions when presenting acoustic results.

Call characteristics are highly dependent on both the animal producing the calls and the

local propagation effects. By comparing properties of the same call across multiple sensors, I found that the mean frequency of M3 calls was most robust to environmental propagation in that differences in call mean frequency across multiple hydrophones contributed the least to total variance. Most published descriptions do not take into account environmental propagation when they report cetacean call characteristics. Simply recording the same call on multiple sensors can improve our understanding of call characterstics that may be most helpful when identifying a specific call type at other locations. The characteristics that are least affected by propagation may also be the most important characteristics to the whales as they communicate. I also provided audio files of the two call types that I recorded in the online Supplemental Information for this publication, and hope that more authors share example audio files in animal bioacoustics publications.

5.2 Gray Whale Migration Behavior on Multiple Timescales

Gray whale migration behavior, and probably most animal behavior, is not constant across multiple timescales. Before applying an average behavior value to a new dataset, we must ensure that the average was taken over a similar timescale as the new dataset.

5.2.1 Diel Cycle

In Chapter 2, I compared acoustic and swimming behavior over a diel timescale. Gray whales increase their calling rate at night, apparent in both the number of calls recorded and the percentage of calls part of a track. I suggest that gray whales may call more when they can no longer use vision to aid their navigation or contact with conspecifics. Any additional anthropogenic sound that we add to the ocean at night may have increased negative effects on species like gray whales that depend more on calling at night.

Mean swimming behavior, however, did not change between night and day. Mean speed

was constant and whales kept direct, straight tracks during both the night and day. Current population abundance models assume that whales increase their migration rate at night (Durban et al., 2015), but this finding suggests that the migration rate of calling whales is the same at night and day and therefore, if non-calling whales are swimming similarly to calling whales, the abundance may be lower than previously reported. Analysis of nighttime swimming behavior should be repeated for multiple migration seasons to ensure that this pattern is consistent.

5.2.2 Southbound Migration

In Chapter 3, I combined gray whale acoustic call localizations and infrared blow detections with southbound gray whale visual sightings to estimate call and blow rates. Blow rates are expected to be stable over time and the average over four days was 49 blows/whale/hour. Call rates however were not stable over the southbound migration and increased by over a factor of five. I hypothesize that different demographics of whales call at different rates with mature animals calling the least often and juveniles calling the most often. I extrapolated the calling rate to the beginning of December to estimate how many whales migrated past before visual observations began. Based on calls detected, I estimated that the number of whales that migrated past was greater than reported using a visual sightings model (Durban et al., 2017). Although these extrapolated calling rates should be checked in another year with concurrent visual observations and acoustic recordings, Chapters 2 and 3 show how multiple detection methods can increase accuracy and precision of marine mammal abundance values.

5.2.3 Southbound Versus Northbound Migrations

In Chapter 2, I compared tracks made from localized gray whale calls between the southbound and northbound migration. Gray whale swimming behavior was similar to what is reported by visual observers. The switch between southbound and northbound tracks occurred in

mid-February and the northbound tracks were on average farther from shore and in deeper water than the southbound tracks. In order for calls to form a track, the animal must be calling at a high enough rate to produce multiple calls detected on all four hdyrophones. More calls were part of tracks during the first part of the southbound migration and the end of the northbound migration. These time periods also have the least total number of calls detected, and, as described in Chapter 3, the first part of the southbound migration has the lowest calling rate. I suggest that a small proportion of the early southbound migrators may be calling at a high rate, but the overall calling rate is low. In the middle of the migration, the overall calling rate is higher, but most whales are not calling at a high enough rate to be tracked. It would be interesting to compare calling rate between the southbound and northbound migration to see if the trend is the reverse of what was observed in the southbound migration. To determine northbound gray whale calling rate, visual sightings would need to be paired with acoustic recordings.

5.2.4 Full Migration Season

Using passive acoustic tracks during the 2014–2015 migration, I estimated that the average swimming speed of migrating gray whales was 1.6 m/s in Chapter 2. In Chapter 3, I combined the visual sightings and acoustic localizations to estimate a mean calling rate of 7.5 calls/whale/day over the full migration season. Future studies should investigate if these values are constant over multiple years and at different locations. For Chapter 4, we assumed the values were constant and used them to estimate the total number of gray whales migrating within the search area of the Southern California Bight HARPs.

5.2.5 Multiple Migration Seasons

In Chapter 4, I used Generalized Additive Models to assess the effects of environmental change on the gray whale migration and I quantified the gray whale migration from three sites

across seven migration seasons. The gray whale migration appears to be more intrinsically driven than affected by ocean temperature or sea ice timing. Future work should investigate the relationship between the environment and the gray whale migration on longer timescales and should also incorporate more environmental variables such as prey abundance in the gray whale feeding areas. Perhaps a long-term acoustic study at Granite Canyon would be a more optimal location to study changes in the gray whale migration without the confounding variables of multiple migration routes through the Southern California Bight.

I compared the exponential growth rate for the two Southern California Bight visual census locations to the population size growth rate as measured at Granite Canyon. The growth rate in number of northbound gray whales estimated to migrate past Santa Barbara was greater than the population size growth rate and the growth rate of the migrating whales passing Los Angeles was greater still. These results could indicate that there are several offshore routes and some offshore whales shifted to a more coastal migration route over these years. The sightings off Santa Barbara were corrected for probability of detection in a similar way as those off Granite Canyon are corrected. An increase in sightings due to an increase in probability of detection off Los Angeles seems unlikely since an experienced observer worked during every shift and the number of days with compromised visibility due to fog was greater during the later migration seasons than the earlier seasons, opposite of what would be expected if visibility was the cause of these results.

When calling rate and swimming speed were applied to the number of gray whale calls detected, the number of whales estimated was lower than expected if most of the population migrates along the offshore route. Perhaps gray whales migrating offshore are more dispersed, or perhaps most take a route that is outside of the search area of the hydrophone. It is also possible that gray whales call at a lower calling rate or source level as they migrate through the deeper waters through the Channel Islands if they perceive there is more danger in deep water. Future studies could incorporate an acoustic "toll-gate" to calculate calling rate for offshore gray whales

and to assess their distribution through the Southern California Bight.

5.3 Methodology Advantages and Potential Improvements

5.3.1 Infrared Methods

Infrared cameras have great potential for detecting whales at night and day since blow rate is likely less impacted by behavior than call rate. However, infrared propagation is affected by visibility, sea state, and humidity, and these effects have not been quantified for probability of detection of whale blows. I tested the potential use of infrared cameras for gray whale blow detections on four days with good conditions according to visual observers and found that probability of detection decreased with range beyond about 2 km. Based on this finding, I recommend that in the future, multiple cameras be used that are optimized to monitor different ranges offshore.

In order to quantify probability of detection of a gray whale blow in a range of conditions, an automatic detector must be developed. Toyon Research Corporation was given the task of creating an automatic infrared blow detector and whale counter for the NOAA infrared cameras. However, although Toyon has shown that in certain days the final count output from their system is similar to the visual observers' count, the blow detection output changes each time a given infrared video is processed with the detector and the locations of the detected blows are much closer to shore than visual sightings. Due to the proprietary nature of the underlying code and the inability to quantify the probability of detection versus false alarm, I abandoned my efforts with this program.

Once a detector with a known performance is developed, physics-based infrared propagation modeling can help assess how the probability of detection and search area are impacted by environmental conditions. Perhaps buoys with weather sensors could be deployed in the search area to match conditions with probability of detection.

Finally, detectors work well when there is a high signal-to-noise ratio. Along the California coast, the water is cold and so the warmer blows are bright against the dark ocean. An infrared camera system may not work as well in a tropical environment and, to the best of my knowledge, has never been tested for whale blow detections in these locations.

5.3.2 Passive Acoustic Methods

Acoustic localization of calls on multiple hydrophones is a tool that should be applied to more marine mammal studies. By localizing calls, we reduce human effort and subjectivity. If a signal is absolutely known, then the optimal detector cross-correlates the data with a kernel of the signal. However, if a signal has ambiguity or variation, a more general detector is often used and these detectors result in many false alarms. Most false alarms that are due to background noise will not be able to be localized since it is unlikely for false alarms to appear on multiple other hydrophones within the range of possible time differences of arrival. Even if noise is localized, it is usually localized far from the center of the range due to the mismatch between the time of arrivals of noise from different sources. Limiting the search area to a region of high probability of detection eliminates most of the remaining false alarms. For instance, the Generalized Power Law (GPL) detector output from a single hydrophone in the array described in Chapter 2 resulted in 22% M3 call detections. However, 48% of the localized detections were M3 calls, and 86% of the localized detections within the array were M3 calls. Without an automatic detector, it would take months for an analyst to detect every call in this 7-month continuous time series, and these detections would be highly subjective, especially for low signal-to-noise ratio calls. With an automatic detector and a single hydrophone, it took weeks to verify detections. With an automatic detector and localizer, it took a day or two to verify detections.

Another benefit of localization is that we are able to limit the search area to a region with a high probability of detection in most noise conditions. With a single hydrophone, source locations are unknown and since we cannot limit the search area, most of the search area has a

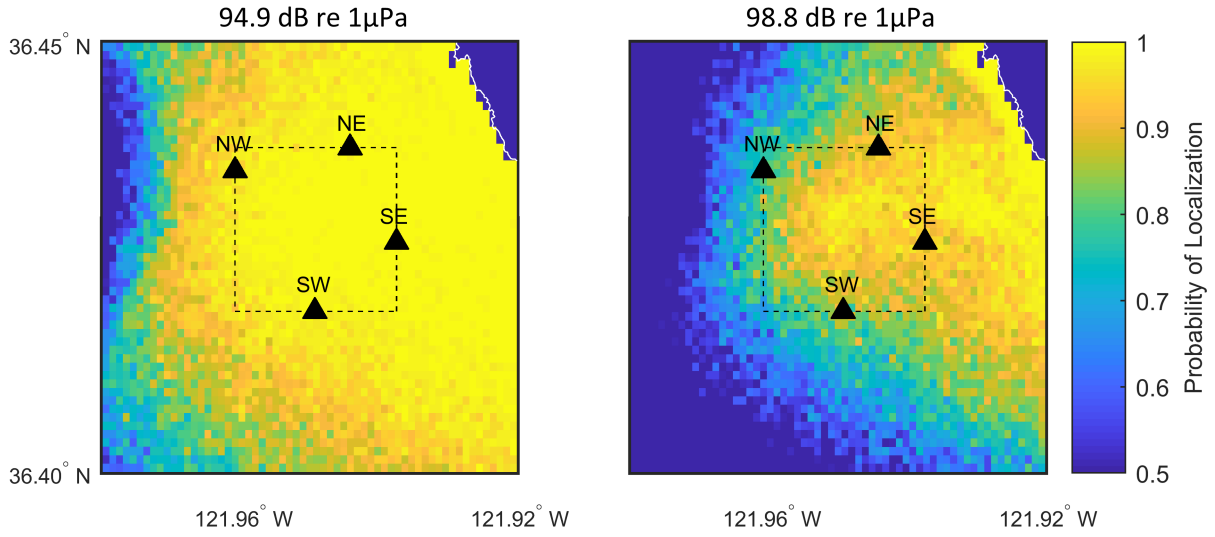

Figure 5.1: Probability of Localization in 94.9 and 98.8 dB re : 1μPa Root Median Square Noise. These maps shows the probability of localization of a call produced at locations close to the hydrophone array in 75th percentile and upper adjacent background noise. In the 75th percentile noise conditions, the probability of localization within the area of the array was approximately 100%. Probability of localization decreases within the area of the array in the higher noise conditions, but it still remains above 80%. The four black triangles mark the positions of the four bottom-mounted hydrophones. The dashed box indicates the area inside the hydrophone array. The axes limits are 36.4° to 36.45° for latitude and -121.98° to -121.92° for longitude.

low probability of detection. Number of estimated calls is inversely proportional to probability of detection, and variance of the estimated calls is inversely proportional to probability of detection raised to the fourth power. Therefore, a low probability of detection greatly decreases the precision in call estimates. Figure 5.1 shows that by limiting the search area, we can keep a high probability of localization (detection on all four hydrophones) in most noise conditions, but if we had a single hydrophone, the search area would be larger and the average probability of detection over the search area would be much lower.

Finally, tracks of localized calls paired with a general detector, can help identify rare or new call types for a species. M1 calls are more rarely detected than M3 calls during the gray whale migration, but tracks with both M3 and M1 calls helped to confidently identify M1 calls. Figure 5.2 shows spectrograms of calls that made up a track which contained eight M3

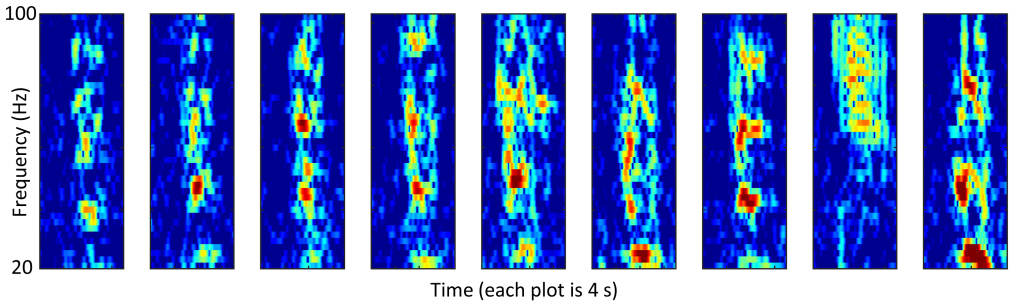

Figure 5.2: Example Track Containing a Gray Whale M1 Call. This sequence of spectrograms are from a track with eight M3 calls and one M1 call (second to last). Each spectrogram has frequency limits of 20–100 Hz and lasts 4 seconds. Color indicates relative amplitude. The spectrograms were produced with an FFT length of 1024 and 99% overlap.

calls and one M1 call.

Even though localization has many advantages, localizing calls from separate hydrophone-recorder packages can be challenging. Each hydrophone-recorder package has a separate clock and these clocks must match for localization to be possible. Small inconsistencies between clocks can result in large differences in localization position. High-quality clocks that do not drift are imperative. In addition, tank experiments would be an easy way to better quantify any remaining clock drift. Currently linear clock drift from the start to the end of the deployment is assumed, but this has never been tested. To verify the accuracy and precision of localizations, sounds of similar frequency and duration of the whale calls of interest could be broadcast at the assumed calling depth from a small boat a few separate times during the deployment. This experiment would help verify (or correct if needed) clock times, propagation distances, and time difference of arrivals to ensure accurate localizations of calling whales.

Finally, instrument noise can create unnaturally high noise levels that make detection of biological signals difficult. The shallow-water environments that gray whales prefer also have increased currents at the depths of the hydrophone-recorder packages than deep-water recording sites. These currents can create low-frequency strumming on the cable, increasing the background noise in the recordings, often to levels that do not allow for effort. One possible solution for low-frequency recordings, is to mount the hydrophone directly to the data logger

package sitting on the seafloor. In addition, disk write noise contaminates 7-seconds out of every 75-seconds in 200 kHz sampling rate recordings. In total, 2.24 hours in each day or 34 days in a year contain disk-writes making detection difficult or impossible. In Chapter 4, I found that the automatic detector could not detect gray whale calls during disk-write times, so I designated these times as no-effort and corrected accordingly. A switch to solid-state drives in the recording packages would fix this problem. Although these drives are more expensive, the extra recording time and increased ability to detect rare animals and call types would pay for itself.

References

Au, W. W. L., Floyd, R. W., Penner, R. H., and Murchison, A. E. (1974). Measurement of echolocation signals of the Atlantic bottlenose dolphin, *Tursiops truncatus* Montagu, in open waters. *The Journal of the Acoustical Society of America*, 56(4):1280–1290.

Au, W. W. L., Mobley, J., Burgess, W. C., Lammers, M. O., and Nachtigall, P. E. (2000). Seasonal and diurnal trends of chorusing humpback whales winteing off western Maui. *Marine Mammal Science*, 16(3):530–544.

Au, W. W. L., Pack, A. A., Lammers, M. O., Herman, L. M., Deakos, M. H., and Andrews, K. (2006). Acoustic properties of humpback whale songs. *The Journal of the Acoustical Society of America*, 120(2):1103–1110.

Bailey, H., Mate, B., Palacios, D., Irvine, L., Bograd, S., and Costa, D. (2009). Behavioural estimation of blue whale movements in the Northeast Pacific from state-space model analysis of satellite tracks. *Endangered Species Research*, 10:93–106.

Baldacci, A., Carron, M., and Portunato, N. (2005). Infrared detection of marine mammals. techreport SR-443, NATO Undersea Research Centre.

Barlow, J., Calambokidis, J., Falcone, E. A., Baker, C. S., Burdin, A. M., Clapham, P. J., Ford, J. K. B., Gabriele, C. M., LeDuc, R., Mattila, D. K., Quinn, II, T. J., Rojas-Bracho, L., Straley, J. M., Taylor, B. L., Urbán R., J., Wade, P., Weller, D., Witteveen, B. H., and Yamaguchi, M. (2011). Humpback whale abundance in the North Pacific estimated by photographic capture-recapture with bias correction from simulation studies. *Marine Mammal Science*, 27(4):793–818.

Bass, A. H. and McKibben, J. R. (2003). Neural mechanisms and behaviors for acoustic communication in teleost fish. *Progress in Neurobiology*, 69(1):1–26.

Boening, C., Willis, J. K., Landerer, F. W., Nerem, R. S., and Fasullo, J. (2012). The 2011 La Niña: so strong, the oceans fell. *Geophysical Research Letters*, 39(19):L19602.

Bond, N. A., Cronin, M. F., Freeland, H., and Mantua, N. (2015). Causes and impacts of the 2014 warm anomaly in the NE Pacific. *Geophysical Research Letters*, 42(9):3414–3420.

Bradford, A. L., Weller, D. W., Wade, P. R., Burdin, A. M., and Brownell, Jr., R. L. (2008). Population abundance and growth rate of western gray whales *Eschrichtius robustus*. *Endangered Species Research*, 6:1–14.

Brodie, P. and Paasche, A. (1985). Thermoregulation and energetics of fin and sei whales based on postmortem, stratified temperature measurements. *Canadian Journal of Zoology*, 63:2267–2269.

Brower, A. A., Ferguson, M. C., Schonberg, S. V., Jewett, S. C., and Clarke, J. T. (2017). Gray whale distribution relative to benthic invertebrate biomass and abundance: Northeastern Chukchi Sea 2009–2012. *Deep Sea Research Part II: Topical Studies in Oceanography*, 144:156–174.

Buckland, S. T., Breiwick, J. M., Cattanach, K. L., and Laake, J. L. (1993). Estimated population size of the California gray whale. *Marine Mammal Science*, 9(3):235–249.

Carretta, J. V., Lowry, M. S., Stinchcomb, C. E., Lynn, M. S., and Cosgrove, R. E. (2000). Distribution and abundance of marine mammals at San Clemente Island and surrounding offshore waters: results from aerial and ground surveys in 1998 and 1999. Technical report, National Oceanic and Atmospheric Administration, U.S. National Marine Fisheries Service, Southwest Fisheries Science Center.

Comiso, J. C. (2012). Large decadal decline of the Arctic multiyear ice cover. *Journal of Climate*, 25(4):1176–1193.

Coyle, K. O., Bluhm, B., Konar, B., Blanchard, A., and Highsmith, R. C. (2007). Amphipod prey of gray whales in the northern Bering Sea: comparison of biomass and distribution between the 1980s and 2002–2003. *Deep Sea Research Part II: Topical Studies in Oceanography*, 54:2906–2918.

Crane, N. L. and Lashkari, K. (1996). Sound production of gray whales, *Eschrichtius robustus*, along their migration route: a new approach to signal analysis. *The Journal of the Acoustical Society of America*, 100(3):1878–1886.

Cummings, W. C., Thompson, P. O., and Cook, R. (1968). Underwater sounds of migrating gray whales, *Eschrichtius glaucus* (Cope). *The Journal of the Acoustical Society of America*, 44(5):1278–1281.

Cuyler, L. C., Wiulsrød, R., and Øritsland, N. A. (1992). Thermal infrared radiation from free living whales. *Marine Mammal Science*, 8(2):120–134.

Dalheim, M. E. (1987). *Bioacoustics of the gray whale (Eschrichtius robustus)*. PhD thesis, University of British Columbia.

Durban, J. W., Weller, D. W., Lang, A. R., and Perryman, W. L. (2015). Estimating gray whale abundance from shore-based counts using a multilevel Bayesian model. *Journal of Cetacean Research and Management*, 15:61–68.

Durban, J. W., Weller, D. W., and Perryman, W. L. (2017). Gray whale abundance estimates from shore-based counts off California in 2014/15 and 2015/16. Paper SC/A17/GW/06 presented to the International Whaling Commission Scientific Committee.

Fish, J. F., Sumich, J. L., and Lingle, G. L. (1974). Sounds produced by the gray whale, *Eschrichtius robustus*. *Marine Fisheries Review*, 36(4):38–45.

Gardner, S. and Chávez-Rosales, S. (2000). Changes in the relative abundance and distribution of gray whales (*Eschrichtius robustus*) in Magdalena Bay, Mexico during an El Niño event. *Marine Mammal Science*, 16(4):728–738.

Gilmore, R. M. (1960). A census of the California gray whale. Number 342 in Special Scientific Reports: Fisheries, pages iv–30. US Department of Interior, Fish and Wildlife Service, Washington, D.C. Edited by Dale W. Rice.

Gordon, J. (2001). Measuring the range to animals at sea from boats using photographic and video images. *Journal of Applied Ecology*, 38(4):879–887.

Guazzo, R. A., Helble, T. A., D'Spain, G. L., Weller, D. W., Wiggins, S. M., and Hildebrand, J. A. (2017). Migratory behavior of eastern North Pacific gray whales tracked using a hydrophone array. *PLoS ONE*, 12(10):e0185585.

Guazzo, R. A., Weller, D. W., Europe, H. M., Durban, J. W., D'Spain, G. L., and Hildebrand, J. A. (In Review). Migrating eastern North Pacific gray whale cue rates estimated from acoustic recordings, infrared camera images, and visual sightings. *Scientific Reports*.

Gulland, F. M. D., Pérez-Cortéz M., H., Urbán R., J., Rojas-Bracho, L., Ylitalo, G., Weir, J., Norman, S. A., Muto, M. M., Rugh, D. J., Kreuder, C., and Rowles, T. (2005). Eastern North Pacific gray whale (*Eschrichtius robustus*) unusual mortality event, 1999-2000. NOAA Technical Memorandum NMFS-AFSC-150, U.S. Department of Commerce.

Hanggi, E. B. and Schusterman, R. J. (1994). Underwater acoustic displays and individual variation in male harbour seals, *Phoca vitulina*. *Animal Behaviour*, 48(6):1275–1283.

Hastie, T. J. and Tibshirani, R. J. (1990). *Generalized additive models*, volume 43 of *Monographs on Statistics and Applied Probability*. Chapman & Hall, London.

Heaney, K. D. and Campbell, R. L. (2016). Three-dimensional parabolic equation modeling of mesoscale eddy deflection. *The Journal of the Acoustical Society of America*, 139(2):918–926.

Heaney, K. D., Prior, M., and Campbell, R. L. (2017). Bathymetric diffraction of basin-scale hydroacoustic signals. *The Journal of the Acoustical Society of America*, 141(2):878–885.

Helble, T. A., D'Spain, G. L., Hildebrand, J. A., Campbell, G. S., Campbell, R. L., and Heaney, K. D. (2013). Site specific probability of passive acoustic detection of humpback whale calls from single fixed hydrophones. *The Journal of the Acoustical Society of America*, 134(3):2556–2570.

Helble, T. A., Ierley, G. R., D'Spain, G. L., and Martin, S. W. (2015). Automated acoustic localization and call association for vocalizing humpback whales on the Navy's Pacific Missile Range Facility. *The Journal of the Acoustical Society of America*, 137(1):11–21.

Helble, T. A., Ierley, G. R., D'Spain, G. L., Roch, M. A., and Hildebrand, J. A. (2012). A generalized power-law detection algorithm for humpback whale vocalizations. *The Journal of the Acoustical Society of America*, 131(4):2682–2699.

Highsmith, R. C. and Coyle, K. O. (1991). Amphipod life histories: community structure, impact of temperature on decoupled growth and maturation rates, productivity, and P:B ratios. *American Zoologist*, 31(6):861–873.

Hu, Z.-Z., Kumar, A., Jha, B., Zhu, J., and Huang, B. (2017). Persistence and predictions of the remarkable warm anomaly in the Northeastern Pacific Ocean during 2014–16. *Journal of Climate*, 30(2):689–702.

Hubbs, C. L. and Hubbs, L. C. (1967). Gray whale censuses by airplane in Mexico. *California Fish and Game*, 53(1):23–27.

Jacox, M. G., Hazen, E. L., Zaba, K. D., Rudnick, D. L., Edwards, C. A., Moore, A. M., and Bograd, S. J. (2016). Impacts of the 2015-2016 El Niño on the California Current System: early assessment and comparison to past events. *Geophysical Research Letters*, 43(13):7072–7080.

Janik, V. M. and Slater, P. J. B. (1998). Context-specific use suggests that bottlenose dolphin signature whistles are cohesion calls. *Animal Behaviour*, 56(4):829–838.

Kahru, M. (2001). Windows image manager: image display and analysis program for Microsoft Windows with special features for satellite images.

Kawanishi, T., Sezai, T., Ito, Y., Imaoka, K., Takeshima, T., Ishido, Y., Shibata, A., Miura, M., Inahata, H., and Spencer, R. W. (2003). The advanced microwave scanning radiometer for the earth observing system (AMSR-E), NASDA's contribution to the EOS for global energy and water cycle studies. *IEEE Transactions on Geoscience and Remote Sensing*, 41(2):184–194.

Kooyman, G. L., Norris, K. S., and Gentry, R. L. (1975). Spout of the gray whale: Its physical characteristics. *Science*, 190(4217):908–910.

Laake, J. L., Punt, A., Hobbs, R. C., Ferguson, M., Rugh, D. J., and Breiwick, J. M. (2009). Re-analysis of gray whale southbound migration surveys, 1967–2006. NOAA Technical Memorandum NMFS-AFSC203, U.S. Department of Commerce.

Laake, J. L., Punt, A. E., Hobbs, R., Ferguson, M., Rugh, D., and Breiwick, J. (2012). Gray whale southbound migration surveys 1967–2006: an integrated re-analysis. *Journal of Cetacean Research and Management*, 12(3):287–306.

Lindquist, O. (2000). *The North Atlantic gray whale (Escherichtius robustus): An historical outline based on Icelandic, Danish-Icelandic, English and Swedish sources dating from ca 1000 AD to 1792*, volume 1. Universities of St. Andrews and Stirling, Scotland.

Liu, J., Curry, J. A., and Hu, Y. (2004). Recent Arctic sea ice variability: Connections to the Arctic Oscillation and the ENSO. *Geophysical Research Letters*, 31(9):L09211.

Malme, C., Miles, P., Clark, C., Tyack, P., and Bird, J. (1984). Investigations of the potential effects of underwater noise from petroleum-industry activities on migrating gray-whale behavior. Phase 2: January 1984 migration. Technical Report PB-86-218377/XAB; BBN-5586, Bolt, Beranek and Newman, Inc., Cambridge, MA.

Mantua, N. J. and Hare, S. R. (2002). The Pacific Decadal Oscillation. *Journal of Oceanography*, 58(1):35–44.

Marques, T. A., Thomas, L., Ward, J., DiMarzio, N., and Tyack, P. L. (2009). Estimating cetacean population density using fixed passive acoustic sensors: an example with Blainville's beaked whales. *The Journal of the Acoustical Society of America*, 125(4):1982–1994.

Mate, B., Lagerquist, B., and Irvine, L. (2010). Feeding habitats, migration, and winter reproductive range movements derived from satellite-monitored radio tags on eastern North Pacific gray whales. Technical Report SC/62/BRG21, International Whaling Commission Scientific Committee.

Mate, B. R. and Urbán-Ramírez, J. (2003). A note on the route and speed of a gray whale on its northern migration from Mexico to central California, tracked by satellite-monitored radio tag. *Journal of Cetacean Research and Management*, 5(2):155–158.

Moore, S. E., Grebmeier, J. M., and Davies, J. R. (2003). Gray whale distribution relative to forage habitat in the northern Bering Sea: current conditions and retrospective summary. *Canadian Journal of Zoology*, 81(4):734–742.

Moore, S. E., Urbán-Ramírez, J., Perryman, W. L., Gulland, F., Perez-Cortes M., H., Wade, P. R., Rojas-Bracho, L., and Rowles, T. (2001). Are gray whales hitting "K" hard? *Marine Mammal Science*, 17(4):954–958.

Moore, S. E., Wynne, K. M., Kinney, J. C., and Grebmeier, J. M. (2007). Gray whale occurrence and forage southeast of Kodiak, Island, Alaska. *Marine Mammal Science*, 23(2):419–428.

Munger, L. M., Wiggins, S. M., Moore, S. E., and Hildebrand, J. A. (2008). North pacific right whale (*Eubalaena japonica*) seasonal and diel calling patterns from long-term acoustic recordings in the southeastern bering sea, 2000–2006. *Marine Mammal Science*.

Noad, M. J., Dunlop, R. A., and Mack, A. K. (2017). Changes in humpback whale singing behavior with abundance: Implications for the development of acoustic surveys of cetaceans. *The Journal of the Acoustical Society of America*, 142:1611–1618.

Overland, J. E. and Stabeno, P. J. (2004). Is the climate of the Bering Sea warming and affecting the ecosystem? *Eos, Transactions, American Geophysical Union*, 85(33):309–312.

Parks, S. E., Johnson, M., Nowacek, D., and Tyack, P. L. (2011). Individual right whales call louder in increased environmental noise. *Biology Letters*, 7(1):33–35.

Payne, R. S. and McVay, S. (1971). Songs of humpback whales. *Science*, 173(3997):585–597.

Perryman, W. L., Donahue, M. A., Laake, J. L., and Martin, T. E. (1999). Diel variation in migration rates of eastern Pacific gray whales measured with thermal imaging sensors. *Marine Mammal Science*, 15(2):426–445.

Perryman, W. L., Donahue, M. A., Perkins, P. C., and Reilly, S. B. (2002). Gray whale calf production 1994–2000: Are observed fluctuations related to changes in seasonal ice cover? *Marine Mammal Science*, 18(1):121–144.

Perryman, W. L., Reilly, S. B., and Rowlett, R. A. (2010). Results of surveys of northbound gray whale calves 2001–2009 and examination of the full sixteen year series of estimates from the Piedras Blancas Light Station. Paper SC/62/BRG1 presented to the International Whaling Commission Scientific Committee.

Petrochenko, S. P., Potapov, A. S., Pryadko, V. V., and Wood, J. S. (1991). Sounds, source levels, and behavior of gray whales in the Chukotskoe Sea. *Soviet Physics Acoustics*, 37(6):622–624.

Piepenburg, D. (2005). Recent research on arctic benthos: common notions need to be revised. *Polar Biology*, 28(10):733–755.

Poole, M. M. (1984). Migration corridors of gray whales along the central California coast, 1980–1982. In Jones, M. L., Swartz, S. L., and Leatherwood, S., editors, *The Gray Whale: Eschrichtius robustus*, chapter 16, pages 389–407. Academic Press, Orlando, FL.

Reilly, S. B., Bannister, J. L., Best, P. B., Brown, M., Brownell, Jr., R. L., Butterworth, D. S., Clapham, P. J., Cooke, J., Donovan, G. P., Urbán-Ramírez, J., and Zerbini, A. N. (2008). *Eschrichtius robustus*. *The IUCN Red List of Threatened Species*, 2008(e.T8097A12885255).

Rice, D. W. and Wolman, A. A. (1971). *The life history and ecology of the gray whale (Eschrichtius robustus)*. Number 3. The American Society of Mammalogists, Seattle, WA.

Rugh, D. J. (1984). Census of gray whales at Unimak Pass, Alaska, November–December 1977–1979. In Jones, M. L., Swartz, S. L., and Leatherwood, S., editors, *The Gray Whale: Eschrichtius robustus*, chapter 10, pages 225–248. Academic Press, Orlando, FL.

Rugh, D. J., Breiwick, J. M., Dahlheim, M. E., and Boucher, G. C. (1993). A comparison of independent, concurrent sighting records from a shore-based count of gray whales. *Wildlife Society Bulletin*, 21(4):427–437.

Rugh, D. J., Ferrero, R. C., and Dahlheim, M. E. (1990). Inter-observer count discrepancies in a shore-based census of gray whales (*Eschrichtius robustus*). *Marine Mammal Science*, 6(2):109–120.

Rugh, D. J., Muto, M. M., Hobbs, R. C., and Lerczak, J. A. (2008). An assessment of shore-based counts of gray whales. *Marine Mammal Science*, 24(4):864–880.

Rugh, D. J., Shelden, K. E. W., and Schulman-Janiger, A. (2001). Timing of the gray whale southbound migration. *Journal of Cetacean Research and Management*, 3(1):31–40.

Salvadeo, C. J., Gómez-Gallardo U., A., Nájera-Caballero, M., Urbán-Ramírez, J., and Lluch-Belda, D. (2015). The effect of climate variability on gray whales (*Eschrichtius robustus*) within their wintering areas. *PLoS ONE*, 10(8):e0134655.

Scammon, C. M. (1874). *The marine mammals of the north-western coast of North America, described and illustrated: Together with an account of the American whale-fishery*. John H. Carmany and Company, San Francisco, CA.

Schonberg, S. V., Clarke, J. T., and Dunton, K. H. (2014). Distribution, abundance, biomass and diversity of benthic infauna in the Northeast Chukchi Sea, Alaska: Relation to environmental variables and marine mammals. *Deep Sea Research Part II: Topical Studies in Oceanography*, 102:144–163.

Shelden, K. E. W. and Laake, J. L. (2002). Comparison of the offshore distribution of southbound migrating gray whales from aerial survey data collected off Granite Canyon, California, 1979–96. *Journal of Cetacean Research and Management*, 4(1):53–56.

Shelden, K. E. W., Rugh, D. J., and Schulman-Janiger, A. (2004). Gray whales born north of Mexico: indicator of recovery or consequence of regime shift? *Ecological Applications*, 14(6):1789–1805.

Spreen, G., Kaleschke, L., and Heygster, G. (2008). Sea ice remote sensing using AMSR-E 89-GHz channels. *Journal of Geophysical Research*, 113(C2).

Sumich, J. L. (1983). Swimming velocities, breathing patterns, and estimated costs of locomotion in migrating gray whales, *Eschrichtius robustus*. *Canadian Journal of Zoology*, 61(3):647–652.

Sumich, J. L. (2014). *E. robustus: The biology and human history of gray whales*. Whale Cove Marine Education, Corvallis, OR.

Sumich, J. L. and Show, I. T. (2011). Offshore migratory corridors and aerial photogrammetric body length comparisons of southbound gray whales, *Eschrichtius robustus*, in the Southern California Bight, 1988–1990. *Marine Fisheries Review*, 73(1):28–34.

Urbán-Ramírez, J., Gómez-Gallardo U., A., and Ludwig, S. (2003). Abundance and mortality of gray whales at Laguna San Ignacio, Mexico, during the 1997-98 El Niño and the 1998-99 La Niña. *Geofisica Internationale*, 42(3):439–446.

Urick, R. J. (1967). *Principles of underwater sound for engineers*. Tata McGraw-Hill Education.

Versluis, M. (2000). How snapping shrimp snap: Through cavitating bubbles. *Science*, 289(5487):2114–2117.

Weller, D. W., Ivashchenko, Y. V., Tsidulko, G. A., Burdin, A. M., and Brownell, Jr., R. L. (2002). Influence of seismic surveys on western gray whales off Sakhalin Island, Russia in 2001. Technical Report SC/54/BRG14, International Whaling Commission Scientific Committee.

Whittaker, J. M., Goncharov, A., Williams, S. E., Müller, R. D., and Leitchenkov, G. (2013). Global sediment thickness data set updated for the Australian-Antarctic Southern Ocean. *Geochemistry, Geophysics, Geosystems*, 14(8):3297–3305.

Wiggins, S. M. and Hildebrand, J. A. (2007). High-frequency Acoustic Recording Package (HARP) for broad-band, long-term marine mammal monitoring. In *2007 Symposium on Underwater Technology and Workshop on Scientific Use of Submarine Cables and Related Technologies*, pages 551–557. IEEE.

Wiggins, S. M., Oleson, E. M., McDonald, M. A., and Hildebrand, J. A. (2005). Blue whale (*Balaenoptera musculus*) diel call patterns offshore of southern california. *Aquatic Mammals*, 31(2):161–168.

Wisdom, S. (2000). Development of sound production in the gray whale (*Eschrichtius robustus*). Master's thesis, University of San Diego.

Wood, S. N. (2006). *Generalized additive models: an introduction with R*. CRC Press, Boca Raton, FL.

Woodward, P. M. (1964). *Probability and Information Theory, with Applications to Radar*, volume 3 of *International Series of Monographs on Electronics and Instrumentation*. Pergamon Press, 2 edition.

Youngson, B. T. and Darling, J. D. (2016). The occurrence of pulse, "knock" sounds amidst social/sexual behavior of gray whales (*Eschrichtius robustus*) off Vancouver Island. *Marine Mammal Science*, 32(4):1482–1490.

Zitterbart, D. P., Kindermann, L., Burkhardt, E., and Boebel, O. (2013). Automatic round-the-clock detection of whales for mitigation from underwater noise impacts. *PLoS ONE*, 8(8):e71217.